A new spatial resampling method for synthetic precipitation generation in the Rhine basin

MSc thesis graduation report

Nynke C.G. Tack

A new spatial resampling method for synthetic precipitation generation in the Rhine basin

MSc thesis graduation report

Graduation committee

TU Delft	Deltares	GIE AXA
Hessel C. Winsemius	Bart J.J.M. van den Hurk	Hugo Rakotoarimanga
Matthijs Kok		

Student:	Nynke C.G. Tack
Student number:	4984900
Institution:	Delft University of Technology
Place:	Faculty of Civil Engineering, Delft
Master track:	MSc Water Management
Specialisation:	Hydrology and Water Resources Management
Project Duration:	March, 2022 - October, 2022

Cover Image: Picture of very local rainfall in Serra do Divisor National Park, Brazil (Salgado, S., 2016)

TU Delft

Het is springen
In het diepe
Zonder te weten
Hoe de golven gaan rollen
Maar ik kan zwemmen ... dus
Laat ik de golven komen ... Ik spring
Na een diepe ademhaling
En kom weer boven
En geniet

- An amazing friend, an incredible woman (2022) -

Abstract

Weather generators (WGs) based on temporal resampling algorithms are not able to generate new extremes with the same or a higher temporal resolution as the historical data series of the thus far observed precipitation. This is problematic for catchments with a time of concentration shorter than the resolution of the used data and conflicts with the increasing occurrence of more local, short duration extremes not yet observed.

In this thesis, it was researched if spatial permutation of precipitation could provide a solution to these problems by introducing historical events from related locations into the area of interest. The generated precipitation series were expected to have a larger variety of precipitation events compared to the historical data, thereby representing the current changing weather patterns better and being more suitable for small basins. This is beneficial for insurance companies, governments and aid organisations which rely on long term precipitation series to generate event catalogues and risk predictions.

To develop, improve and widen the knowledge about the effects of spatial permutation, four different questions were formulated for a case study on spatial permutation in the Rhine basin. A literature study showed that precipitation regimes in Europe can be defined based on spatial and temporal variability, precipitation amounts and the influence of controlling factors like atmospheric circulations, topography and climate change. This information was used to built three permutation models. The first model shifted historical precipitation fields over fixed distances and directions. In the second model this fixed approach was replaced by semi-random vectors including spatial and temporal correlation. The last model used a vector approach with vectors conditioned with historical wind data. The effect of each model on the Generalized Extreme Value (GEV) distributions, the cumulative distribution functions (cdfs) and the main characteristics of precipitation for different basins and aggregation times was determined. The July 2021 Meuse flood was used as example to show the working method of each model visually and to better understand the effect of each permutation model on individual extreme events.

The results showed that spatial permutation did influence precipitation patterns, characteristics and statistics. Strongest changes in extreme precipitation events were seen for small basins and short aggregation times. The permutation direction and distance were important determinants for the outcome of each model. Precipitation permutation with semi-random vector fields was shown to be a promising method which allowed for the inclusion of both spatial and temporal correlation. However, the model had a high sensitivity to the initial and boundary conditions. Wind based vector fields were able to replicate the most important historical precipitation characteristics while at the same time generating new extremes. Yet, a clear trade off was visible between similarity of the historically observed and modelled precipitation characteristics and the number of new extremes introduced.

With the knowledge obtained, it can be concluded that spatial permutation is a promising method to generate more divers precipitation time series for the Rhine basin. Both semi-random and wind-based vector permutations can already be used to generate new precipitation series as long as the initial and boundary conditions are chosen carefully. To improve the results, a fusion of spatial and temporal relations and a physically wind-based vector generation method is advised. In addition, possibilities are seen in a combination of the currently used temporal resampling algorithms and a spatial permutation approach. The outcomes of these suggestions are not known yet. Nevertheless, it is expected that a better understanding of spatial permutation, on top of the results presented in this thesis, can advance the current methodologies used to generate long term precipitation series. Therefore, it is hoped that this research provides the incentives to explore spatial permutation of precipitation patterns in more detail and in such, contributes to a more accurate risk profile for the livelihoods of people worldwide.

Keywords: weather generators (WGs), spatial permutation, extreme precipitation, Rhine basin

Résumé

Les générateurs stochastiques de temps (GT) basés sur des algorithmes de rééchantillonnage temporel ne sont pas capables de générer de nouveaux extrêmes avec une résolution temporelle identique ou supérieure à celle des séries de temporelles historiques de précipitation observées jusqu'à présent. Ceci est problématique pour les bassins versants dont le temps de concentration est plus court que la résolution des données utilisées et n'est pas compatible avec l'apparition croissante de phénomènes extrêmes plus locaux et de courte durée qui n'ont pas encore été observés sur la période historique, liée au changement climatique.

Dans cette thèse, nous avons cherché à savoir si la permutation spatiale des précipitations pouvait apporter une solution à ces problèmes en introduisant des événements historiques provenant de lieux connexes dans la zone d'intérêt. Nous nous attendons à ce que les séries de précipitations présentent davantage de variabilité par rapport aux données historiques et représentent ainsi mieux les régimes météorologiques changeants actuels. Un tel modèle est important pour les compagnies d'assurances, les gouvernements et les organisations en charge de la coordination de la réponse aux désastres naturels qui s'appuient sur des séries de précipitations à long terme pour générer des catalogues d'événements et des prévisions de risques.

Pour développer, améliorer et approfondir les connaissances sur les effets de la permutation spatiale, quatre questions différentes ont été formulées pour une étude de cas dans le bassin du Rhin. Une étude documentaire a montré que les régimes de précipitations en Europe peuvent être définis sur la base de la variabilité spatiale et temporelle des quantités de précipitations et de l'influence de facteurs de contrôle tels que les circulations atmosphériques, la topographie et le changement climatique. Ces informations ont été utilisées pour construire trois modèles de permutation. Le premier modèle, cette approche fixe a été remplacée par des vecteurs semi-aléatoires incluant une corrélation spatiale et temporelle. Le dernier modèle a utilisé une approche vectorielle avec des vecteurs basés sur des données historiques de vent. L'effet de chaque modèle sur les lois d'extremum généralisée (GEV), les fonctions de distributions cumulative (cdfs) et les principales caractéristiques des précipitations pour différents bassins et temps d'agrégation a été déterminé. La crue de la Meuse de juillet 2021 a été utilisée comme exemple pour illustrer visuellement la méthode de travail de chaque modèle et pour mieux comprendre l'effet de chaque modèle de permutation sur les événements extrêmes individuels.

Les résultats ont montré que la permutation spatiale influence effectivement les modèles, les caractéristiques et les statistiques des précipitations. Les changements les plus importants dans les événements de précipitations extrêmes sont observés pour les petits bassins et les temps d'agrégations courts. La direction et la distance de la permutation sont des facteurs déterminants pour les résultats de chaque modèle. La permutation des précipitations avec des champs vectoriels semi-aléatoires s'avère être une méthode prometteuse qui permet d'inclure la corrélation spatiale et temporelle. Cependant, le modèle reste très sensible aux conditions initiales et aux conditions aux limites. Les champs vectoriels basés sur le vent ont permis de reproduire les caractéristiques historiques les plus importantes de précipitions tout en générant de nouveaux extrêmes. Toutefois, un compromis doit être déterminé entre la similarité des caractéristiques des précipitations historiquement observées et modélisées et le nombre de nouveaux extrêmes introduits.

Forts de cette étude, il est possible de conclure que la permutation spatiale est une méthode prometteuse pour générer des séries temporelles de précipitations plus diversifiées pour le bassin du Rhin. Les permutations vectorielles semi-aléatoires et basées sur le vent peuvent d'ores et déjà être utilisées pour générer de nouvelles séries de précipitations, à condition que les conditions initiales et limites soient choisies avec soin.

Pour améliorer les résultats, une fusion des relations spatiales et temporelles et une méthode de génération de vecteurs basée sur le vent physiques sont conseillées. En outre, des possibilités sont envisagées dans une combinaison des algorithmes de rééchantillonnage temporel actuellement utilisés et une approche de permutation spatiale. Les résultats de ces suggestions ne sont pas encore connus. Néanmoins, nous pouvons nous attendre à ce qu'une meilleure compréhension de la permutation spatiale, en plus de résultats présentés dans cette thèse, puisse faire progresser les méthodologies actuelles utilisées pour générer des séries de précipitations à long terme. Par conséquent, nous espérons que cette recherche incitera à explorer plus en détail la permutation spatiale des modèles précipitations et contribuer ainsi à la détermination d'un profil de risque plus précis dans l'intérêt des populations.

Mots clés : générateurs météorologiques (GT), permutation spatiale, précipitations extrêmes, bassin du Rhin.

Contents

1 Introduction

Climate change influences the intensity and frequency of extreme precipitation events. As a result, storms with a duration and depth exceeding the thus far historical observed values are recorded at more and more locations [1]. A recent example of such a storm is the deep, stationary depression called 'Bernt' causing the July, 2021 flood covering parts of Germany, Belgium and The Netherlands. In total 240 people lost their lives and the economic damage was estimated to be 38 billion euros. Thereby, the flood was ranked as the second most expensive natural disaster of 2021 [2].

The fact that a flood could cause such damage in some of the world's wealthiest and most technologically advanced countries sparked the interest of society. Companies, governments and researches are looking into how current practices and tools can be improved to reduce the impact of future disasters. The focus is two-sided. On the one hand, measures are investigated which reduce the impact of a storm, such as the Dutch "Room for the River" project which aims at giving rivers the possibility to retrieve their meandering behaviour. On the other hand the attention has been drawn to flood risk profiles which are used by insurance companies, governments and aid organisations. These profiles are generated with the help of hydrological-hydraulic models.

Hydrological-hydraulic models are models which combine weather data with the characteristics of water flow, conveyance, sub-soil and landscape characteristics. They are used to determine the probability, frequency and impact of floods resulting from different types of extreme precipitation events. On top, they are employed to calculate the characteristic storms and floods belonging to different return periods. To do so the input weather data must be of sufficient length which is especially important for extreme and rare events. Therefore, long precipitation series with an accurate reconstruction of precipitation dynamics and statistical characteristics are necessary to make a credible description of the flood risk present in an area [3].

The most commonly employed method to reconstruct the required long-term precipitation series are weather generators (WGs) [4]. WGs are a group of models which produce long-term synthetic weather series based on historical data and re-sampling algorithms. The advantages of these models are that they can produce rainfall series applicable to different catchments, can generate times series much longer than the length of the observed data and can be used for catchments for which not much data are present. In addition, they are used to produce 'design storms' which generation is less computational intensive due to the assumption of uniformity in time and space. This can speed up the hydrological-hydraulic modelling process [5].

The large drawback of the use of these 'design storms' is that they do not generate new and more extreme events at the time resolution of the historical data of a certain location. They also do not account for the high degree of spatial and temporal variability which is observed during extreme rainfall events [5]. Yet, it is especially this variability together with the heterogeneous state of the catchment which determines the final flood response and the corresponding flood risk of an area.

Fed by observations of changing frequencies of more local and extreme precipitation events in our present-day climate, the interest into new methods to generate long term synthetic weather series at a larger spatial scale is sparked. Several papers are published which show the first results of new temporal re-sampling methods [6], [7], which are proven to shown satisfactory results. However, with regard to the spatial scale, most methods are limited to a local scale [8] or focus on large areas with long times of concentration in which most variability originates from multi-day events. Nevertheless, it is mostly the basin scale which is relevant with regard to the interrelated and international risk- and finance dependencies. As such, it becomes important to know what the influence of the spatial component is on long term precipitation series generation.

Objective

Therefore, this MSc thesis has as goal to look into the effects of including spatial variability explicitly in generating long term precipitation series. It will do so by developing a method which can be used to apply spatial permutation over a basin size area. As case study, the Rhine basin is used due to its central position in Europe and the large economic and social values associated with Rhine basin floods. The research builds on the vast amount of research done into WGs, temporal re-sampling and recent initiatives into small-scale spatial re-sampling [8]. The results of the different steps in the development processes of the permutation model will be analysed with extreme value analysis, correlation coefficients and compared to the current extreme value statistics and physical boundaries of the catchment under consideration. Based on the conclusions drawn, the knowledge obtained from the spatial permutation models can be used as input for the next generation flood risk models.

To be able to reach the goal of this MSc thesis as described above, the following main objective was formulated:

"To develop a method to include, improve and widen the knowledge and understanding of the effects of spatial permutation of historical precipitation data on the generation of precipitation time series for the Rhine basin."

In order to reach the main objective, several questions and sub-questions are defined.

1. How can the annual precipitation regimes above the Rhine basin be defined in terms of temporal and spatial characteristics?
    I. What are the temporal and spatial characteristics of a precipitation regime?
    II. What are the main factors influencing the characteristics of a precipitation regime?
    III. Which macro-scale precipitation regimes can be distinguished in Europe?
    IV. What are the macro-scale precipitation regimes covering the Rhine basin?
        i. What are the spatial and temporal characteristics of these precipitation regimes?
        ii. What are the main factors influencing the characteristics of these precipitation regimes?
2. How does spatial permutation of historical gridded precipitation series influence the extreme precipitation patterns and statistics in the Rhine basin?
    I. How do extreme value statistics and precipitation patterns in the Rhine basin change when historical gridded precipitation series are shifted in space?
    II. What is the effect of basin size on the influence of spatial permutation on the extreme precipitation patterns and statistics?
    III. What is the effect of the duration of the rainfall event on the influence of spatial permutation on the extreme precipitation patterns and statistics?
    IV. What is the effect of shifting direction and distance on the extreme precipitation patterns and statistics?

3. How can a semi-random vector approach be used to spatially shift historical gridded precipitation series over the Rhine basin?
    I. Which parameters and methodologies are needed to develop a semi-random vector approach?
    II. What is the sensitivity of the outcomes to the different parameters and the methodology?
    III. How do extreme value statistics and precipitation patterns change when historical gridded precipitation series are shifted in space with a semi-random vector approach?
    IV. What is the influence of basin size, direction and duration on the extreme value statistics and precipitation patterns obtained with a semi-random vector approach?
4. How can historical wind data be used to generate a physically based vector approach which shifts historical gridded precipitation series over the Rhine basin?
    I. How can wind data be used to condition displacement vectors to move historical gridded precipitation series over the Rhine basin?
    II. How well does the shifted precipitation patterns maintain the main temporal and spatial characteristics of the historical precipitation patterns?
    III. How do extreme value statistics and precipitation patterns change when historical gridded precipitation series are shifted in space with wind based displacement vectors?
    IV. What is the sensitivity of the outcomes to the assumptions made in the methodology?
    V. What is the influence of basin size, direction and aggregation time on the extreme values statistics and precipitation patterns obtained with a wind based shifting approach?

Report structure

This report starts in Chapter 2 with an overview of the historical developments in the field of WGs. Based on literature research, the past and current knowledge is summarized in order to position this research into the correct context. In Chapter 3 an elaboration is given about the 'Materials & Methods' which are used to answer the different research questions. The data preparation, modelling steps and the statistical analysis performed are explained in different sub-sections for each type of model. Subsequently, the results are presented in Chapter 4 including a discussion of the results on model level. The general discussion is presented in Chapter 5 and focuses on the comparison of the results of the different models, The report closes with Chapter 6 which summarizes the answers to the sub-questions and main objective. References are provided at the end of the report as well as additional information captured in the appendices.

2

Literature review

With an estimated damage up to 600 million euros in The Netherlands alone, the recent flood in the Meuse basin has renewed the interest into flood risk assessment strategies [9]. At the base of all these strategies lies a large variety of combined hydrological-hydraulic models. A common characteristic is their dependence on environmental forcing factors of which one of the most important are precipitation data [10].

In early approaches to determine flood risk frequencies, precipitation statistics were derived with the help of an event-based approach. Statistical parameters were fit to point rainfall observations and used to obtain local peak discharge distribution functions [11]. Successive research has extended this application of stochastic methods to hydrological models which rely on long precipitation series [12]. To estimate the probabilities associated with rare and extreme events, data series with lengths up to 10,000 years are sometimes needed. This requirement is problematic since no historical records of this length are available.

A solution to this problem can be found in the creation of synthetic weather series by Weather Generators (WGs). WGs exist in many forms which vary in complexity. The most intuitive WGs are physically based models which estimate weather variables from physical relationships between one or multiple known characteristics. An example is the numerical Weather Research and Forecasting (WRF) model which generates weather series based on the physical relation between radiation, wind speed, surface thermodynamics and moisture content [13]. The disadvantage of physically based models is that their computational costs often exceed the available resources for risk modelling. Besides, they rely on sufficient and well distributed data within the system of interest. In absence of these data, results can become inaccurate, biased and limited by the imposed initial and boundary conditions [14].

Weather generators based on Artificial Intelligence (AI) partly fill this gap. AI models can deal with non-linear, uncertain, and irregular data. Artificial Neural Networks (ANN) can deduce patterns in various ranges of data which can subsequently be used to create new precipitation series. However, it was also concluded that the type of ANN used, and the temporal scale of interest determine the outcome of the model [14]. So far, no frameworks are known to determine the most appropriate AI model for a certain area thereby leaving the choice for an ANN up to the researcher.

Despite the promising development in the field of AI WGs, the most common method to develop long-term rainfall series up to today is by means of Stochastic Weather Generators (SWGs). SWGs treat precipitation as a stochastic process which can be described by mathematical parameters. Depending on the type of SWG, a chosen probability distribution is applied to simulate precipitation occurrence, spatial distribution and intensity over a predefined time step, e.g. monthly, daily, or sub-daily [12].

The advantage of stochastic methods compared to, for example methods which re-sample historical data into new weather time series, is the possibility to generate new daily extremes. Serinaldi & Kilsby (2014) [15] showed that the use of model approaches including fat/heavy tailed distributions created over dispersion within the models. This allowed for simulation of more extreme events without the need of including supplementary random fields. Difficulties remain, however, in capturing the spatial-temporal dynamics of precipitation events, especially over large geographic areas. Nevertheless, a spatial coherent representation of precipitation is indispensable for well-defined and realistic flood risk scenarios. Precipitation amounts and occurrence at various locations are correlated. The degree of correlation depends on distance, but also on the climatology and orography [16]. WGs should capture the spatial correlation to produce credible weather data.

Within the last decade, several approaches are studied which intend to capture the spatial correlation in the produced weather data. A univariate Markov process for multi-site precipitation occurrence including spatial correlation was developed by Breinl *et al.* (2013) [6] but could not produce new precipitation fields which accurately reflected the seasonal variability of rainfall. Gaussian probability density functions were fit to the covariance values of the Danube basin. Applying the continuous distributions of rainfall amounts and occurrence was used to generate new precipitation patterns. The inclusion of the covariance values guaranteed that the relation between time and space was maintained while still generating new random precipitation events. Though the model performed well, a tendency of overestimation for precipitation sums and aggregates was observed. Recently, an auto-regressive model in which precipitation was modelled as a censored latent Gaussian process was applied to Europe. The spatial correlation was proven to be low for most cells (<0.5). Yet, the correlation structure of highly correlated locations was underestimated [7].

Applications of WG models to basin scale areas are rare [7]. Nevertheless, this scale becomes more and more important considering the interconnected disaster financing, insurance regulations and climate adaptation strategies in the European Union (EU). Single flood-events have been shown to cover large parts of a basin and thereby affecting multiple countries simultaneously. As such, not only the local but also the surrounding weather patterns become relevant to determine flood risk [3]. More insight into the spatial dependency of these basin scale events is necessary to answer questions about probabilities, the accuracy of events catalogues and impact forecasts, which gained renewed attention because of the July 2021 Meuse basin flood.

Therefore, the development of a WG, which captures both the temporal and spatial dependency of extreme rainfall events over a larger area, will be an advancement for a better understanding of flood risk. The WG should capture the local dynamics of an extreme event, while at the same time representing the climatology of the wider region within the physically possible boundaries. A valid WG should be able to reproduce the stochastic structure of observed precipitation series [17]. In this way, the WG can be applied as input for the future generation of basin wide flood risk assessment models.

3

Materials & Methods

In this chapter, the data and methodologies used to answer the research questions are explained. Each sub-chapter concerns a separative research question. A summary of all the steps and their relations can be seen in the flowchart at the end of this chapter introduction (figure 3.1).

In the first sub-chapter, the structure of the performed literature review is explained. The focus of this review is to find out which different precipitation regimes exist in Europe and how factors like wind, pressure regions and topography influence these patterns. A more detailed attention is paid to precipitation and environmental factors in the Rhine basin, since this is the area of interest of this study.

Sub-chapter two focuses on the development of research model[1] 1 which is based on fixed spatial permutation. This model has the goal to determine whether spatial permutation does alter precipitation occurrence and statistics in different catchments compared to the historically observed data and can therefore be considered as a sensitivity study. Input data of the model consisted of historical precipitation values on a daily basis. The generated precipitation fields were compared with the historically observed precipitation by means of the Anderson-Darling test and the Pearson correlation coefficient. On top, the July 2021 flood was visualized in order to determine the effect of research model 1 on the total amount of rainfall simulated over the affected areas.

In sub-chapter three, the data and methodologies behind the more complex research model 2 are explained. The purpose of research model 2 is to see if semi-random state-space correlated vectors can be used to shift precipitation in a credible way. Artificial temporal, spatial and boundary conditions were determined to create the vectors. By varying the conditions, several iterations were made to determine the sensitivity of the final precipitation fields to the initial assumptions made. The data and statistical tests to analyse the difference between the modelled and observed precipitation are similar to research model 1, but extended with an analysis on the methodology itself. The sensitivity of the model to the chosen initial vector field, the direction of the methodology and the weighting factors used was examined. With the obtained information conclusions were drawn about the influence of the assumptions on the final vector and precipitation fields created.

In the last sub-chapter, the focus is put on model 3 which is the final and most complex model of this research. The motivation behind model 3 is to investigate whether it is possible to move precipitation with vectors which are conditioned based on historical wind speeds and directions observed over the Rhine basin. Therefore, in addition to the historical precipitation data, daily mean wind speeds in north-south (v) and east-west (u) direction and historical wind angles were used.

[1]The indication 'research model' is used in this report to indicate that the permutations applied in the model are based on methodological choices instead of physical observed quantities, e.g. wind, which can be used to condition displacement vectors. The goal of each research model is to determine the working principles, sensitivity, challenges and advantages which the taken modelling method entails.

Conditioning displacement vectors for precipitation based on historical wind date was considered as an appropriate next step to shift precipitation more objectively, since the natural movement of precipitation is to a large extent determined by wind directions and speeds [18] [19].The analysis of the results consisted of two steps. First, the temporal and spatial correlation, and the mean difference between the modelled precipitation fields and the historical fields were compared on a monthly and seasonal basis and visualised. Next, the same statistical procedure as described for research models 1 and 2 was performed on the newly created precipitation values.

A final important note to make with regard to the methodology behind each model, is that the temporal order of the historical gridded precipitation series is maintained in all cases. As such, changes observed in the resulting statistics, analysis and comparisons can be solely attributed to spatial permutation. Generated time series which exceeded that duration of the historical time series consisted of multiple repetitions of the historical time series. No changes in the underlying order of the precipitation events were made.

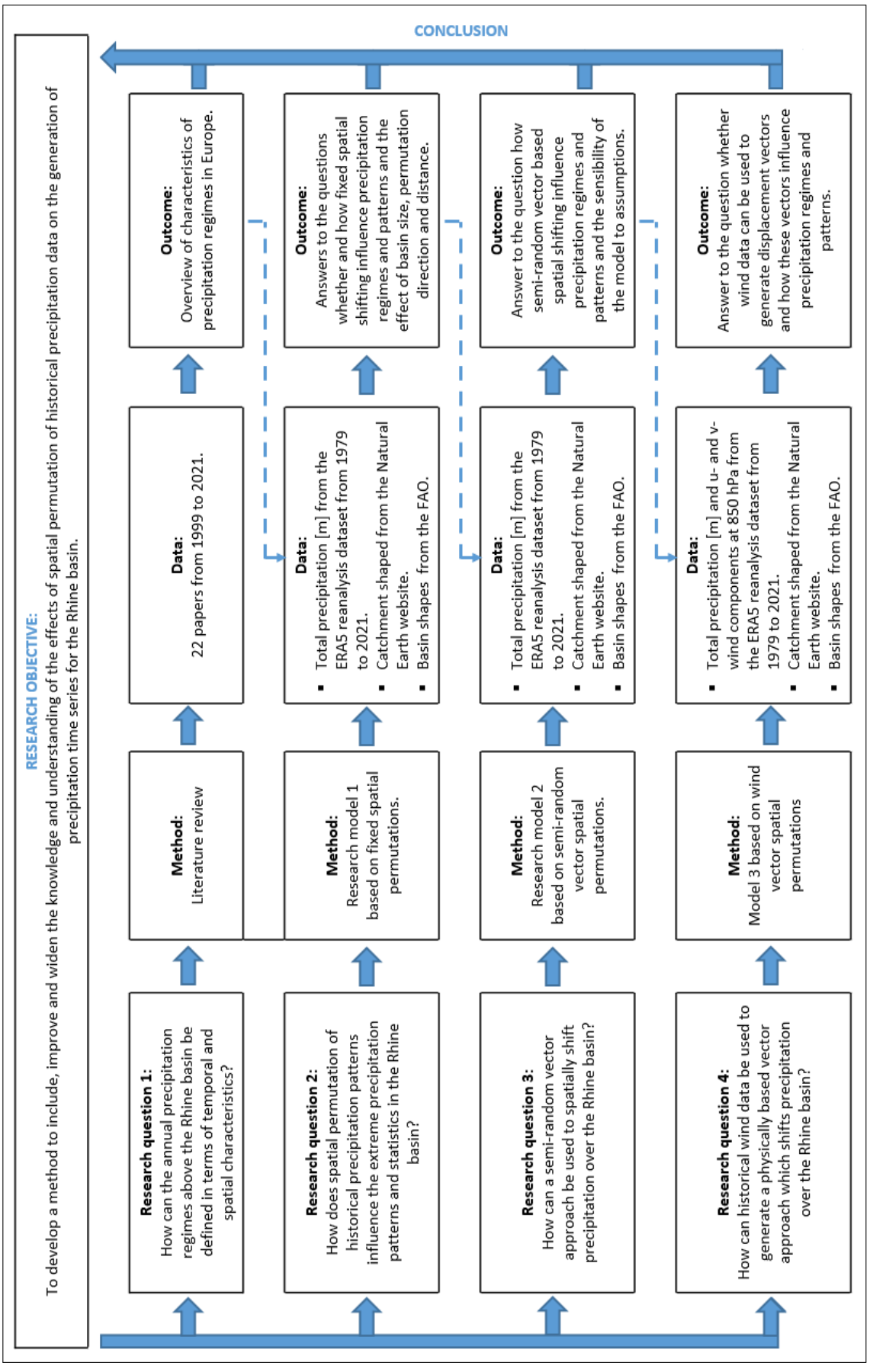

Figure 3.1: Flowchart showing the connection between the main objective, research questions and materials & methods. Blue dotted arrows indicate that results are used as input for the next step.

3.1. Literature review

The aim of the literature research was to get more insights into the basic mechanisms of precipitation formation and movement in Europe in order to answer the sub-questions of research question one. Google Scholar was used as main search engine. No restrictions on publication datum were applied since early research into generally accepted atmospheric phenomena was deemed to be of importance for the overall understanding. Search terms varied based on the sub-question under consideration.

In total, 22 papers were selected with publication dates between 1999 and 2021. From each paper, the abstract, introduction and conclusion were read. Main points were summarized and if necessary some further reading into the data and methodology was done. The acquired information was combined into a literature review which can be found in section 4.1.

3.2. Research model 1: fixed spatial permutation

Model 1 is a research model based on fixed spatial permutation. The model has been used to answer the sub-questions set for research question two. The main goal of the research model was to determine if spatial permutation of precipitation influences extreme rainfall statistics compared to historical observed statistics, and what the effect of catchment size and the duration of the rainfall is on the obtained results.

3.2.1. Methodology research model 1

Research model 1 is based on fixed spatial permutation. Fixed spatial permutation was in this case defined as: 'one uni-directional permutation which is fixed for the whole record length of the historical observations'. Permutations were chosen to be uniform and independent to isolate the effect of shifting on the statistics from other potentially determining variables, like the shape of the low pressure area and topography.

The following equations described how fixed spatial shifting, as defined above, is applied to ERA5 reanalysis precipitation data.

$$P\left(t,x,y\right) = \mathrm{s}(Pr\left(t,x,y\right), Pr'\left(t,x,y\right)) \tag{3.1}$$

$$Pr'\left(t,x,y\right) = Pr\left(t, x + D_x\left(\boldsymbol{l},\boldsymbol{d}\right), y + D_y\left(\boldsymbol{l},\boldsymbol{d}\right)\right) \tag{3.2}$$

In which, P is the modelled precipitation value [mm/day], t is the time [days], x is the longitude coordinate [degrees], y the latitude coordinate [degrees], s refers to a selection function, Pr is the historical precipitation value [mm/day], Pr' is the shifted precipitation value [mm/day] and D_x and D_y are the permutation functions with which the historical coordinates were perturbed in both x (longitude) and y (latitude) direction, respectively. Bold parameters indicate scalars which are varied for different iterations in the modelling process.

For research model 1, the permutation functions D_x and D_y are based on the parameters $\boldsymbol{l}$ and $\boldsymbol{d}$. They determined the permutation length [degrees] and direction, respectively, over which historical precipitation was shifted. For both length and distance, different values were examined. Values considered for length $\boldsymbol{l}$ were one, two, three, five and ten pixels, which is equivalent to 0.25, 0.5, 0.75, 1.25 and 2.5 [degrees], respectively. The analysed values of length $\boldsymbol{l}$ were chosen such that the effect of small (one pixel), medium (five pixels) and large (ten pixels) permutations could be compared with each other. Also, it allowed for analysing the differences a shift of only one pixel made by comparing the precipitation values resulting from either one, two or three pixels with each other.

For the permutation direction d each half-wind direction of the wind rose, i.e. north, north-east, east, south-east etc. was examined. The modelled precipitation series consisted of all values corresponding to a fixed value of l and the eight possible values of d. As such five data sets with a length of 378 years, i.e. eight times 42 years of shifted data plus one time 42 years of the historical data, were created for further analysis. A visual representation of the permutation methodology with l = 0.25 [degrees], i.e. one pixel, is shown in figure 3.2.

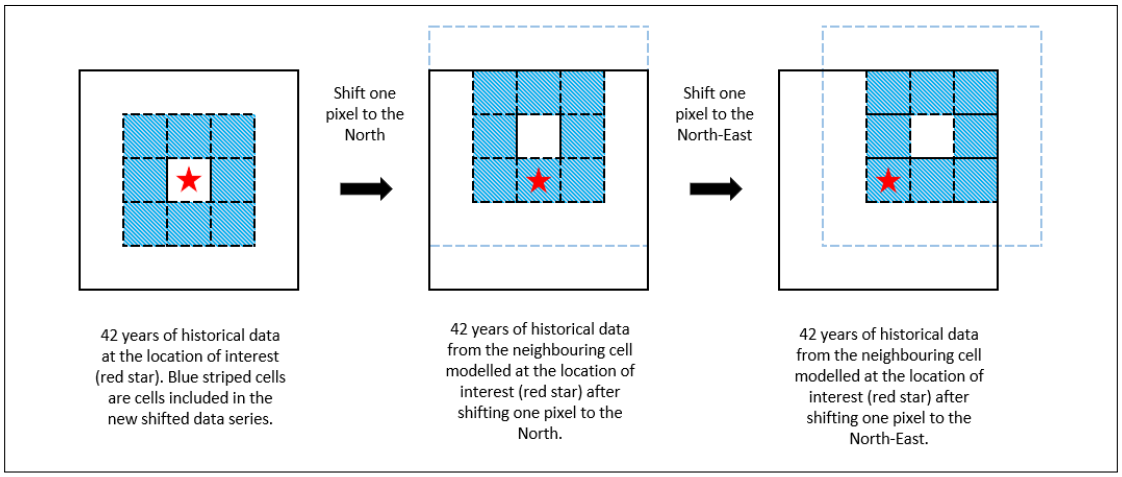

Figure 3.2: Schematic representation of the permutation mechanism employed in research model 1. Blue striped cells indicate cells included in the new shifted time series. The red star is the location of interest. The black solid line shows the initial grid boundary, while the blue striped line indicate the shifted grid boundary.

Based on the five data sets generated, analysis of the model results was performed. The one, two and three pixels shifted data sets were used for the creation of the cumulative distribution function (cdf) and fitted to a Generalized Extreme Value (GEV) distribution. The five and ten pixels shifted data sets were used to study the behaviour of the model when limits were increased to larger values. All data sets were analysed by means of statistical tests (see section 3.2.3).

3.2.2. Data research model 1

Precipitation data

Total precipitation [m] from 1979 to 2021 was extracted from ERA5 reanalysis data set from the climate data store of the Copernicus climate change service website [20]. The spatial coverage of the initial data set was -0.25 to 16.25 degrees longitude and 43.75 to 55.25 degrees latitude, roughly corresponding to the Rhine basin. The resolutions of the initial data set were 0.25°x 0.25°for the horizontal component and 37 pressure levels for the vertical component which cover pressure levels from 1,000 to 1 hPa. However, to handle data more efficiently, the vertical component of the data set was aggregated to one mean value in the vertical. In addition, the temporal resolution was up-sampled to daily values since this time step was deemed suitable for capturing the main precipitation dynamics over the Rhine basin while at the same time eased the further data handling. The final data set contained daily total precipitation values expressed in [mm/day].

Catchment and basin shapes

To determine the effect of catchment size on the results of precipitation permutation, shapes of European countries and hydro basins were used to clip data to different areas of interest. The countries shape file was obtained from the Natural Earth website [21]. Subsequently, a new shape file was created containing all countries on the European continent except Russia, since this country will not be part of the study area. A third shapefile was created only containing the countries covering the Rhine basin.

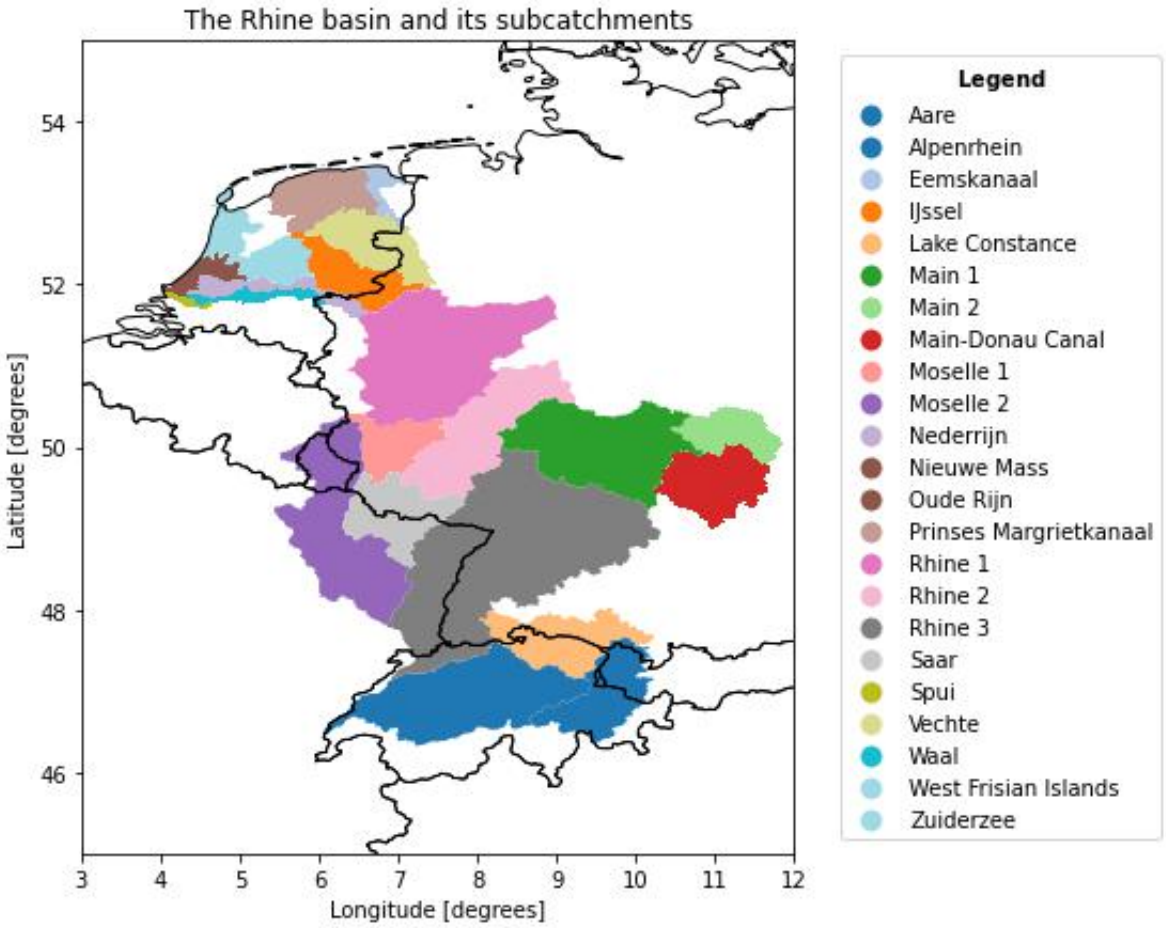

Figure 3.3: The Rhine basin and its sub-catchments

For the hydro basins, the shapes of the Rhine basin and its 23 sub-catchments were downloaded from the Food and Agriculture Organisation of the United Nations (FAO) [22]. Subsequently, the co-ordinate reference system (crs) of the shapes was set to EPSG:32632 - WGS 84/UTM zone 32N to be able to calculate the total area of the different catchments in the local reference coordinate system. For further analysis, three catchments at different locations and with different sizes were selected and saved as separate shape files. The catchments chosen were: the Ijssel, the Moselle (merging the shapes 1 and 2 together, see figure 3.3) and the whole Rhine basin.

3.2.3. Analysis research model 1

Quantification of statistical similarity between historical and modelled precipitation values

Quantification of the statistical similarity between the historical and modelled precipitation values was done with the Anderson-Darling (AD) test. The AD-test is a statistical test which can be used to determine whether a certain sample is drawn from a defined probability distribution. AD-test statistics can be either positive or negative. The lower the statistics, the more likely it is that two samples come from the same distribution,

Application of the AD-test to the precipitation values obtained from research model 1 was done with two purposes. First, the test was used to compare the cumulative distribution function (cdf) of the observed precipitation data with cdf of the shifted data. Low AD-test statistics indicated a high likelihood that two precipitation regimes came from the same climatology.

High values indicated that precipitation permutation led to a new climatology in the region. This could indicate a violation of the physical limits and possibly the need to define a boundary to the length l over which precipitation can reasonably be shifted.

The second purpose of using the AD-test was to quantify the goodness of fit of the Generalized Extreme (GEV) distribution to the historical and shifted data. The AD-test adds more value to the tails of the distribution and is therefore a suitable test to use for extreme events. Low AD-values indicated a good agreement between the fitted GEV-distribution and data. By performing the AD-test on the GEV distributions of different catchments and aggregation times, it was examined how the statistics of the shifted values differed from the historical values. Comparing the shifted data between catchments and aggregation times was used to see the influence of size and aggregation time on the obtained results.

For both cases, the AD test statistics was implemented with the *scipy.stats.anderson_ksamp()* function [23]. Critical values of the AD-test can be found in table 3.1. Note that α values above 0.25% will result in negative AD-test statistics.

Table 3.1: Critical values for the Anderson-Darling test including significance [%] with which the null-hypothesis: 'The samples come from the same distribution', can be rejected.

	Critical values of the Anderson-Darling test						
α [-]	**0.25**	**0.1**	**0.05**	**0.025**	**0.001**	**0.0005**	**0.0001**
Test statistics [-]	0.325	1.226	1.961	2.718	3.752	4.592	6.546

Correlation between historical and shifted precipitation maxima under different circumstances

The Pearson correlation coefficient was used to quantify the correlation between the historical and shifted annual maxima for different catchments, durations and shifting distances l. A high correlation between maxima indicated that maxima did not differ a lot. By applying the Pearson correlation coefficient to different combinations of catchments, durations and shifting distances, it was examined to what extent these factors influence the generation of maxima which differ compare to the historical data. Besides, the correlation coefficient was employed to show over which distance rainfall events correlate and if direction and basin size influenced the correlation. Outcomes of this process helped to get a first feeling about the distances over which precipitation could be shifted. To automate the calculation of the correlation coefficient, the *scipy.stats.pearsonr()* was used [24].

3.3. Research model 2: random based vector permutation

Model 2 is a research model which moved precipitation based on generated semi-random vector fields. This research model was built to answer the sub-questions asked under research question three. The main purpose of the research model was to determine whether artificial vector fields can be used to generate new precipitation patterns. In addition, the research model was used to determine the sensitivity of a vector based approach to assumptions made in the methodology about the initial and boundary conditions. It was expected that a semi-random vector based approach would move rainfall more credible compared to a fixed permutation approach, but that the final results would highly depend on the conditions set. Therefore, knowledge about the controlling parameters of the random vector field was essential to determine whether and how this approach could be used to generate vector fields on a physical basis in model 3. An overview of the codes used for research model 2 can be found in appendix I.1.

3.3.1. Methodology research model 2

The working mechanism of research model 2 is based on the same methodology as presented for research model 1 (see section 3.2.1). However, instead of using fixed permutations based on a chosen length $\boldsymbol{l}$ and direction $\boldsymbol{d}$, the permutations equations D_x and D_y of research model 2 were altered to generate state-space correlated vector components. The generation of these components was controlled by the spatial and temporal averaged vector components of the grid cells neighbouring the cell of interest. In addition a range $\boldsymbol{r}$ [degrees] was defined to set the variability between the spatial averaged component and the newly selected component. A maximum length $\boldsymbol{m}$ [degrees] was used to set the upper and lower limits of the vector components. The resulting modelling equations are as follows:

$$P\left(t,x,y\right) = \mathsf{s}(Pr\left(t,x,y\right), Pr'\left(t,x,y\right)) \tag{3.3}$$

$$Pr'\left(t,x,y\right) = Pr\left(t, x + D_x\left(\boldsymbol{r},\boldsymbol{m}\right), y + D_y\left(\boldsymbol{r},\boldsymbol{m}\right)\right) \tag{3.4}$$

$$D_x\left(\boldsymbol{r},\boldsymbol{m}\right) = \mathsf{U}(\mathsf{max}\left(\bar{p}\left(t,x\right) - \boldsymbol{r}, -\boldsymbol{m}\right), \mathsf{min}\left(\bar{p}\left(t,x\right) + \boldsymbol{r}, \boldsymbol{m}\right)) \tag{3.5}$$

$$D_y\left(\boldsymbol{r},\boldsymbol{m}\right) = \mathsf{U}(\mathsf{max}\left(\bar{q}\left(t,y\right) - \boldsymbol{r}, -\boldsymbol{m}\right), \mathsf{min}\left(\bar{q}\left(t,y\right) + \boldsymbol{r}, \boldsymbol{m}\right)) \tag{3.6}$$

In which, U is an uniform distribution which limits are determined by $\boldsymbol{r}$ and $\boldsymbol{m}$, $\bar{p}$ is the spatially and temporally averaged horizontal vector component [degrees] and $\bar{q}$ is the spatially and temporally averaged vertical vector component [degrees]. Bold parameters indicate scalars which are varied over different iterations in the modelling process.

To set up the modelling process, an initial field was generated. This initial field started with a semi-random horizontal and vertical permutation in the north-west corner of the grid. These permutations were determined by using equations 3.5 and 3.6, respectively, with a value of zero for both $\bar{p}$ and $\bar{q}$. Subsequently, the top row and first column of the grid where filled with permutations based on equations 3.5 and 3.6 with the permutations of the preceding row and column cell set as values for $\bar{p}$ and $\bar{q}$. Next, the other grid cells were filled based on the same equations, but $\bar{p}$ and $\bar{q}$ were determined by the spatially averaged value of the permutations of the three cells north and the cell west of the cell of interest. This was done since the permutations south and east of the cell of interest were not known yet.

To derive the spatially averaged value for $\bar{p}$ and $\bar{q}$, fixed weights were used. These weights were based on the rationale that neighboring cells in parallel with the direction of the permutation are more influential for the new permutation. This arbitrary assumption was made based on the empirical observation that wind vectors close to each other exhibit a similar direction and speed in most cases. The resulting weights for $\bar{p}$ were: 1, 1.25, 1 and 1.5, for the three cells north and the cell west (see figure 3.4), respectively. For $\bar{q}$ weights of 1, 1.5, 1 and 1.25, for the cells north and west were used, respectively.For the last column of the initial field, no cell in the north-east corner of the cell of interest existed. Therefore, the value of $\bar{p}$ and $\bar{q}$ was solely based on the permutations of the cells neighboring the cell of interest in the north-west corner, the north and the west.

After the initial field was filled, subsequent permutations were determined based on spatial-temporal averaged values for $\bar{p}$ and $\bar{q}$. An arbitrary weights vector, based on the same empirical observation as explained above, was assigned to calculate the average value of the neighboring permutations in the previous time step. The weights assigned were: [0.75, 1, 0.75], [1.25, 1.5, 1.25], [0.75, 1, 0.75], for the cell north-west till south-east, respectively in case of $\bar{p}$ (see figure 3.4). For $\bar{q}$, the weights slightly differed because the direction of $\bar{q}$ is 180°shifted compared to the $\bar{p}$. The weighting vector used for the $\bar{q}$ was therefore: [0.75, 1.25, 0.75], [1, 1.5, 1], [0.75, 1.25, 0.75]. As a result, permutations in line or parallel with the direction of the component of interest had more influence on the final value of $\bar{p}$ and $\bar{q}$.

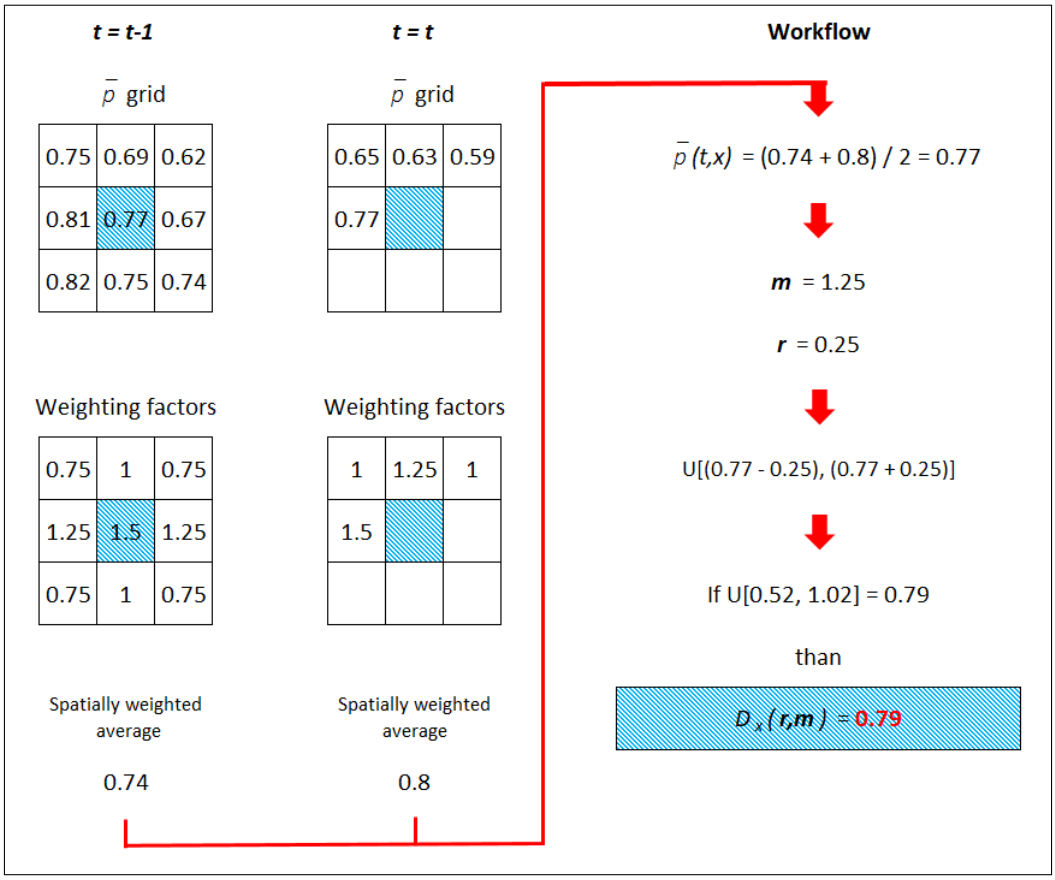

Figure 3.4: Example of the calculation procedure executed in order to generate the new $D_x\,(\boldsymbol{r}, \boldsymbol{m})$ for at time $t = t$ in a centrally located cell. The blue striped cell is the cell of interest. Values shown in white cells are values calculated according to the same procedure but at an earlier point in the process. The grid is filled from north-west to south-east.

The final values of $\bar{p}$ and $\bar{q}$ used for D_x and D_y in equations 3.5 and 3.6 were determined by taking the mean value over the average permutation of the previous time step and the current time step. The new permutation was drawn randomly from the uniform distribution U limited by the parameters r and m. The full procedure as described above and which can be seen in figure 3.4 was repeated for each cell for a time series of 42 years to ease the comparison with the historical data series.

Table 3.2: The different parameter combinations tested for the semi-random vector based approach of research model 2. Range r [degrees] defined the variation around either $\bar{p}$ and $\bar{q}$. The maximum absolute length was determined by m [degrees].

	Parameter	
	m [degrees]	***r*** [degrees]
Vector T1	1.25	0.25
Vector T2	1.25	0.75
Vector T3	2.50	0.25

In addition, different combinations of the controlling variables r and m of the permutation equations D_x and D_y were tested. This resulted in three different vector types T1, T2, and T3 with distinct combinations of r and m (see table 3.2). The values for m were chosen such that the different vector types could be compared to the five and ten pixels shifted data of research model 1.

For each vector type eight series of 42 years of permutation fields were generated. These permutation fields were used to generate new coordinate fields. Each grid cell contained a set of latitude and longitude coordinates which referred to the new location from which the shifted precipitation value Pr' was selected. This value was obtained by means of linear regression and was imposed on the original coordinates of the grid cell resulting in a new precipitation field filled with the modelled precipitation values P for each cell. An example of the result with $\boldsymbol{r} = 0.75$ [degrees] and $\boldsymbol{m} = 1.25$ [degrees] can be seen in figure 3.5. The observed loss of spatial correlation in the modelled precipitation field (middle figure) can be related to the high value of $\boldsymbol{r}$ which allows for much temporal and spatial variation between neighboring permutations and thereby a loss of spatial coherence. As such, the difference between historical Pr and modelled P precipitation values became larger as well (right figure).

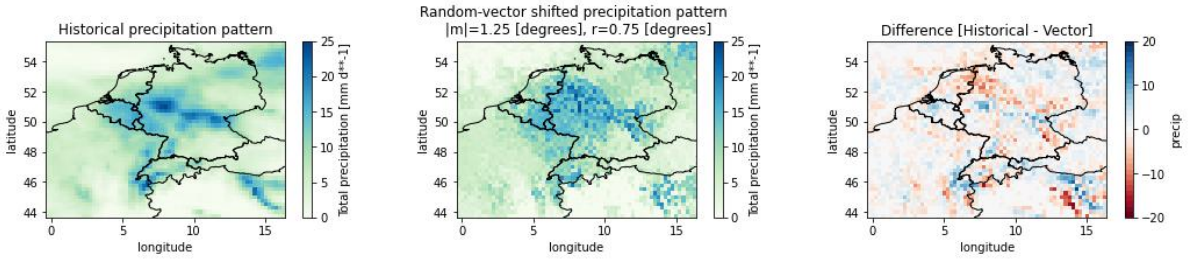

Figure 3.5: Visual representation of the outcome of research model 2 for vector type T2 at February 14, 1997 in the Rhine basin. From left to right: historical precipitation, modelled precipitation and difference between the two patterns.

3.3.2. Analysis research model 2

Quantifying similarity between historical and modelled precipitation values

The Anderson-Darling test and the Pearson correlation coefficient were used to quantify the extent to which the different vector types, i.e. T1, T2 and T3, were able to generate new extremes compared to the historical observed precipitation values Pr. In addition, the influence of aggregation time and basin size on the generated precipitation extremes was examined for each vector type in the same way as described for research model 1.

Sensitivity of the model to the used methodology

The goal of the sensitivity analyses performed on research model 2 was to determine the influence of the choices made in the methodology on the resulting semi-random permutation fields and the final precipitation values. In total, three different features which are described in subsection 3.3.1 were tested. These features were:

1. The initial permutation field
2. The weighting factors
3. The direction of permutation generation in the current time step

During the sensitivity analysis only the feature tested was changed while all other parameters and calculation methods remained as described in subsection 3.3.1. The base precipitation values were taken from the historical data of the year 2021 for all sensitivity analyses. The range $\boldsymbol{r}$ and length $\boldsymbol{m}$ were fixed for all analyses at a value of $\boldsymbol{r} = 0.25$ and $\boldsymbol{m} = 1.25$. An overview of the used code can be found in appendix I.2.

The initial permutation field

Three different variants of initial permutation fields were tested to determine the influence of the initial field on the generated precipitation means of the different basins. Variants of initial permutation fields tested were:

- Ten varying initial permutation fields produced with the methodology described in subsection 3.3.1.
- One fixed initial permutation field.
- An initial permutation field filled with zeros.

Precipitation means were compared at times 1, 2, 4, 7 and 14 days, 1 and 6 months, and 1 year after the start of the simulation. At each time, the coefficient of variation (cv) was calculated by dividing the standard deviation of the ten iterations by their mean. With the obtained values it could be concluded whether or not the initial field influenced the precipitation means generated and at which moment in time this effect was diminished.

Information about the influence of the initial permutation field on the generated precipitation values could be used to determine whether the model had a spin up time. If so, the results would indicate a time at which the results could be considered independent of the initial field. Besides, the variant which showed the least influence on the final precipitation values could be considered as the most suitable initial field for further development of vector based permutation models according the proposed methodology.

The weighting factors

Weights were used to generate the new value for $\bar{p}$ and $\bar{q}$ based on past and current surrounding values as shown in figure 3.4. As such, the weights determined the final values of the permutations which create the semi-random vector fields. To test the sensitivity of the model, different combinations of weights were tested. The combination tested are shown in figure 3.6 in which the parallel and perpendicular matrices are depicted for $\bar{p}$. For $\bar{q}$ these matrices turn 90°in agreement with the changing direction from east-west ($\bar{p}$) to north-south ($\bar{q}$). The initial permutation fields used for all iterations were similar.

For each vector generated, the maximum annual precipitation for different aggregation times was calculated to determine whether different weights influence precipitation extremes. If extremes were shown to be influenced by the weights assigned without a physical explanation, it could be concluded that weights should be chosen as neutral as possible, i.e. all similar. In addition, the average latitude (row) and longitude (column) correlation between the produced $D_x\,(t,x)$ and $D_y\,(t,y)$ was computed for several distances to see how weights altered the dependency between permutations. In the ideal case, latitude and longitude correlation would be similar and only vary with the randomness of the model. If weights appeared to force certain differences in correlation, it indicated that in further development weights should be omitted, be chosen with a physically substantiated reasoning or set all similar.

The direction of vector generation in the current time step

The calculation of $D_x\,(t,x)$ and $D_y\,(t,y)$ was executed from left, e.g. the most north-west grid cell, to right, e.g. the most south-east grid cell. As such, the new permutation depended more on the three known permutations at its north side and at its west boundary. This methodological choice could potentially create a high latitude correlation and directional bias in the permutation fields. To test whether this was the case, two different variants of permutations were created. The first variant started from a fixed initial permutation field but only the past permutations were used to calculate the new permutations. This eliminated the potential bias introduced by using the three cells north and cell at the west boundary in the current time step. The second variant started from an initial permutation field filled with zeros and only the past permutations were used to calculate the new permutations. This prevented both the potential bias of the current time step and the bias introduced in the procedure of creating the initial field to influence the results. Comparison of the latitude and longitude correlation between the two variants, and the correlation values obtained from the original methodology were used to determine whether a directional bias was present in the generated permutation fields.

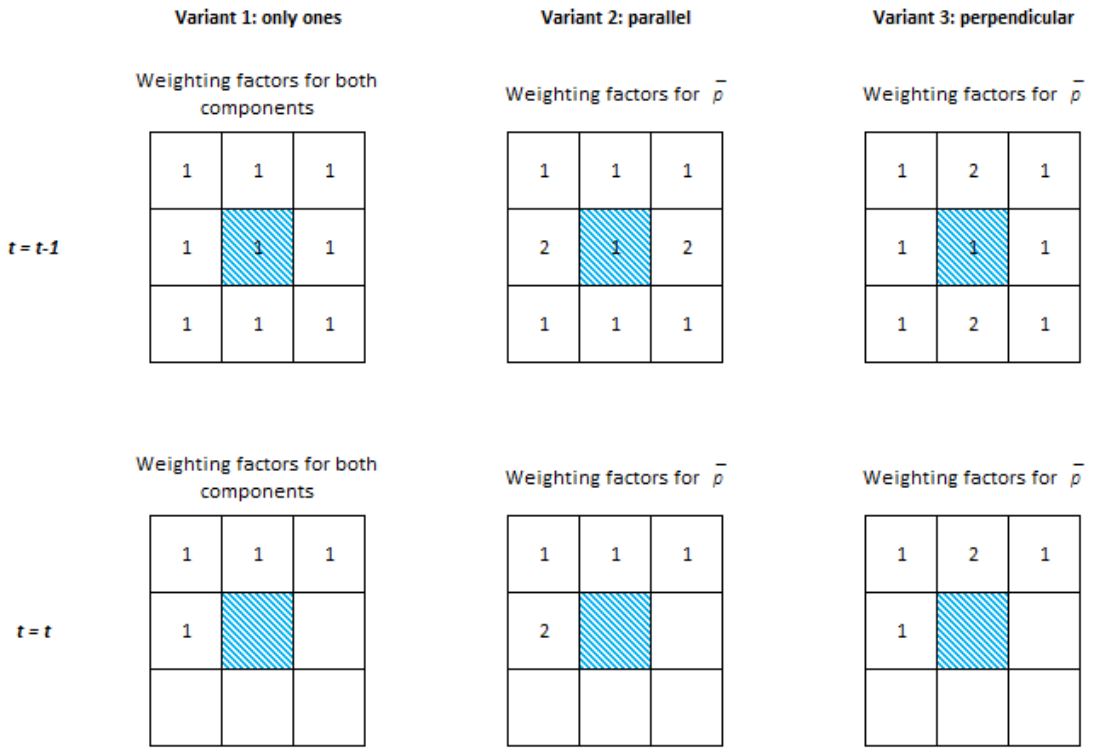

Figure 3.6: Weighting vectors used for the sensitivity analysis of the convolution matrices. Parallel and perpendicular matrices are shown for $\bar{p}$. The matrices for the $\bar{q}$ are opposite since the parallel and perpendicular direction changes from east-west to north-south.

If a directional bias originating from the methodology was proven to be present, a change in the methodology should be applied. Subsequent models should not show any directional preference which cannot be explained by natural phenomena. Other options should then be explored such as iterating two times over a vector field or using only the surrounding past values in the calculations process.

Extent of variation

To determine the extent to which research model 2 was able to generate clear variation in extremes, 1,000 times one year of data was generated based on the methodology as described in subsection 3.3.1 and with different combinations of weights and initial field as tested in the sensitivity analysis. From the historical data, the date of the maximum precipitation in the Ijssel, Moselle and Rhine catchments were derived. These dates were used to select the maxima on the same date from each iteration. A histogram was made with the 1,000 extracted values to visualize the extent to which the model was able to generate variation compared to the historical observed maxima.

3.4. Model 3: wind based vector permutation

Model 3 is a wind vector based model. The goal of this model was to determine if precipitation permutation can be done with displacement vectors based on observed historical wind data. Analyses of the model and its results was done to answer the sub-questions of research question four. The motivation to use wind data as starting point was that wind direction and speed is an important factor for precipitation movement. By using the observed wind vectors it was possible to include both local speed and directional limits to the displacement vectors based on a physically substantiated reasoning. The model framework of model 3 was comparable with research model 2, but the lessons learned resulted in some methodological changes which are explained in the subsections below. An overview of the codes used for model 3 can be found in appendix II.

3.4.1. Methodology model 3

The methodology of model 3 is an extension of the methodology presented for research model 2. Yet, instead of semi-random state-space correlated vectors, permutations are imposed with displacement vectors. Displacement vectors are vectors which are conditioned based on the historical wind vector field $\vec{V_h}$ and a selected proxy vector $\vec{V_p}$. To select $\vec{V_p}$, a subset of $\vec{V_h}$ was used which fulfilled the required temporal and spatial characteristics. The resulting displacement vector was decomposed in a horizontal permutation $D_x\left(\vec{V_p}\right)$ [degrees] and a vertical permutation $D_y\left(\vec{V_p}\right)$ [degrees]. The permutations were used to select the location from which the modelled precipitation value P was selected. The equations belonging to this process can be seen below.

$$P\left(t,x,y\right) = \mathsf{s}(Pr\left(t,x,y\right), Pr'\left(t,x,y\right)) \tag{3.7}$$

$$Pr'\left(t,x,y\right) = Pr\left(t, x + D_x\left(\vec{V_p}\right), y + D_y\left(\vec{V_p}\right)\right) \tag{3.8}$$

$$\vec{V_p} = \mathsf{s}(\vec{V_h}\left(t_m, \vec{V_{hc}}\left(t,x,y\right), \pm\boldsymbol{f}\right)) \tag{3.9}$$

In which t_m [month] is the month corresponding with the time t [day] of the historical wind vector of a specific grid cell, $\vec{V_{hc}}\left(t,x,y\right)$ is a historical wind vector of a specific grid cell at time = t, longitude = x and latitude = y and $\boldsymbol{f}$ [-] is a fraction of the monthly standard deviation of the wind angle and speed of $\vec{V_{hc}}\left(t,x,y\right)$. Bold parameters indicate scalars which are varied over different iterations in the modelling process.

To select a proxy vector $\vec{V_p}$ based on the historical wind vector $\vec{V_{hc}}\left(t,x,y\right)$ of one particular cell, a subset of the historical vector field $\vec{V_h}$ was made based on two requirements:

I. Each vector in the subset must have been observed in the month t_m to which the time t of the historical wind vector $\vec{V_{hc}}\left(t,x,y\right)$ belonged.
II. The vector length and angle of each selected vector should fall within a subspace around the length and angle of $\vec{V_{hc}}\left(t,x,y\right)$ which limits are defined by the fraction $\boldsymbol{f}$ of the monthly standard deviation of the wind angle and speed of $\vec{V_{hc}}\left(t,x,y\right)$.

The temporal component of these requirements was used to enable a seasonally dependent conditioning of the displacement vectors. The fraction $\boldsymbol{f}$ was the only scalar in model 3 and was varied between 0.05 and 0.5 [-]. As such, the extent of the subset from which $\vec{V_p}$ could be chosen was varied. In figure 3.7 an example of a subset of historical wind vectors with $\boldsymbol{f} = 0.05$ selected based on the historical wind vector $\vec{V_{hc}}\left(t = 10, x = 11.5, y = 46.75\right)$ observed in the Italian city Vahm at January 11th, 1980, is shown. The figure indicates that for this day and location, 17 historical wind vectors fulfill the requirements as explained above.

During the modelling process, similar subsets were generated for each location and time step. From each subset, one vector was randomly selected as $\vec{V_p}$. The final displacement vector was constructed with a length based on $\Delta\vec{V} = \vec{V_p} - \vec{V_{hc}}\left(t,x,y\right)$. The angle of the displacement vector was similar to the angle of $\vec{V_p}$. This process can be seen in figure 3.8 steps one to four.

Next, $\vec{V_p}$ was broken up into a horizontal $D_x\left(\vec{V_p}\right)$ and vertical $D_y\left(\vec{V_p}\right)$ permutation by means of equations 3.10 and 3.11. Since the resulting permutations were still in [m/s], their values were integrated over the temporal resolution of the historical data set, i.e. one day, and divided by the number of meters in one degree latitude/longitude. Projection on the earth's surface was assimilated to the tangent plane at the grid cell center.

$$D_x\left(\vec{V_p}\right) = -|\Delta\vec{V}| * \sin(\angle\vec{V_p}) \tag{3.10}$$

$$D_y\left(\vec{V_p}\right) = -|\Delta\vec{V}| * \cos(\angle\vec{V_p}) \tag{3.11}$$

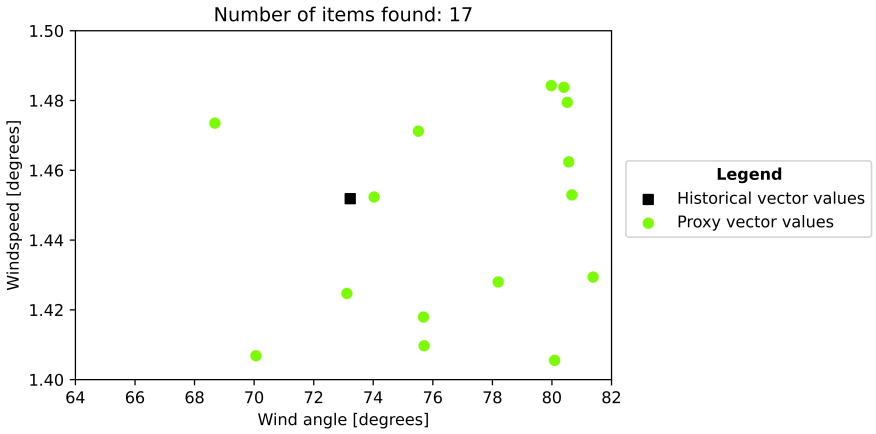

Figure 3.7: Visual representation of a subset of historical wind vectors selected (green dots) based for the historical wind vector $\vec{V_{hc}}\,(t, x, y)$ (black square) observed at 1980-11-01 in Vahrn, Bozen, Italy [longitude = 11.5, latitude = 46.75].

By adding permutations to the original coordinates of the grid cell, a new position was obtained. From this position, the precipitation value was derived by means of linear regression of daily precipitation values from the historical data set. This process was similar to research model 2. The new precipitation value Pr' was plotted on the original coordinates of the cell center. A visualisation of the process can be seen in figure 3.8 steps five and six.

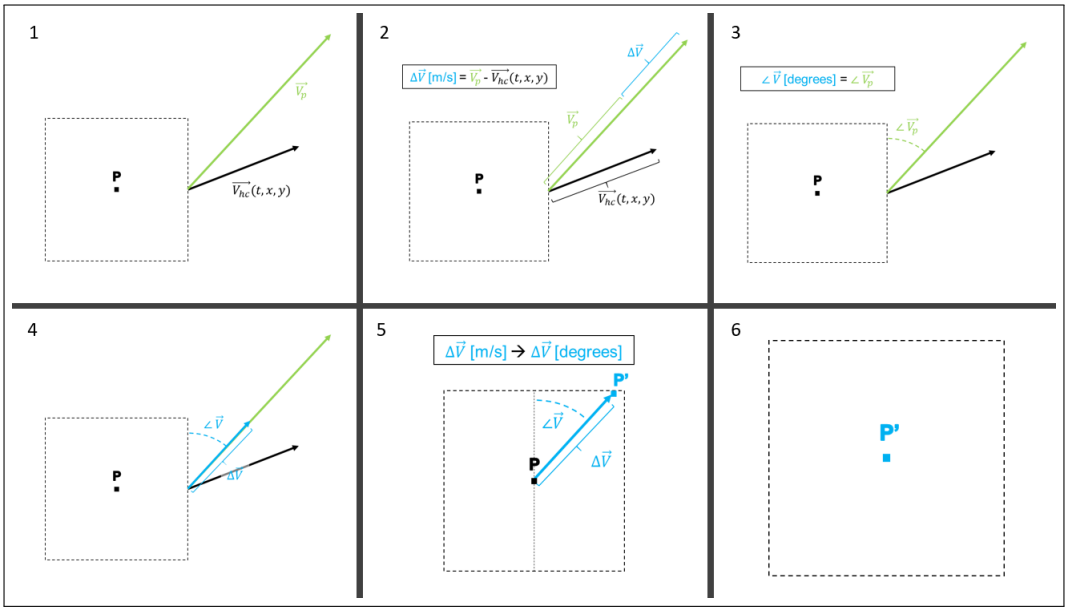

Figure 3.8: Visual representation of the steps taken to derive the new displacement vector (blue) based on the historical $\vec{V_{hc}}\,(t, x, y)$ (black) and proxy vector $\vec{V_p}$ (green).

The process described above was repeated at the same historical day for all grid cells. As such, a new coordinate field based on the displacement vectors conditioned with the historical wind data was created. When the full grid was generated, the next day of the historical wind vector field $\vec{V_h}$ was used as starting point. The process was repeated till the desired length of the time series was reached. When the desired length was longer than the amount of days in the historical data set, historical data was reused. The random selection of $\vec{V_p}$ within the limits set by $\boldsymbol{f}$ and $\vec{V_{hc}}\,(t, x, y)$ ensured that the resulting coordinate fields and thereby precipitation patterns were not repetitive.

3.4.2. Data model 3

Precipitation data

For the development of model 3, the same precipitation data as described for research models 1 and 2 were used. Not additional changes were made.

Wind data

Historical wind vectors (u and v components of wind in [m/s]) were obtained from raw hourly data from 1979 to 2021 from the climate data store of the Copernicus climate change service website [20]. Data was retrieved at a pressure level of 850 hPa which is in agreement with the methodology of Huidong *et.al.* [18] which studied the relation between regional-scale circulations and the observed clouds in Ny-Ålesund, Norway. They showed that wind direction had a strong correlation with the presence of clouds above Norway. At the 850 hPa pressure level this correlation was clearly visible. Assuming that these clouds are in most cases also responsible for the observed precipitation, a height of 850 hPa can be considered suitable for wind vector retrieval to steer precipitation movement.

The historical u and v components were converted to wind speeds, i.e. vector lengths, and angles, i.e. vector directions with the method suggested by the European Centre for Medium-Range Weather Forecasts (ECMWF) in their ERA5 documentation [25]. The results were stored in a file for later use.

3.4.3. Analysis model 3

Quantifying similarity and variance of historical and modelled precipitation values

The Anderson-Darling test and the Pearson correlation coefficient were used to quantify the extent to which model 3 was able to generate new extremes compared to the historical observed values. In addition, the influence of duration, basin and fraction f on the generated extremes was examined. The methodology behind the AD-test and the Pearson correlation coefficient was similar as described in the methodology sections of research models 1 and 2. The procedure behind the variation histograms was the same as well though the amount of repetitions was reduced to 100 to speed up the calculation process.

Spatial correlation of precipitation

The spatial correlation coefficient was used to validate to what extent the correlation observed in the historical precipitation fields was maintained in the generated precipitation fields. The mean spatial correlation of each grid cell to its 5x5 surrounding grid cells was calculated for each of the four seasons. The months belonging to each season were in agreement with the Gregorian calendar and defined for the Northern hemisphere. The correlation coefficient was based on the whole data series corresponding to one season. For each grid cell in the 5x5 grid, a Pearson correlation coefficient with the center grid cell was calculated. The final spatial correlation value of the center grid cell was set to be the average of the correlation coefficients with all 24 surrounding cells. No spatial correlation coefficients for the two boundary rows and columns of the study area were calculated. These values could introduce unwanted noise in the spatial correlation field since they required assumptions about the unknown data outside the study area. Differences between correlation values were visualised by subtracting vector correlation values from historical correlation values for each grid cell for each season. The results were plotted and analysed visually.

Temporal autocorrelation of precipitation

The temporal autocorrelation coefficient was calculated to examine how well model 3 was able to maintain the historical autocorrelation between precipitation values for each grid cell. Values for the autocorrelation were determined for each season, in which the months belonging to a season are as defined in subsection 3.4.3. Lags of one, three, five and seven days were tested. At the end of each season, the time lags resulted in the introduction of new values which originally belonged to another season. However, since human introduced seasonal boundaries are no strict natural boundaries for abrupt changes in weather patterns, this was not seen as an issue. Shifts at the end of the data series resulted in seven NaN values which were omitted from the calculation of the final autocorrelation coefficient.

4

The results and model discussion

In this chapter, the results of the research are presented and discussed. Each sub-chapter deals with another research question which is connected to a distinct research approach as defined in chapter 3. The first sub-chapter presents a summary of the literature review which had as main goal to define the different precipitation patterns in Europe, their influencing factors and to give a more detailed description about the precipitation regime in the Rhine basin. The second sub-chapter deals with the results of research model 1 to answer the question whether spatial permutation did influence extreme rainfall statistics and how basin size and aggregation time influenced the results. The third sub-chapter discusses the results of research model 2 which was used to determine whether a vector-based approach could be used to shift precipitation and which variables and steps were most determining for the final results. The final sub-chapter of this chapter presents the results of model 3. The results were used to answer the sub-questions of research question four which were centered around the question if historical wind data could be used to spatially shift precipitation without violating the main characteristics observed in the historical precipitation series.

4.1. Literature review of European precipitation regimes

4.1.1. Characteristics of a precipitation regime

A precipitation regime is defined as the assembly of 'characteristics of the seasonal distribution of precipitation at a particular place' [26]. The characteristics of a regime can be roughly subdivided in two main groups: precipitation variability and precipitation amounts, like annual or seasonal means and maxima.

Precipitation variability

Precipitation variability can be split in temporal and spatial variability. Temporal variability refers to the variability in time at a specific location and can be analysed at different resolutions. At a low temporal resolution, precipitation variability is often analysed on a seasonal scale. For example, in the famous Koppen-Geiger climate classification, the presence or absence of dry and wet summers or winters is used as one of the three major classification parameters to define the climatology of a region [27]. However, temporal variability can also be analysed at a high resolution if the goal is to define very local precipitation regimes. Lana *et.al.* [28] used daily rainfall data to analyse the time variability of intense rainfall in Catalonia to determine strategies to effectively target soil erosion and water resources problems. They concluded that temporal variability, as defined by the monthly standard deviation and average rainfall rates, differed between 6 and 24 [mm/day] over the 75 measuring locations resulting in a very irregular regime over Catalonia.

On the other hand, spatial variability refers to the variability in space at a given moment in time and can be analysed at scales varying from local to regional and even global. Spatial variability is often examined by clustering of areas based on certain variables of interest, like daily and monthly total precipitation and geographic and atmospheric patterns [28]. Spatial variability can be different depending on the variable and location under study. Emmanual *et.al.* [29] showed that the decorrelation distance of precipitation varied depending on the type of precipitation. Storms were characterized by a dual structure of small intense clusters with low spatial correlation located within areas with a higher spatial correlation. Light rain periods on the other hand showed very high spatial correlation values, which reduced when showers became more intense.

Precipitation amounts

The most common precipitation amounts which are used to classify a precipitation regimes are the maximum and mean precipitation averaged over a long historical time series. Values can be calculated at different temporal and spatial resolutions. Time scales vary between hourly to annual values while spatial scales range from point locations to continental regions. Changes in precipitation amounts can be used to detect cycles in precipitation patterns or to study the effect of climate change [30]. In addition, the amounts are often used as input to calculate the temporal and spatial variability. In the Koppen-Geiger system seasonal mean precipitation is used as input to determine presence or absence of rainfall periods [27]. Monthly mean rainfall was used to define the distinct spatial and temporal rainfall regimes in Catalonia [28], while maximum hourly precipitation was used to define diurnal cycles in the UK [31].

4.1.2. Main factors influencing precipitation regimes

The variability and precipitation amounts which define a certain precipitation pattern are determined by several environmental factors. These factors differ per location and the interplay between them determines the physical boundaries of the precipitation pattern present. While multiple environmental factors and their complex relationships have been shown to influence meso-scale precipitation patterns, three major components can be distinguished which are discussed in the below subsections.

The subsections are divided as follows. In the first subsection, atmospheric circulation patterns with a focus on the North Atlantic Oscillation (NAO) are presented. The second subsection describes the influence of topography on rainfall. The effect of orography is central in this subsection. The final subsection deals with the effects of climate change and spatial dependency associated with it.

Atmospheric circulation patterns

The movement of precipitation fields is largely determined by major atmospheric circulation patterns. An atmospheric circulation pattern can be defined as a large and consistent movement of air driven by thermal energy and its associated pressure differences. For the North Atlantic-European (NAE) sector, to which the area of Rhine basin belongs, the North Atlantic Oscillation (NAO) is the most important circulation pattern. This oscillation is driven by the difference between two distinct pressure regions. The first region is the 'sub-polar low' which is located at the high latitudes near Greenland and Iceland and is characterized by a lower air pressure compared to its surroundings. The second region is located in the central North Atlantic Ocean. This region is characterized by a high pressure field and is therefore referred to as the 'subtropical high' [32].

The strength of the NAO is not constant in time and can be indicated by the NAO index. A positive NAO index means that both the sub-polar low and the subtropical high are stronger than normal. A stronger Atlantic jet stream occurs, shifting the average storm track more northward. Consequently, the storminess, amount of precipitation and temperature increases in the North of Europe. This correlates with less precipitation and colder temperatures over the Mediterranean area. A negative NAO index displays a reversed pattern, with warm, wet and stormy conditions across the Mediterranean and cold and dry weather patterns over the Scandinavian regions [32].

The NAO index is also correlated with wind speed. Positive NAO indices create strong westerlies over the north of Europe with an average wind speed of 5 [m/s]. Over the Iberian Peninsula, wind speeds drop till average values of approximately 2 [m/s]. Negative NAO indices indicate an opposite wind pattern with lower wind speeds in the North of Europe and higher wind speeds over the Mediterranean area [33]. As such, the NAO can be considered as an important binding and steering factor between climate variables like wind speed and direction, heat and moisture transport, and the frequency and strength of storms [19].

However, besides the NAO, other atmospheric circulations do influence the occurrence or absence of precipitation. Wibig *et.al* [34] discussed the contribution of the Scandinavian (Sc), East Atlantic (EA), East European (EE) and Central European (CE) pattern to the observed precipitation amounts during winter between 1951-1990 in Europe. He concluded that the variance in the amount of rainfall was mainly explained by the NAO (>23%), but that also the Scandinavian and Central European pattern explained over 17 and 15% of the total variance, respectively.

Important to note is that the influence of each pattern depends on the region of interest. Great Britain and Ireland, Scandinavia, Western Europe, Central and East Europe, the Iberian Peninsula and the Mediterranean were all shown to exhibit different dependencies on the most prevailing circulation patterns [34]. These dependencies are also shown in the different mean annual rainfall amounts in Europe. Great Britain and Ireland, The Alps, the Scandinavian mountains and Western Europe contain regions with the largest annual amounts up to 1,500 [mm/year]. Regions with the smallest amounts are observed in Eastern Europe and the east side of the Iberian Peninsula with values between 250 - 500 [mm/year] [35].

In addition, Alvarez *et.al* [35] showed that the Pearson correlation coefficient can be used to cluster areas in Europe exhibiting a comparable rain series dynamics. By calculating the correlation coefficient for different spatial scales, a threshold was chosen which marked a clear change in correlation between regions. At a value slightly higher than 0.2, ten distinct regions were identified. Most of these regions were also shown to be influenced by a common atmospheric circulation pattern, whereas differences in the prevailing atmospheric pattern were the main drivers for the distinct rainfall anomalies observed.

Topography

It is well known that the presence of distinct topographic elements has a large influence on precipitation [36]. Especially, mountain ranges are known to affect wind patterns since they alter air flows and respond differently to solar radiation compared to their lower lying surroundings. By forcing air to rise or fall they promote either condensation or evaporation creating distinct areas with higher or lower amounts of precipitation with regard to neighbouring regions. The shape, extent and orientation of the mountain range defines the final precipitation pattern, which is often very local [37].

This local dependency originates from the balanced interplay between microphysics, (thermo) dynamics and the geometry of the terrain. Together they determine the growth and fallout of precipitation. By studying this interplay in more detail, Houze *et.al.* [36] defined twelve different types of mechanisms behind precipitation patterns which were induced by topography (see figure 4.1). These types are not mutually exclusive but can be observed simultaneously in a mountain area or can alter based on seasonality. For example, Anders *et.al* [37] showed that in the Alps both rain shadow (figure 4.1 (a)) and blocking (figure 4.1 (i)) are the dominant types behind the observed precipitation pattern. At the Scottish highlands, rain shadow is considered to be the leading mechanisms behind the precipitation differences observed [38]. However, the relation between a rainfall pattern and the mechanisms behind it is often non-linear and locally dependent. This makes the comparison of mountainous regions among each other and the definition of general precipitation responses difficult [36].

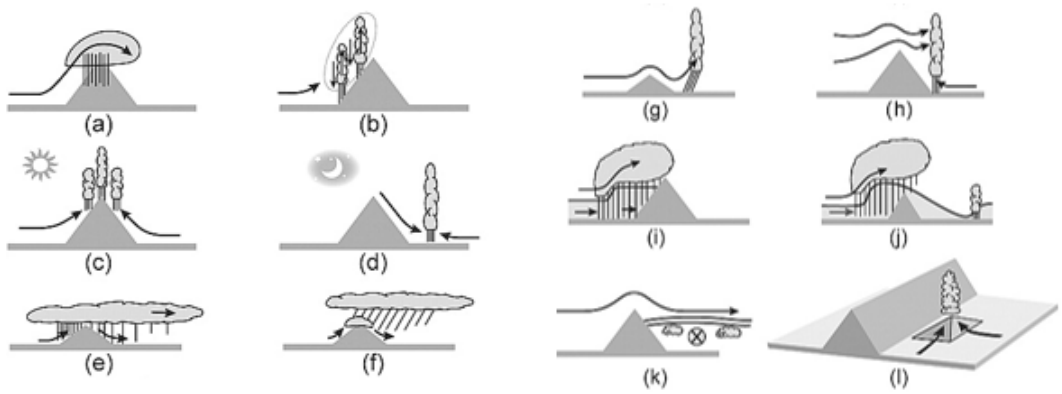

Figure 4.1: Main mechanisms by which mountains influence precipitation (Fig. 3 in Houze (2012)).

Comparing the spatial patterns in mountainous regions with plains can be done more easily. For example, Touma *et.al* [39] showed that the length scales over which precipitation events correlate in mountainous areas are relatively constant between summer and winter. This reflects the dominant influence of the non-seasonal topographic structure on the occurrence of rainfall. The correlation distances were found to be short varying from 150 to 200 [km]. In contrast, at plains a clear distinction between correlation lengths is seen over the seasons. The largest distances occur over winter up to 350 [km] and the smallest lengths in summer, i.e. 200 [km]. This seasonal difference is most likely caused by the characteristic storm type of each season. During summer, small scale extreme convective storms are more common, while winter rainfall is characterised by long-duration, large scale stratiform fronts [40].

The differences in spatial relevant scales for precipitation patterns between mountainous and flat areas makes it necessary to consider them carefully when defining distinct analysis regions. In Europe, the main mountain regions were precipitation is distinct at small scale caused by the mechanisms shown in figure 4.1 are the Alps, the mountain chain consisting of the Pyrenees and the Cantabrian mountains and the Scandinavian mountain range. Increasing the resolution in these areas show clear wind and lee-side differences, up to 250 [mm/year] for some locations [38]. As such, spatial shifting at these locations should take place over smaller distances to prevent violation of the clear physical limits which define the distinct precipitation patterns at locations which are in relative proximity of each other.

A second clear topographic element which creates distinct local precipitation patterns are coastlines. Due to the presence of the ocean-land boundary, precipitation is enhanced in the first 150 [km] of the land surface. Especially during the winter period, the first 50 [km] of land surface is likely to receive more rain compared to the hinterland. This difference is less pronounced in summer. On average, the amount of rainfall reduces with 14% in the first 100 [km] from the coast, with another 8% between 100 and 150 [km] [41].

Not only the presence of large water bodies, but also the type of land cover does influence the spatial pattern of precipitation. The type of land cover determines the radiation and aerodynamic characteristics of the land surface, which influences the local water cycle. Trusilova *et.al.* [42] modelled the influence of increased urbanisation with a 30-[km] resolution and concluded that rural areas downwind of large cities receive less precipitation, but that small urban patches increase downwind precipitation. Overall difference were higher in summer but did depend on the location of the area in either East, Central or West Europe. Absolute difference were all found to be <1 [mm/day] which leads to the conclusion that the influence of urban areas are relevant for modelling microclimates but are less essential for mesoscale extremes.

A similar conclusion was drawn for the effect of de- and afforestation in Europe with regard to extreme precipitation. Deforestation leads to a reduction of precipitation events in the 95th and 99th percentile. Less vegetation leads to a decrease in evaporation causing a dryer climate. Afforestation creates the opposite effect. Changes are most visible at a local level (±50 [km]) and reduce when the spatial scale coarsens. In addition, deforestation was shown to take place mainly in eastern and northern Europe, while afforestation was concentrated in central Europe. When this trend continues, more extreme events can therefore be expected in the central part of Europe based on this parameter [43].

Climate change

Changing temperatures as result of climate change are undoubtedly related to changes in precipitation. The physics behind this relation is captured in the Clausius–Clapeyron equation, which expresses the change in saturation vapor pressure when temperature increases or decreases. Though, general global warming does not mean that changes in precipitation are similar everywhere. In Europe, increasing temperatures and shifting circulation patterns result in a predominantly increasing trend in annual precipitation in northern Europe, while a decrease is observed in the southern part. The changes are most pronounced during summer with increases of +20 [mm/decade] in Scandinavia and reductions of -10 [mm/decade] in the Mediterranean and the Iberian Peninsula [44].

When looking at a more regional scale, a more patchy pattern can be seen with regard to the occurrence of extreme events. In winter, mean and extreme precipitation is estimated to increase with a spatial pattern reflecting the orography of Europe. Increases on the north-west side of the main mountain ranges are relative small compared to the rest of the mountain range. Nevertheless, due to the high amount of rainfall in these areas, the absolute changes are large [45].

Aalbers *et.al.* [45] also concluded that the response to climate change for mean and extreme precipitation in summer was not similar. For the mean precipitation, they found the same drying gradient from North to South as the European Environmental Agency (EEA) did in her research [44] with exceptions in the high elevation areas like the Scottish highlands, Scandinavian mountains and the Alps. In these areas, increased mean precipitation is observed despite drying in the surrounding areas. Extreme precipitation was shown to increase over the whole domain especially for storms with a return period >20 years. The pattern of increase was very patchy and did not resembled the orography. The probability density functions confirmed this observation by showing a clear shift to higher values and broadening of the distribution for longer return periods. This indicates that an increase in spatial variability is likely to be observed for extreme precipitation events.

The influence of orography on the response of precipitation to climate change was also researched by Moreno *et.al.* [46]. They showed that the strongest decrease in total precipitation is observed in the Pyrenees in areas with an altitude between 500 and 800 [m.a.s.l]. Overall, precipitation decreased on the Southern side of the Pyrenees while an increase was seen at the Northern side. Locations closer to either the Atlantic or Mediterranean sea showed an increase in precipitation amount compared to a decrease more in the middle of the mountain range. Seasonality was also shown to be important with overall drying in the summer and a spatial variable increase or decrease in winter months.

Seasonality is a parameter which appears to be vary important with regards to climate change. Papers generally agree on the changes in precipitation over the winter season, with drying in the Southern part of Europe and wetting in the northern part [44] [46] [47]. Predictions about summer precipitation are more complex and highly depending on the initial situation, region and forcing method [47]. In general, a clear division is found between Scandinavia, Central Europe, Western Europe and the Mediterranean area. Each area was shown to have different mean precipitation values, changes in return periods, daily precipitation values and dry and wet spell duration making local research, testing and analysis of observations and (modelling) results indispensable.

4.1.3. Major precipitation regimes in Europe

Precipitation regimes depend on the location. Their variability and characteristic average, minimum and maximum amounts are determined by factors like atmospheric circulation patterns, topography and climate change. These factors and their interaction vary depending on the area of interest. Knowing these factors and the characteristics of an area can be valuable for modelling since it gives a first indication of the importance of several variables in the area. Therefore, a clustering based on the information retrieved from the literature review presented was done in order to determine the main precipitation regimes above Europe.

Below, the results of the clustering are presented. In total seven distinct precipitation regions were defined based on their climatic, topographic and atmospheric characteristics. Subsection two focuses on the two major precipitation patterns covering the Rhine basin. For both patterns, their main characteristics are discussed. Values in this section are derived from the ERA5 wind and precipitation data which is described in subsections 3.2.2 and 3.4.2.

The seven clustered precipitation regions in Europe

The factors defining a precipitation regime are non linear phenomena with no strict boundaries. As such, Europe can be divided in different combinations of precipitation regions depending on the importance given to the several influencing factors and the final goal of the clustering. For this research, it was chosen to cluster regions based on the characteristics and influencing factors presented in the sections above. In this way, the knowledge of each region can be used in a later modelling stage to validate the effects of spatial shifting by examining whether or not the model violates the precipitation characteristics and factors as defined for the region.

The Koppen-Geiger climate classification was used as starting point for the clustering since the level two precipitation category is based on the main characteristics of precipitation as defined in subsection 4.1.1. When neglecting the third category based on temperature, four different climate zones were distinguished:

1. The area covering Scandinavia and Eastern Europe with a cold, no dry season climate.
2. The area covering Great-Britain and Western Europe with a temperate, no dry season climate
3. The area covering the Mediterranean area excluding the Iberian Peninsula, having a temperate, dry summer climate.
4. The Iberian Peninsula having a mix of climates between arid and temperate with and without dry seasons.

Precipitation regimes in each region can be assumed approximately similar with regard to their major characteristics like seasonality and mode of precipitation, e.g. rain or snow, short and intense or long and moderate [27].

An extra level of detail was added to the division based on the Koppen-Geiger classification by considering the most important atmospheric circulation patterns. As shown by Wibig *et.al.* [34], Alvarez *et.al.* [35] and Lindsey *et.al.* [32], the impact of the NAO and other circulation patterns differs over Europe. In general, a strong north-south gradient is observed for the NAO while other atmospheric patterns act more locally. As such, Great-Britain and Ireland can be assumed as a separate area relying more on the NAO circulation compared to the rest of Western Europe which is highly influenced by the East-Atlantic and East-European circulations. A similar reasoning was made to split Scandinavia from Eastern Europe. Whereas Scandinavia relies most heavily on the NAO and the Scandinavian circulation, Eastern Europe depends mainly on the Scandinavian and Central-Europe circulation patterns [34].

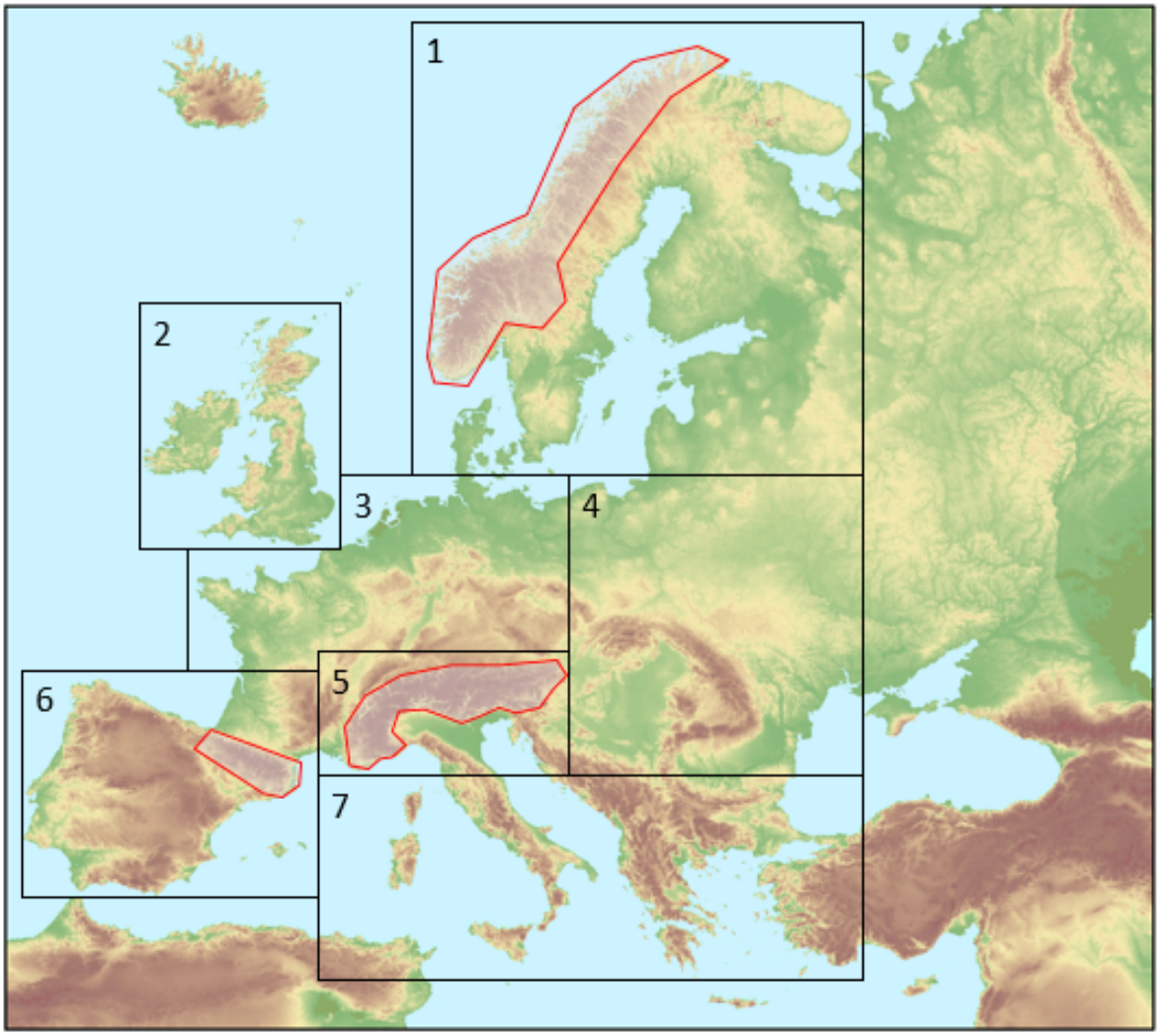

Figure 4.2: The 7 analysis regions which will be used in this study. 1) Scandinavia, 2) Great-Britain, 3) Western Europe, 4) Central Europe, 5) The Alps, 6) Iberian Peninsula, 7) Mediterranean. Shaded, red-contoured areas indicate main mountainous areas in which precipitation does differ compared to the surroundings. Elevation map retrieved from [48]

On top, also topography, most dominantly the orography of a region, was indicated to be an important factor especially for regional precipitation patterns. In figure 4.2 the main mountain areas, which were shown to exhibiting distinct characteristics, are indicated by their red contours. However, with regard to the purpose of the use of spatial perturbation for flood risk impact models, it was chosen to only separate The Alps as distinct area from its surroundings. The Alps are centered in an area with high economic value and lay at the origins of many important river basins in Western Europe. On the contrary, the economic value of the areas influenced by the Scandinavia mountains is relatively low, with some exceptions in the most southern part of Norway. For the Pyrenees, its influence on the precipitation dynamics at the larger Iberian Peninsula is deemed to be low compared to the several climatic regions in which the peninsula can be subdivided. On top, as result of its location at the boundary of the analysis region it is expected that a larger uncertainty of the spatial dynamics in this region will not hamper the spatial permutation in the more economically important regions at the coastlines of Spain and Portugal.

Last, a bird's eye view was given concerning the impact of climate change. Most papers seemed to confirm a clear north-south gradient with regard to the annual amount of precipitation. In addition, it was mentioned that mountainous areas often react distinct to climate change compared to their surroundings. Regional differences in precipitation were shown to be largely dependent on the orientation and location of the area in the mountain range. In addition, also seasonality was proven to control a regions response to climate change. However, all these factors are for their largest part captured in the characteristics of climatic zones, atmospheric circulation patterns and topography. As a result, climate change itself is not seen as a parameter which creates the need to define additional areas on top of the seven final regions which are shown in figure 4.2.

Precipitation regions in the Rhine basin

Figure 4.2 shows that the Rhine basin is covered by the Western Europe and the Alps precipitation regions. The distinguishing factor between the two regions is the orography with high and steep mountains in the Alpine region, while the rest of Western Europe is characterized by relative flat to hilly terrain.

The effects of the Alps were seen in all of the characteristics of the precipitation regions which were defined over the Rhine basin. Figure 4.3 shows the mean monthly precipitation values. Highest mean precipitation values were seen in the Alps during the summer months. Warm moist air is lifted by the mechanisms shown in figure 4.1 and cooling at higher altitudes results in cloud formation and subsequent precipitation. Maximum mean values were found to be around 14 [mm/day], while minima in the Northern part of the basin were around 1 [mm/day]. Patterns of maximum monthly precipitation and standard deviation show similar differences between the Alps and the surrounding area, though maxima are found at the edges of the Alpine region instead of at the center. Figures can be seen in appendix III, figures III.1 and III.2.

Wind speed and direction was also different when comparing the two regions. Mean wind speeds were as low as 1 [m/s] in the Alps for all seasons, while at the Northern part of the Rhine basin mean wind speeds increased up to 14 [m/s] during winter (see figure 4.4). The most common wind direction observed was South-West, which is in agreement with the prevalence of Westerlies in Western-Europe as result of the NAO. Varying directions at the grid cell spatial resolution were observed around the Alps (see appendix III, figure III.5). Minimum wind speeds were observed in the center of the Alpine region while maximum speeds up to 40 [m/s] were seen in the most North-Western part of the Rhine basin. Figures can be seen in appendix III, figures III.4 and III.3, respectively.

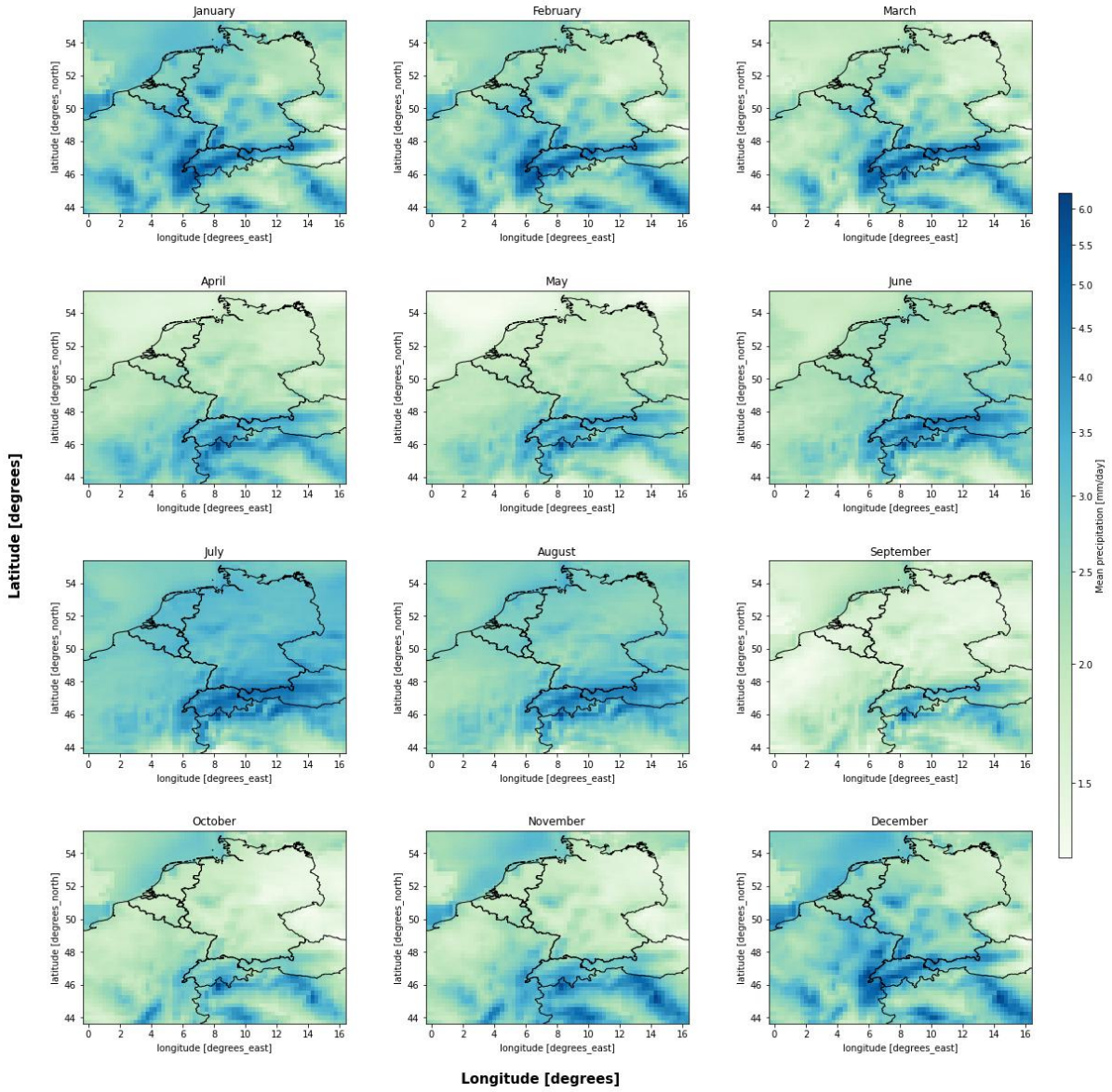

Figure 4.3: Mean historical daily precipitation values [mm/day] observed over the Rhine basin. Data is retrieved from the ERA5 reanalysis data set from 1980-2021. Values shown are average values over each month.

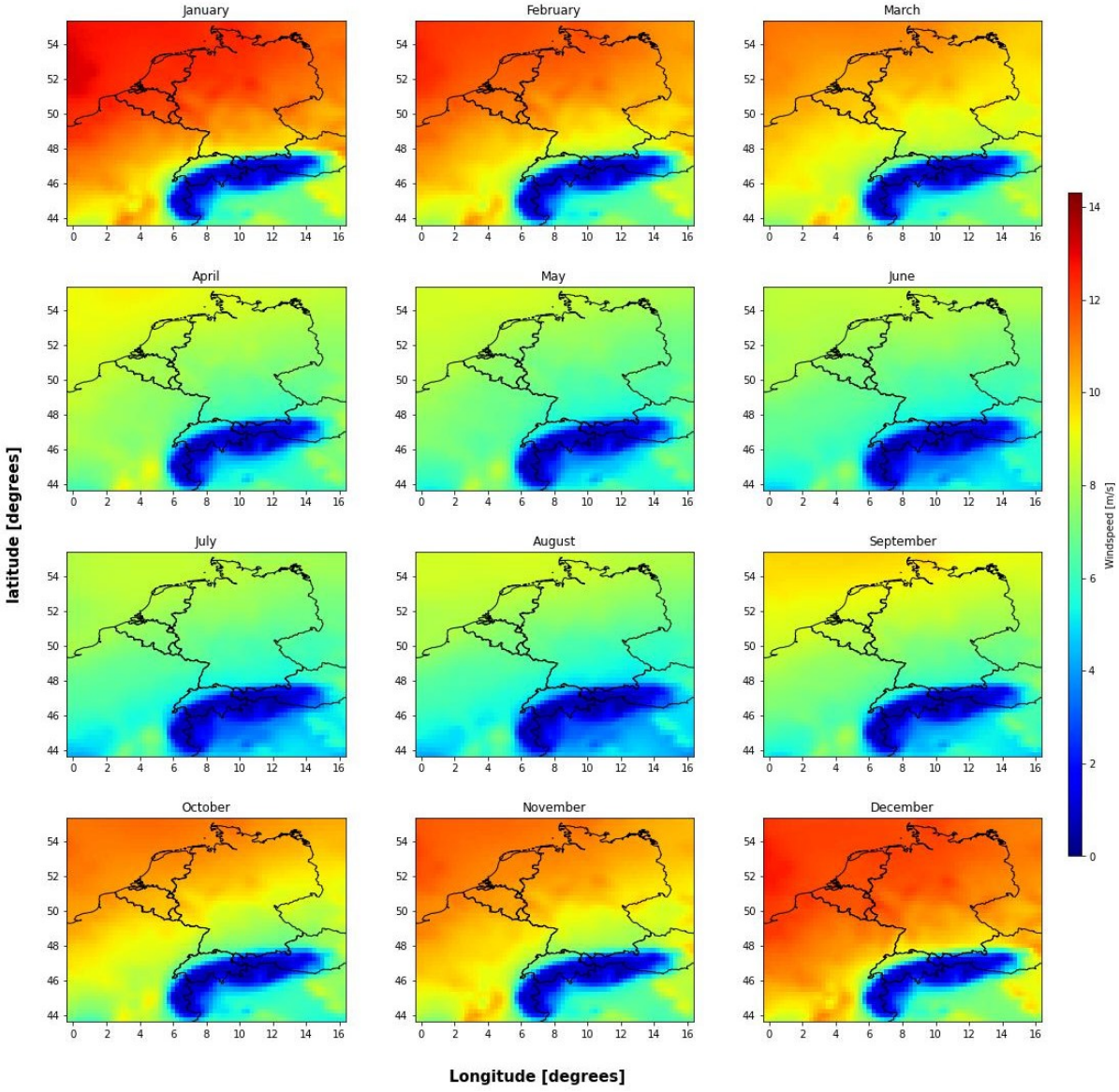

Figure 4.4: Mean historical daily wind speed values [m/s] observed over the Rhine basin. Data is retrieved from the ERA5 reanalysis data set from 1980-2021. Values shown are average values over each month.

Summary literature review

- Rainfall regimes are characterized by their temporal and spatial variability and their characteristic amounts, like mean and maximum precipitation.
- Rainfall regimes are influenced by many environmental and physical factors. The most important are:
  - Atmospheric circulation patterns.
  - Orography and land surface.
  - Climate change
- Seven different rainfall regimes were defined above Europe based on grouping of rainfall characteristics and influencing factors.
- The Rhine basin is covered by two distinct rainfall regimes: The Alpine regime and the Western Europe regime.

4.2. Results and discussion: fixed spatial permutation

The objective of research model 1 was to research if spatial permutation influences extreme precipitation values and how the results depend on catchment size, permutation direction and permutation distance. To answer these questions, the extreme value distribution and the cumulative distribution function (cdf) of the generated data was compared with the historical distributions. In addition, the effect of the model on the observed precipitation during the last day of the July 2021 flood was visualised.

In the following subsections, the results of research model 1 are presented and discussed. The first section focuses on the extreme value distribution. Differences are quantified with the Anderson-Darling (AD) test statistics (see subsection 3.2.3). In the second subsection the cumulative distribution function (cdf) is examined by means of the AD-test and the Pearson correlation coefficient. On top, the coefficient is used to test the relation between shifting distances and the difference between historical and shifted precipitation extremes. The final subsection visualizes the working method of the model by showing its effect on the precipitation event of July 15th, 2021.

4.2.1. Extreme value distribution

The mean observed daily precipitation for the Rhine, Moselle and Ijssel basins were tested against five different statistical distributions by means of the Anderson-Darling (AD) test. The results showed that the observed data was most likely distributed according to a Generalized Extreme Value (GEV) distribution, with an average AD-test statistic of -1.11. The Gumbel distribution was shown to be the second best fit with an AD-test statistic of -0.86.

Fitting the GEV distribution to the observed and one, two and three pixels shifted data revealed some general trends. First, the GEV fit to the shifted data resulted in higher AD-statistics in all cases independent of the basin and aggregation time under consideration (see figure 4.5). It indicated that the GEV fit to the shifted data is worse compared to the historical data. This can be explained by the fact that the Generalized Extreme Value (GEV) distribution is based on the assumption that the underlying data is independent and identically distributed (IID). For historical precipitation maxima, this assumption is met. Therefore, the GEV statistics is the most widespread used distribution for the analysis of extreme rainfall events and the calculation of return periods exceeding the length of the observed data records [49]. However, the assumption of independence was not met for the shifted data since the introduction of a new extreme event was highly correlated with the presence of an extreme in the historical data series. This dependency was most severe for large basins and short shifting distances since under these circumstances the influence of shifting is minimal compared to the historical observations. This led to a repetition of historical extreme events in the modelled data series. As such, independence cannot be guaranteed shown by the higher Anderson-Darling (AD) test statistics for all shifted data sets.

Higher AD-values were also seen when extreme outliers were present in the historical data. By shifting the precipitation fields 360°around, these outliers were replicated in a slightly different way. While the introduction of these new extremes was the ultimate goal of the model, these outliers could not be well captured by the parameters of the GEV distribution. The higher sensitivity of the AD-test to the tails of the distribution caused the statistics to increase quickly [50]. This was most obviously seen for the smaller Ijssel basin in which an extreme historical event was replicated eight times (see figure 4.7b). On top, the the introduction of pixels with new extremes resulted quickly in new high mean values because the relative contribution of each pixel to the basin's mean precipitation was large.

(a) The Rhine basin

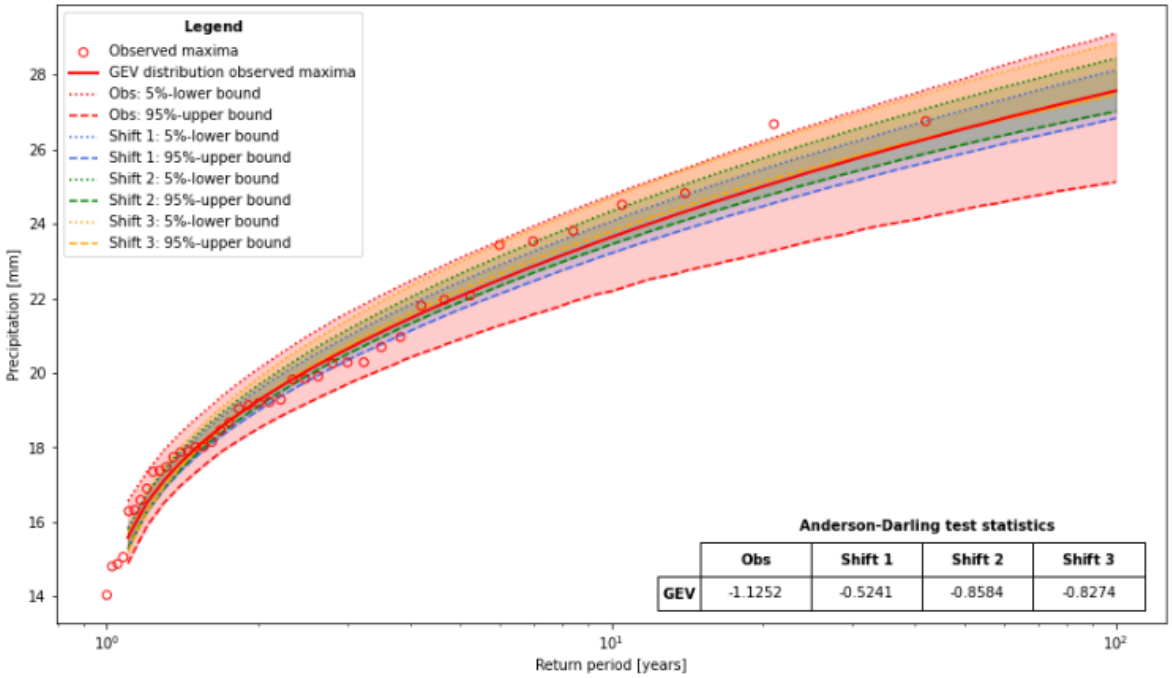

(b) The Ijssel basin

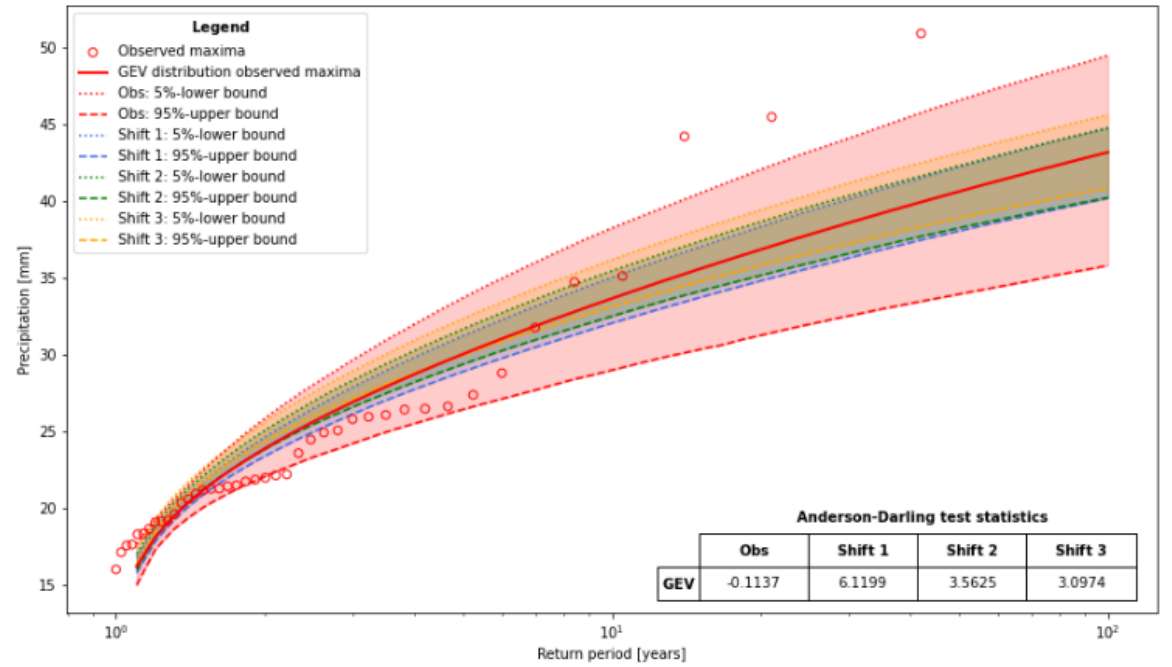

Figure 4.5: The Generalised Extreme Value (GEV) distribution for annual daily precipitation maxima of the Rhine (top) and Ijssel (bottom) basin. Shaded areas show the 95% confidence intervals. The red dots represent the observed maxima. Shifted maxima are not shown. The table shows the Anderson-Darling (AD) test statistics between the historical and shifted precipitation data for different shifting distances, i.e. Shift 1 = 1 pixel, Shift 2 = 2 pixels and Shift 3 = 3 pixels.

The second observation made was that the uncertainty interval of the GEV distribution of the shifted data reduced with a factor three compared to the observed data (see figure 4.5). The cause for this observation could be found in the increased sample size from 42 years of historical data to 378 years of shifted data, which resulted in more information about the underlying data [51]. On top, the dependency between the historical and shifted data caused the change in standard deviation of the shifted data set to be minimal compared to the historical variability. As such, the calculated 5- and 95-percentile intervals reduced.

Moreover, it was shown that the shifted data felt within the uncertainty boundaries of the historical data for each shifting distance. This indicated that the introduced events could have happen in the region of interest by chance as well. Thereby, it proved that shifts of up to three pixels did not cause the unwanted introduction of rainfall events from other climate regimes which was in agreement with the extent of the Koppen-Geiger climate regions identified in Europe [27]. Nevertheless, the uncertainty intervals could not be used to determine whether the introduction of new extremes at a higher spatial resolution, i.e. grid cells, did violate any physical limits. This could be especially the case in mountainous areas in which spatial variability is large [36]. Therefore, a more spatially differentiating permutation approach will be needed to take this local limits into account and having a more realistic permutation mechanism over varying locations.

Next, it was seen that the relative position of the uncertainty intervals of the shifted data compared to the bounds of the observed data differed, but the direction was not consistent for either basins or aggregation time. The overlap between the uncertainty bounds for larger basins was more coherent, whereas for the IJssel basins the bounds did vary most. Moreover, an increase in absolute value of the uncertainty intervals was seen when basin size decreased (see figure 4.5).

This overall dependency of the results to the basin size and aggregation time observed for the uncertainty intervals was also seen in the values of the AD-test statistics. AD-test statistics for all shifted data was higher compared to the historical data but the mutual values of the shifted data varied. For the Rhine basin, the shifted data was still well fitted with a GEV distribution. The maximum AD-test statistic observed was 0.42. For the Moselle basin, AD-test statistics increased since the shifted data introduced new extremes in the data set. These extremes did act as outliers in the data set and as result, the AD value for the GEV fit increased. The same observation was made for the Ijssel basin, in which even more extreme events were introduced by shifting the data. The maximum AD-test statistic was found to be 6.12. However, removing the six most extreme events from the shifted data set resulted in a decrease of the AD-test statistic to 4.91,

Last, increasing the rainfall aggregation time from one day to one week caused a reduction in the AD-test statistics for all basins. For longer time spans, i.e. weekly, variability in the historical data set was shown to be less and also the newly introduced extremes deviated less compared to the historical observed values shown by the lower AD-test statistics. This difference in variability was also observed by Zhang *et.al* [52] who showed that the already existing difference of variability between time scales will be amplified by the effects of climate change. Short duration extremes will likely become more extreme and more local [44]. This change in frequency is valuable for the modelling of rainfall return periods in a certain area. Spatial permutation could therefore be used as tool to introduce these short and very local events in the time series of a location which historical data did not contain these extremes yet.

4.2.2. Cumulative distribution function

The cumulative distribution function (cdf) of the precipitation extremes was analysed with two tests. First, the Anderson-Darling (AD) test was used to test the similarity between the historical and shifted data. Next, the Pearson correlation coefficient was used to determine the extent to which historical and shifted maxima were related.

The AD-test statistics showed that the similarity between the observed and shifted data related to basin size. Smaller basins had higher absolute differences in AD-test statistics for each aggregation time compared to larger basins such as the Rhine basin. In addition, smaller basins showed higher AD-test statistics for increasing shifting distances which indicated a decrease in similarity to the observed data when shifting distance increased. The cause for this observation is the relative sensitivity of small basins to permutations. Even permutations over short distances will introduce relatively many new precipitation values in a small basin compared to a larger basin in which only a minority of the area is exposed to new precipitation values. As such, the mean precipitation over a small basin will change more compared to a larger basin, resulting in bigger differences in AD-test statistics.

This reasoning was confirmed by the finding that the AD-test statistics of the larger Rhine basin showed an irregular trend over shifting distance and aggregation time with varying AD-test statistics. However, the absolute differences between the AD-test statistics for each aggregation time were smaller compared to the Moselle and Ijssel basins. For all basins, the direction of change of the AD values was similar for all shifting distances when considering one aggregation time, but no trend in AD-test statistics was visible over time (see figure 4.6).

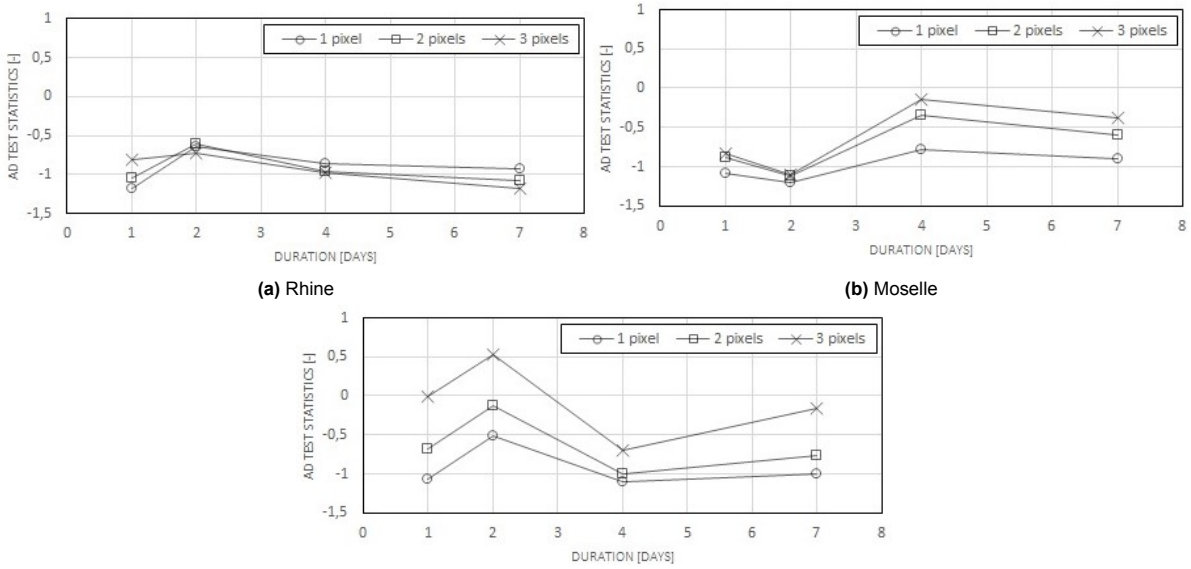

(a) Rhine **(b)** Moselle

(c) IJssel

Figure 4.6: The Anderson-Darling (AD) test statistics to compare the historical and shifted cumulative distribution functions (cdfs) of the annual precipitation maxima for different basins, aggregation times and permutation distances. The lower the AD-test statistics, the more similar the cdfs were. One pixel is similar to a shift of ±27.75 [km] or 0.25 [degrees lat/lon].

The Pearson correlation coefficients varied between 0.92 and 0.99, indicating a clear dependency between the observed and shifted maxima for all basins. The differences between Pearson correlation coefficients for one aggregation time became smaller when the aggregation time increased. Though, the largest correlation coefficients did not always coincide with the longest duration. The smallest correlation coefficients were seen for the two days aggregation time in all basins. On top, the lowest absolute values of the correlation coefficients were seen for the smallest basins, which agreed with the earlier observation that even small permutation distances introduce relatively many new precipitation values into a small basin. As such, the differences between the historical and shifted precipitation values will become more evident even for small permutation distances. This is reflected in the faster decrease of the correlation coefficient observed for small basins.

Between the permutation distances and the correlation values the opposite relation was seen. When shifting distance increased, the correlation values decreased. The decrease was largest for the Ijssel basin, with a correlation value of 0.987 for one pixel shifted daily data and a value of 0.61 for 10 pixels shifted daily data. For the Rhine basin, the same shifts on daily data resulted in correlation values of 0.997 and 0.80, for one and 10 pixels shifts, respectively.

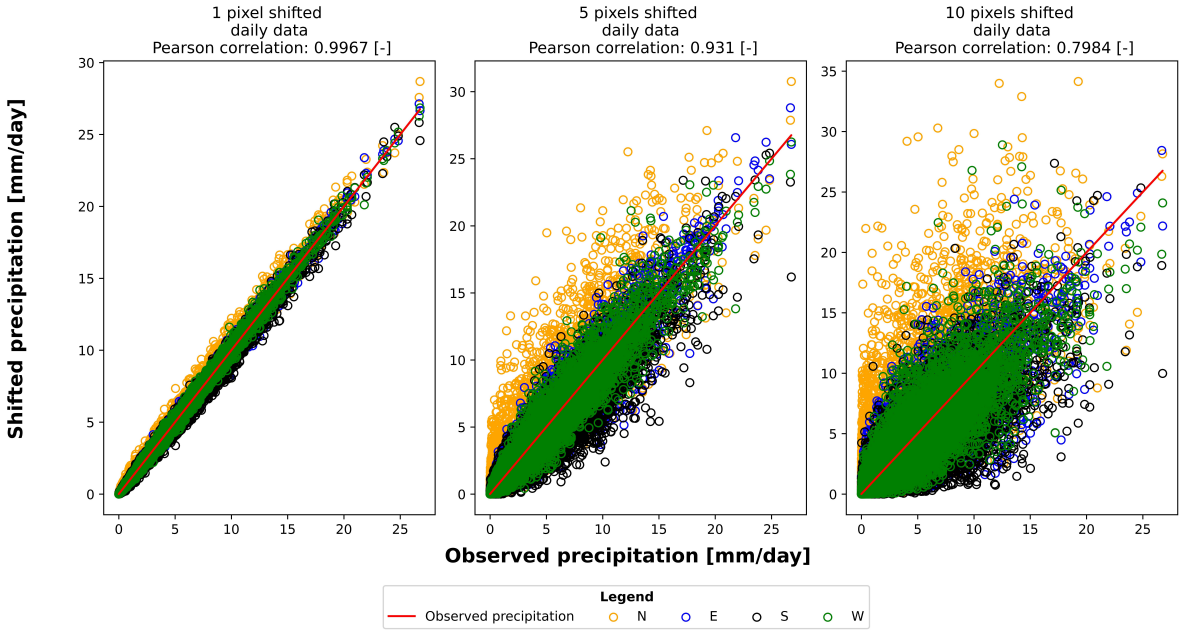

(a) The Rhine basin

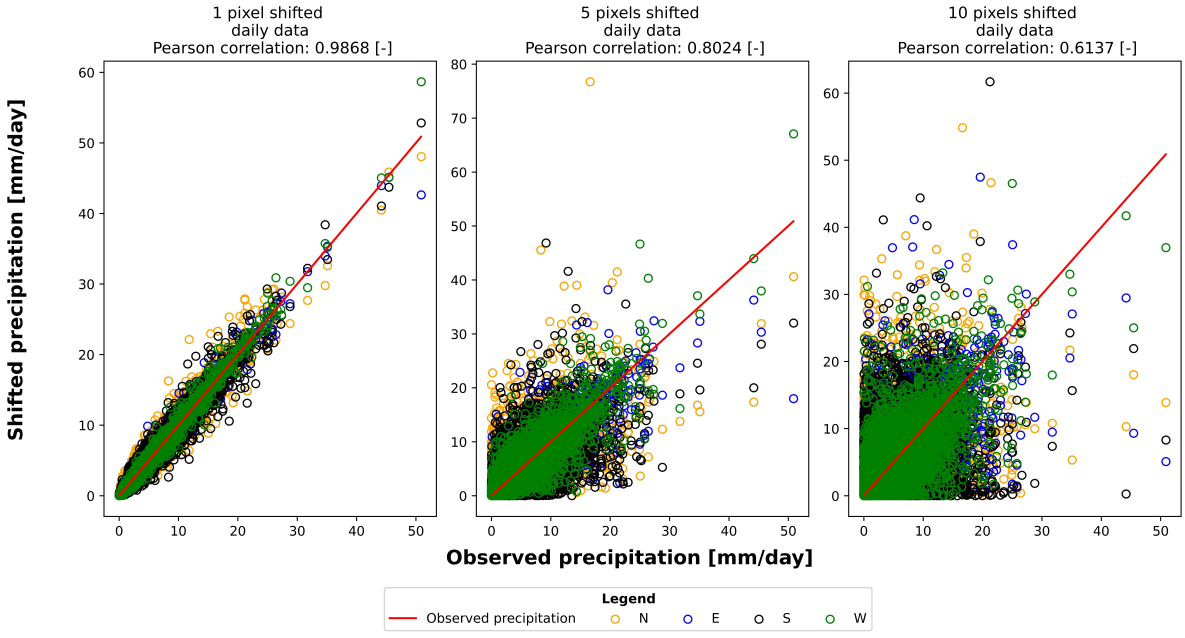

(b) The Ijssel basin

Figure 4.7: The influence of permutation distance and direction on the correlation coefficient between the observed total daily precipitation and shifted total daily precipitation of the Rhine basin (top) and Ijssel basin (bottom). Only the main wind-rose translation directions are shown.

With regard to the permutation direction, a strong relation with the correlation coefficient was seen for the Rhine basin. More extreme events were introduced with a northward shift while less extreme events were seen when the shifting direction was opposite (see figure 4.7a). The same trend was present in the Moselle basin. A possible explanation could be found in the orography of the two basin. Basist *et.al.* [53] showed that mountainous areas were strongly related to more extreme precipitation events. As such, northward permutations could introduce extreme events from The Alps and its foothills into the shifted data series whereas southward shifts did not. On the other hand, the Ijssel basin, characterised by a uniform orography, did not show a clear north-south trend. This resulted in a more random introduction of extremes and less influence of permutation directions on the final result. However, permutation distance became more important for the results of the Ijssel basin. The most extreme event in the historical data (50.90 [mm/day]) was re-sampled in all directions for a one pixel shift but the event disappeared when the permutation distance increased till five or 10 pixels. At these distances, other extremes were introduced which were not observed in the historical data (see figure 4.7b).

4.2.3. Influence on the July 2021 flood

To visualise the working mechanism of research model 1 and its effect on extreme precipitation events, the most extreme precipitation event in the Moselle catchment had been selected as example. This event took place on July 15th, 2021, which was the last day of the low pressure area called 'Bernt'. Bernt caused major flooding in parts of Germany, Belgium and The Netherlands and was the direct cause for the questions raised about the spatial component of extreme rainfall.

The results of figure 4.8 proofed that spatial permutation had a large effect on the observed mean precipitation value over a catchment. Both shifting distances and directions influenced the final mean value observed. For this specific event, southward shifting resulted in a larger part of the precipitation event to be located above the catchment. Larger permutation distances on the other hand led either to larger values when the depression was more centered above the catchment or lower when the center of the depression was shifted away from or over the catchment. Therefore, multi-directional shifting can be considered necessary to create reliable new precipitation time series in which biased introduction of new extreme events is prevented. This is especially important for basins which consisted of distinct precipitation regimes causing a strong directional dependency of the results as was shown for the Rhine basin.

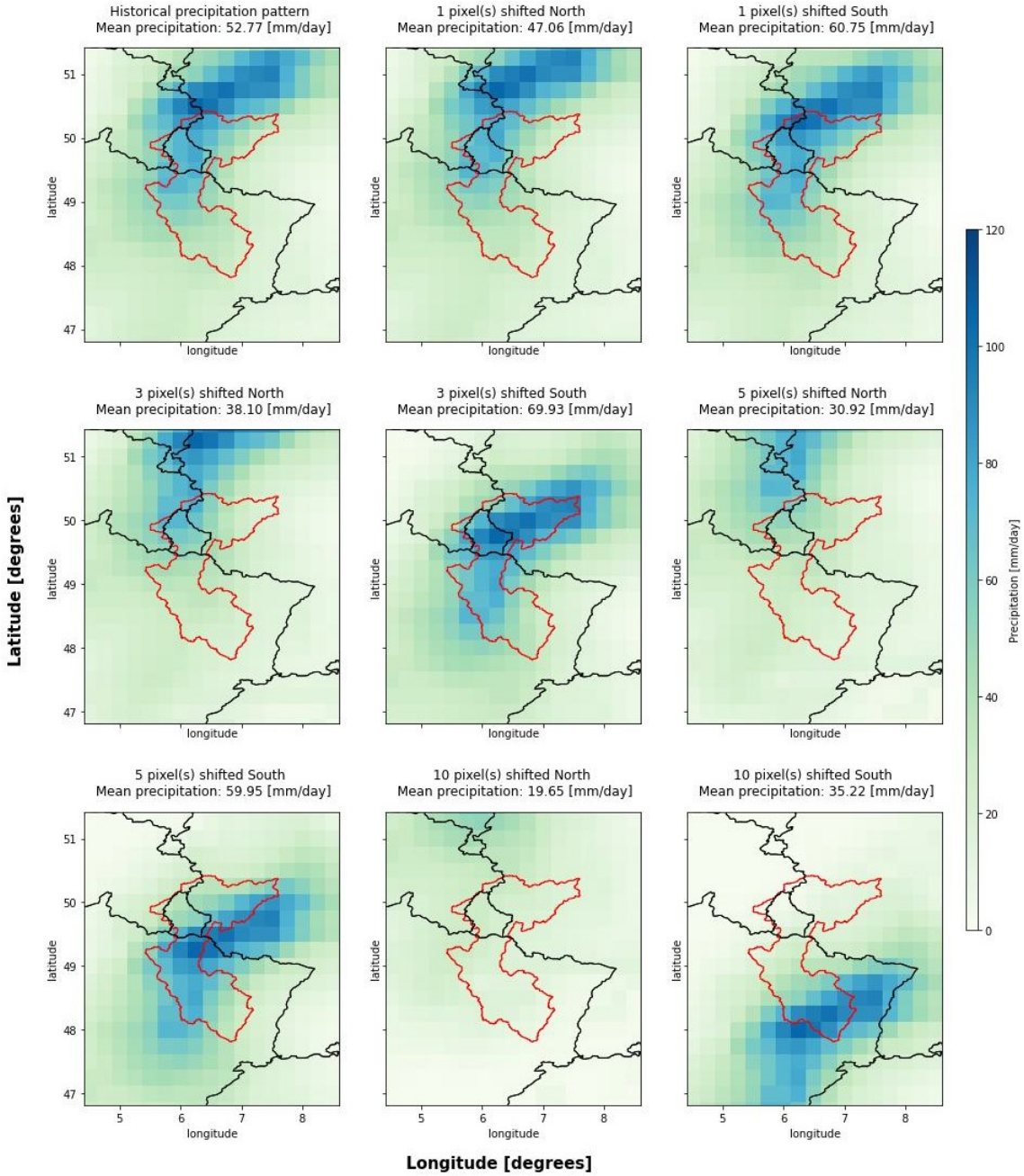

Figure 4.8: Visual representation of the effect of research model 1 on the modelled precipitation in the Moselle catchment on July 15th, 2021. Shifts are shown for the north and south direction over a distance of one, three, five and 10 pixels.

Summary research model 1

- The Generalized Extreme Value (GEV) distributions and the cumulative distribution functions (cdfs) of the historical observed precipitation extremes are altered by spatial permutation indicated by the changing Anderson-Darling (AD) test statistics.
- Spatial permutation created most variation in extremes for large distances, small basin sizes and short aggregation times.
- Longer aggregation times and larger basins resulted in higher correlation values between historical and shifted precipitation series. Shorter aggregation times and smaller basins resulted in lower correlation values.
- The magnitude of extreme precipitation events introduced by spatial permutation depends on the direction in which precipitation is shifted. This effect is most clear for areas which cover different rainfall regimes, i.e. the Rhine basin, and when analysing individual events, i.e. the July 2021 floods.

4.3. Results and discussion: vector based permutation

The fixed based permutation approach of research model 1 showed that spatial permutation influenced the precipitation values observed in a basin. However, the fixed method was rigid and did not allow for local modification while aggregation time, basin size and shifting direction were shown to influence the final results. As such, the need to develop a more differentiable approach emerged in precipitation could by shifted without violating the varying temporal and spatial characteristics of precipitation patterns.

For that reason, research model 2 was developed with as main objective to research how a semi-random vector based approach could be developed and used to shift precipitation over the area of interest. It was tested to what extent this approach could generate new extremes, what the influence of basin size and aggregation time was on the obtain results and last, how the different model steps, assumptions and variables did affect the outcomes of the model.

Subsection one of this section presents the generalized extreme value (GEV) distributions of research model 2 and the differences between the distributions for several combinations of basins and aggregation times. In the next subsection, the cumulative distribution functions (cdfs) are shown. In the third subsection, the displacement vector fields are analyzed and the influence of different parameters on the vectors fields is discussed. The fourth subsection shows the effect of the model on the July 2021 event in the Moselle basin. Subsequently, the sensitivity of the methodology to several features and steps taken is examined. Features discussed are the initial vector field, the weighting factors and the directional component of the methodology. Besides the results, each subsection provides a discussion of the meaning, consequences and implications of the findings.

4.3.1. Generalized extreme value distribution

The AD-test statistics of the GEV showed a strong relation with basin size. Average AD-test statistics became higher when basin size decreased for all vector types (see table 4.12 for the parameter combination per vector type). The range of the average AD-test statistics varied between -0.36 and -1.09. Highest scores pointed towards the presence of a larger variation in precipitation extremes, while the lowest score indicate a more even distribution which could be better fitted by the GEV distribution. Though, since all AD-test statistics were still well below zero, it indicated that all vector-shifted data were still likely to be distributed according a GEV distribution.

In addition, 56% of the combinations of aggregation time, basin and vector type led to lower average AD-test statistics compared to the historical data. This observation can be explained by splitting the vector data into the individual repetitions for each vector type (see figure 4.9). Repetitions with a small range between minima and maxima were shown to be fitted better by a GEV distribution resulting in low AD-test statistics. When the variation in a repetition became larger, the GEV fit became worse resulting in higher AD-test statistics.

This reasoning is supported by the observed decrease in AD-test statistics of the different basins when aggregation time increased. Longer aggregation times resulted in smaller relative ranges between precipitation minima and maxima for all repetitions of each vector type. This directly translated into lower AD-test statics. However, two days rainfall events had the highest AD-test statistics for all basins and vector types which was caused by the largest variation observed in these repetitions.

Considering individual vectors, the maximum and minimum AD-test statistics found were 0.55 and -1.20, respectively. No relation between AD-test statistics and vector type was observed. Yet, it must be noticed that a better or worse fit of the GEV distribution does not provide a conclusion about the usefulness of the data. Even the repetitions which had the worst fit to a GEV distribution can be useful for risk analysis. Especially these data sets will be likely to include more extreme events and can be employed for modelling the increased variability and extremity observed in our current day climate as a result of climate change.

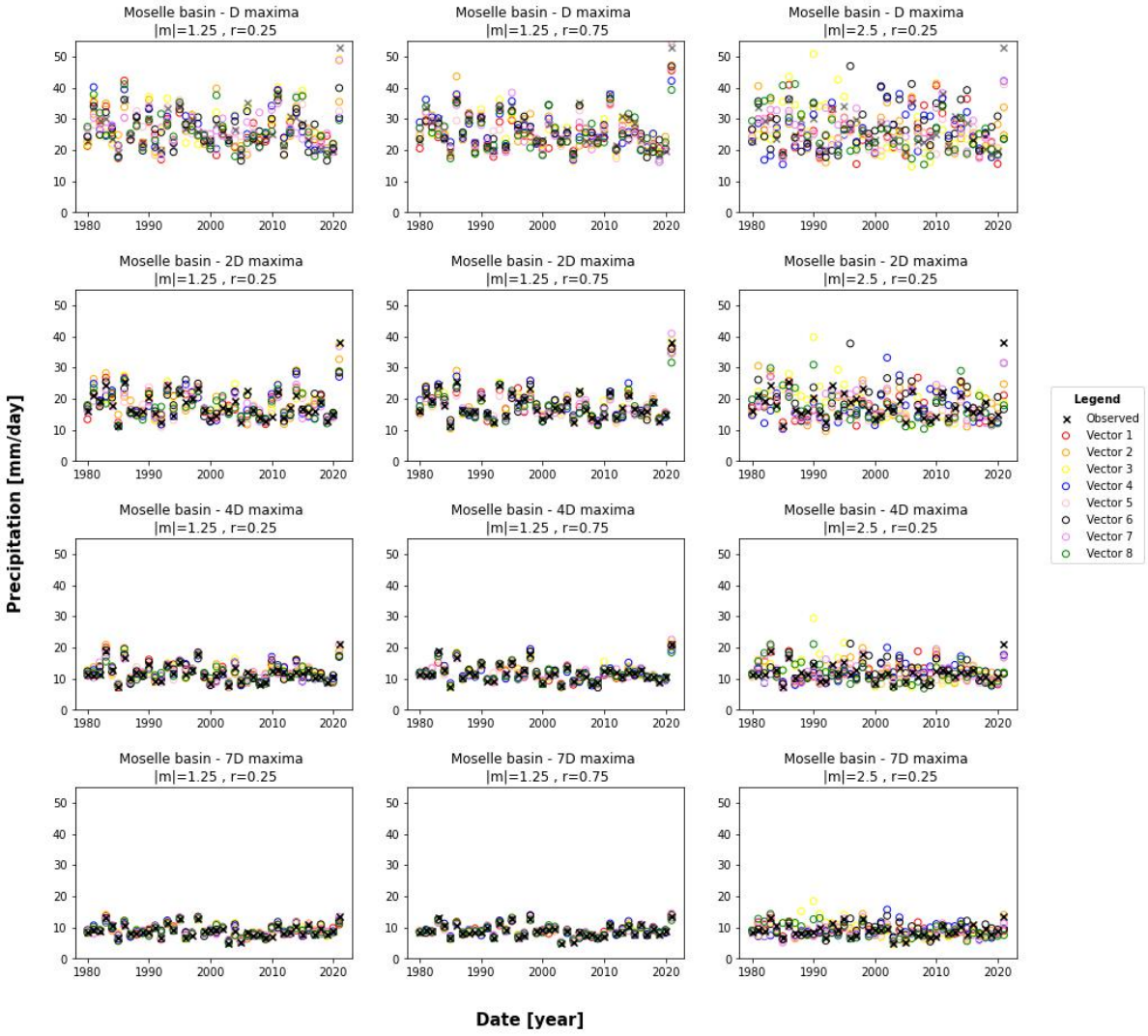

Figure 4.9: The annual precipitation maxima of the Moselle basin for all vector types and aggregation times for the eight repetitions separately. Black crosses show the historical observed values. Distinct coloured open circles represent independent repetitions of the semi random-based vector shifted maxima.

With regard to the uncertainty intervals, it was seen that for 72% of the tested combinations between aggregation time, basin and vector type, the shifted-data had a smaller average maximum uncertainty interval compared to the historical data. This was interesting since data sets had the same length as the historical data, i.e. 42 years. A larger sample size could therefore not be an explanation for the reduced uncertainty as was the case for research model 1. Carlson [54] suggested that a better fit of the underlying distribution could lead to smaller confidence intervals since residuals are and the standard deviation is smaller. However, the results did not show a relation between AD-test statistics and the absolute magnitude of the corresponding confidence intervals. As such, this explanation did not hold.

A reason which can be explanatory for the average decrease in uncertainty intervals can be seen when considering the results for the Moselle basin. In the historical data, the year of 2021 had a very distinct maximum with a value more than 10 [mm/day] higher than the second highest value (see figure 4.9). As a result, the uncertainty interval of the observed data was large. Random re-sampling and the use of linear regression to determine the new grid cell precipitation value led in most cases to a decrease of the largest annual maxima. However, vector repetition three of type T3 sampled an even higher maxima. A corresponding larger uncertainty interval was indeed observed.

Larger uncertainty intervals were also seen for longer aggregation times for all basins because the absolute range of observed extremes was larger. The lowest average values for each aggregation time were found for the Rhine basin, while the uncertainty for the Moselle was the highest, except for daily data. In view of the vector types, a similar pattern was observed with lowest values for the Rhine basin and highest values for the Moselle, except for vector type T1 ($|\boldsymbol{m}| = 1.25$ [degrees], $\boldsymbol{r} = 0.25$ [degrees]). Though, when neglecting the extreme 2021 annual maximum, again a clear influence of catchment size was seen in the uncertainty intervals. Smaller catchments had more variable maxima leading to larger uncertainty intervals and higher AD-test statistics for the GEV fit.

4.3.2. Cumulative distribution function

The cdf curves of the observed and vector-shifted data were compared with the AD-test. The average AD-test statistic for each combination of vector type and aggregation time varied between 1.02 and -1.08. In total, 88.9% of the AD-values were below the $\alpha = 0.25$ critical value for the AD-test, indicating a high likelihood that the vector shifted precipitation data came from the same distribution as the historical data. Nevertheless, higher AD-test statistics were a clear indicator for the presence of more variability and were mainly seen for small basins. This confirmed that especially for small basins, spatial permutations resulted in the introduction of more new precipitation events which made these time series interesting for risk analysis.

When the average AD-test statistic over all aggregation times for each vector type and basin was calculated, the effects of limit $\boldsymbol{m}$ became visible. Changing the limit from |1.25| [degrees] to |2.5| [degrees] resulted in higher AD-test statistics for all basins which was confirmed by a clear visible change in cdf-curves. The larger the basin, the lower the AD-test statistics. This indicated that new events introduced by spatial permutation differed less compared to the historical observed extremes when basin size increased.

A remarkable exception on this general relation between basin size and AD-test statistics was seen in the results of one of the iterations for vector type T3 (see figure 4.10). For this particular vector, highest AD-test statistics were seen for the Rhine basin, meaning that the difference between the vector shifted and historical events was large. Examination of the underlying vector field revealed that the mean $D_x(\boldsymbol{r}, \boldsymbol{m})$ and $D_y(\boldsymbol{r}, \boldsymbol{m})$-permutations were 1.28 [degrees] and 1.06 [degrees], respectively, which was more than 50% higher compared to the other iterations of vector type T3. As such, an almost unidirectional re-sampling of precipitation from the northeast direction took place.

This translation direction could directly be compared with a southward shift in research model 1. For this shifting direction, introduced extremes were shown to be less intense compared to the historical data in case of the Rhine basin. A cause for this observation was found in the presence of the Alpine region. Basist *et.al.* [53] showed that mountainous areas are a source of more extreme events. The biased sampling from the northeast direction causes a replacement of the historical values observed in the Alpine region, with less extreme events observed in the more northeast located areas. This resulted in a decrease of the cdf-curve compared to the historical data and as consequence a large AD-test statistic reflecting the difference between the historical and shifted cdf-curves.

Varying the range ($\boldsymbol{r}$) did not result in large changes in the AD-test statistics and order. Highest values were still observed for the Ijssel basin and lowest for the Rhine basin. The influence of the range on the AD-test statistics was largest for the Moselle basin, while the values for the Ijssel and Rhine hardly changed.

The average correlation between the historical and vector-shifted data showed the largest correlation values for the Rhine basin and the smallest values for the Ijssel, independent of vector type (see figure 4.11). This underlined again that smaller basins are more influenced by spatial permutation compared to larger basins. Yet, differences between the Ijssel and the Moselle were small. Correlation increased when the aggregation time of the precipitation events became longer, since longer aggregation time averaged out the most extreme daily precipitation values.

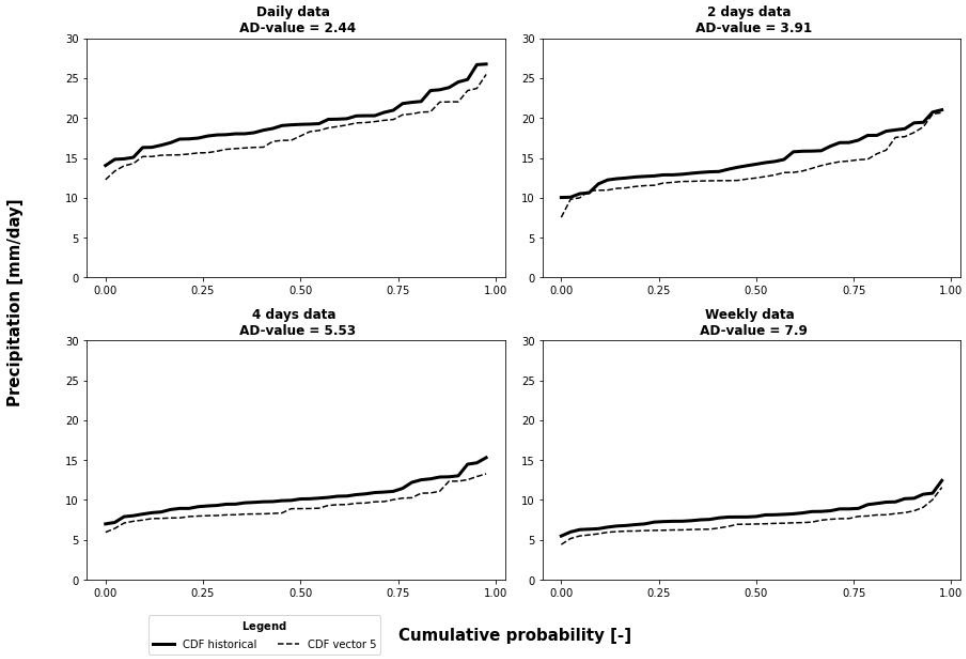

Figure 4.10: The cumulative distribution function (cdf) of annual maximum precipitation values in the Rhine basin of the historical data (black solid line) and the most extreme iteration of vector type T3 (m=2.50 [degrees], r=0.25 [degrees]) data (black dotted line). Corresponding AD-test statistics are: 2.44, 3.91, 5.53 and 7.90 for daily, 2-days, 4-days and weekly data, respectively.

For the average correlation for each vector type, the highest correlation values were observed for vector type T2. Increasing the range while maintaining the same value of m led to a higher correlation between the observed and shifted precipitation data (see figure 4.11). Intuitively, this higher correlation seems unexpected when considering the displacement vectors and resulting precipitation fields. As can be seen in figure 4.13b a high value for r resulted in a fragmented precipitation field which did not resemble to original coherent historical precipitation pattern. However, the fragmentation prevented the model to shift low pressure areas in or out an area of interest as a whole. As such, the mean precipitation modelled over an area was almost similar to the historical mean, while the precipitation pattern from which the mean was derived was a lot different.

The lowest correlation values were observed for vector type T3 with the highest value of m of all vector types, i.e. $\boldsymbol{m} = |2.5|$ [degrees]. As a result of this higher limit, the average displacement vectors became longer. Longer displacement vectors meant that precipitation was shifted over larger distances which created larger changes in precipitation patterns compared to short displacement vectors which kept the historical precipitation approximately at the same location. As such, the larger differences caused by longer displacement vectors were reflected in lower correlation values.

This phenomenon can be compared with the negative relation between correlation and shifting distances in research model 1. Yet, the obtained correlation coefficients for research model 2 were still higher compared to the five and 10 pixels shifted correlation values of research model 1. This can be explained by the fact that the pixel shifted approach ensured that precipitation was shifted the exact amount of indicated pixels, i.e. 1.25 [degrees] (five pixels) or 2.5 [degrees] (10 pixels), in all cases. While theoretically these limits could also be reached with the semi-random vector approach in research model 2, the average length of vector type T3, with limit $\boldsymbol{m} = |2.5|$ [degrees], was only 0.4 [degrees] and 0.2 [degrees] for the $D_x(\boldsymbol{r}, \boldsymbol{m})$ and $D_y(\boldsymbol{r}, \boldsymbol{m})$-permutations, respectively. These lower values resulted in smaller shifting distances of the precipitation fields with as consequence higher correlation values between historical and vector shifted precipitation data.

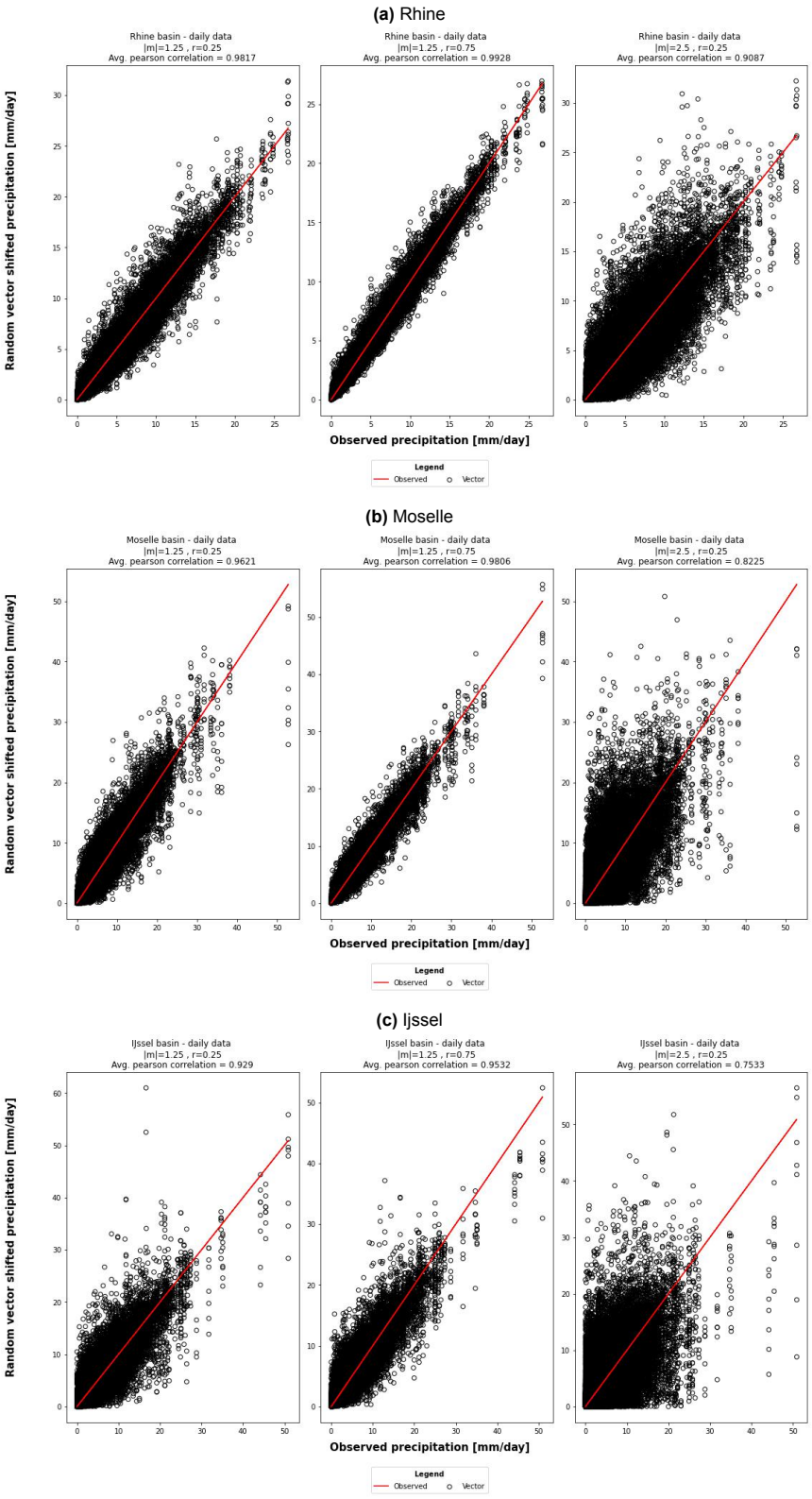

Figure 4.11: The correlation plots and average correlation values for daily precipitation data. Each plot shows the results of a different vector type. From left to right: T1, T2 and T3 (for parameter values see table 3.2). Observed precipitation is shown as a straight red line. Notice that vertical axis values differ per plot.

The knowledge obtained about the influence of the parameters m and r can be translated to a more physical meaning by relating them to the characteristics of precipitation regimes. As discussed in section 4.1.1, temporal and spatial precipitation variability have distinct values depending on the location. Therefore, they can be seen as important boundaries for precipitation permutation in an area. For the current modelling approach, these boundaries can be created by varying the parameter r on grid cell level. High values of r will reflect areas in which spatial and temporal correlation is low, like mountainous areas. Low values will be appropriate for the low lands and over large waters, such as the North sea, The Netherlands and the North of Germany, where temporal but mainly spatial correlation is higher. Limit m can be connected to the average distance over which precipitation or wind moves. Areas in which large travel distances of precipitation events are observed will allow for a higher limit, while areas with very local precipitation patterns will be confined by a smaller limit. As such, the methodology of research model 2 allows for local adjustments when further developments are done.

4.3.3. Displacement vector fields

The influence of the three vector types with different combinations of parameters m and r (see table 3.2) on the resulting vector fields was tested visually (see figure 4.12). Each vector type was examined at $t > 365$ [days] to ensure that the initial field did not influence the examined vector fields.

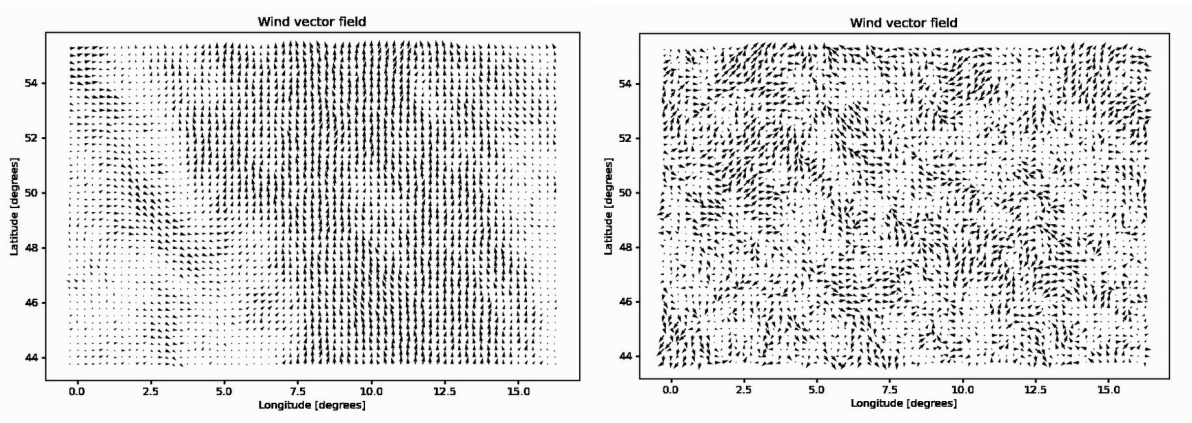

(a) Vector type T1 : $|m|$=1.25 [degrees], r=0.25 [degrees]

(b) Vector type T2 : $|m|$=1.25 [degrees], r=0.75 [degrees]

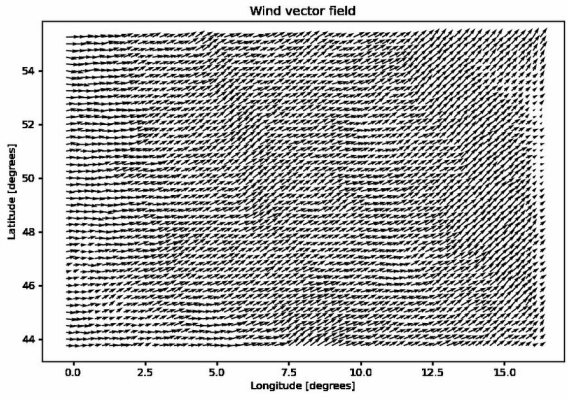

(c) Vector type T3 : $|m|$=2.50 [degrees], r=0.25 [degrees]

Figure 4.12: Visual representation of the different vector types T1, T2 and T3. Parameter combinations for each vector type can be found in table 3.2. Days are chosen randomly after the spin up time of $t > 365$ [days] to indicate the differences between the vectors types clearly

The results showed that an increase of the limit m from |1.25| (T1) to |2.5| (T3) [degrees], respectively, resulted in longer vectors. The mean absolute length for the $D_x(\boldsymbol{r}, \boldsymbol{m})$ and $D_y(\boldsymbol{r}, \boldsymbol{m})$-permutations of the type T3 vectors was 1.09°and 1.20°compared to 0.46°and 0.44°for type T1 vectors. Parameter r determined the coherence at one time step between vectors. The low r-value of 0.25 [degrees] for vector types T1 and T3 lead to a strong coherence with long stretching vector patterns (see figures 4.12a and 4.12c). Increasing the r-value to 0.75 [degrees] for vector type T2 resulted in less coherence and a dynamic vector field with distinct clusters of vectors (see figure 4.12b). The average length of the $D_x(\boldsymbol{r}, \boldsymbol{m})$ and $D_y(\boldsymbol{r}, \boldsymbol{m})$-permutations did not change for different values of r.

The proof that the choice of the parameters m and r do influence the final vector fields in distinct ways, confirmed that these parameters can provide a strong base for reflecting physical limits like atmospheric circulations and variability. This was already observed and described for the resulting cdf-curves (see section 4.3.2). However, between the created vector fields and the resulting cdf-curves one step is left. This step concerns the influence of m and r on a precipitation event itself and is discussed in the next subsection.

4.3.4. Influence on the July 2021 flood

The differences in the displacement vector fields as caused by the varying combinations of the parameters m and r persisted into the generated precipitation field. This was made visible for the rainfall event of July 15th, 2021. In figure 4.13, it can be seen that type T1 displacement vectors fields caused the least changes in precipitation. Almost all fields shifted the center of the event away from the Moselle basin resulting in lower mean values for all repetitions compared to the historical observed value of 52.77 [mm/day] (see figure 4.13a).

The precipitation fields resulting from vector type T2 showed the same disruption as the displacement vector field itself. The spatial coherence of the original precipitation event was lost resulting in unrealistic, scattered precipitation patterns. Grid cells with high precipitation values were spread over the area without a clear direction. Mean values of the eight repetition varied around the observed value with two repetitions creating a more extreme event compared to the historical event (see figure 4.13b).

Vector type T3 resulted in coherent precipitation patterns which were shifted over larger distances compared to the results obtained with vector type T1. This was in agreement with the expectation based on the longer, but still spatially correlated displacement vectors observed in the displacement vector field of type T3 (see figure 4.12c). In addition, no persistent shifting direction was observed. The repetitions with shifts in the southward direction resulted in the highest mean precipitation, while northeastward shifts created very low mean values. None of the repetitions created a more extreme mean value compared to the historical observed value for the Moselle basin (see figure 4.13c).

When considering the different vector types, the amount of variation in the mean values created by vector T2 can be considered most promising. New extremes were introduced compared to historical observed precipitation values. However, vector type T2 showed also a clear trade-off between the created extremes and the loss of the spatial coherence. This conflicts with the notion that spatial correlation is an important characteristic of a precipitation regime. The uncorrelated precipitation fields thereby weaken the argumentation that the modelled precipitation values could have occurred by chance in the area of interest, which is the basic assumption behind the application of spatial permutation.

The loss of spatial coherence was prevented when keeping r low while changing m. Larger values of m resulted in more variation, though for this specific event no more extreme precipitation values were introduced. This can be a matter of chance, but to conclude about this more repetitions should be made. Yet, when indeed a larger value of m is proofed to create more variation, this value cannot be increased endlessly. If m is used to reflect the atmospheric circulations in a certain area, a limit should be chosen based on values typical for the local wind speed and -direction. Too extreme values can lead to precipitation shifts which conflict with the distance over which precipitation moves is reality and should therefore be prevented despite their possibility to introduce more extremes.

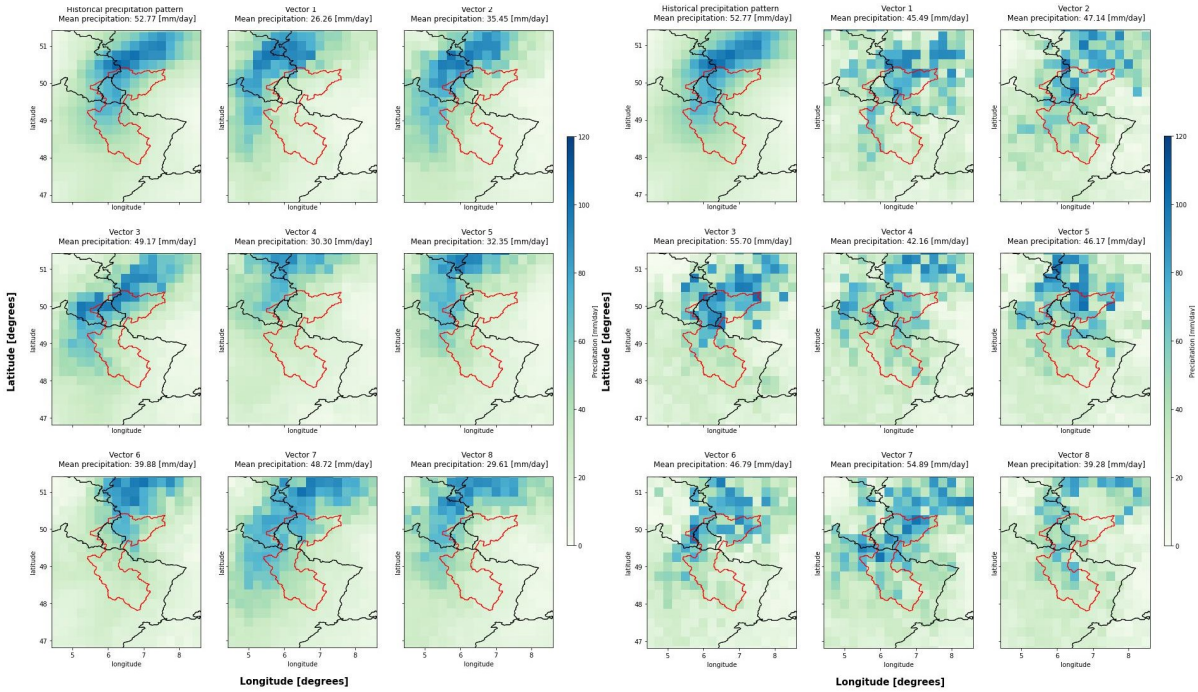

(a) Vector type T1 : $|\boldsymbol{m} = |1.25||$ [degrees], $\boldsymbol{r} = 0.25$ [degrees]

(b) Vector type T2 : $|\boldsymbol{m} = |1.25||$ [degrees], $\boldsymbol{r} = 0.75$ [degrees]

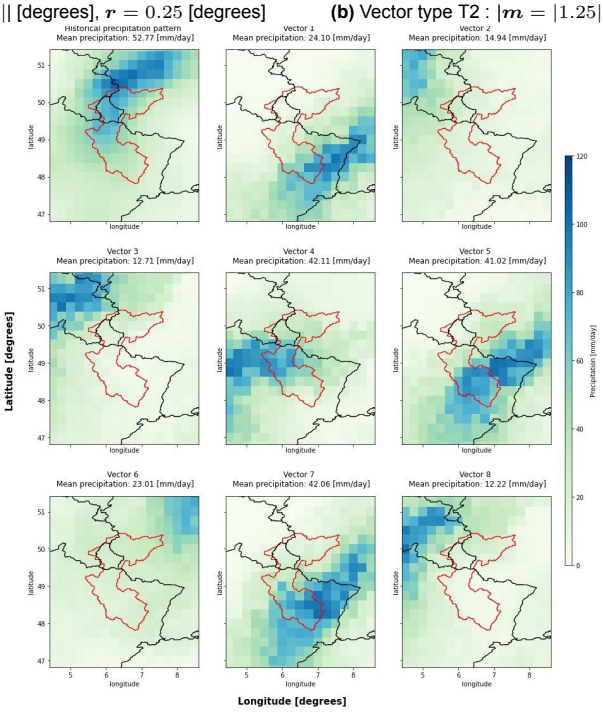

(c) Vector type T3 : $|\boldsymbol{m} = |2.50|$ [degrees], $\boldsymbol{r} = 0.25$ [degrees]

Figure 4.13: Visual representation of the influence of the different displacement vector types on the precipitation event of July 15th, 2021

4.3.5. Model sensitivity

The methodology of research model 2 contained assumptions about boundary and initial parameter values which were not based on physical arguments but rather on practical modelling reasons. In addition, the underlying code had a strong directional component caused by a constant array fill direction from northwest to southeast. To determine the influence of the assumptions and methodology, the different parts were analysed. The starting situation for each analysis was the methodology as explained in subsection 3.3.1. Sensitivity to different features was tested by varying only the feature of interest and run the model over a period of one year with as base precipitation values the historical values of 2021.

Sensitivity to the initial field

The initial field did influence the variation in precipitation values observed for each basin. Largest coefficients of variation (cv) were seen when varying initial fields were used as starting point. This can be explained by the diversity of initial permutation fields which were used as starting point for the simulation. The cv decreased when the same initial field was used, thereby reducing the diversity in the permutation fields with regard to varying initial fields. Lowest cv values were obtained when the simulations were started with initial fields consisting of zeros. Cv for all initial fields for all basins were in the same order of magnitude after one month, which can be seen as the spin up time of the model. As such, the spin up time can be considered negligible compared to the long time series which are used for flood risk predictions, i.e. often more than 1,000 years. Cv were shown to be strongly correlated to basin size. Smallest values were found for the Rhine basin and largest for the Ijssel.

Sensitivity to the assigned weights

The rainfall maxima observed over the different basins did not show a sensitivity towards the weights assigned during the displacement vector generation. Independent of the weights used, a strong relation between maxima and basin size was observed. Lowest maxima were seen for the Rhine, while highest values were found for the Ijssel basin.

The assigned weights had a large influence on the spatial correlation of displacement vectors. When cells parallel to the permutation direction were given higher weights, the correlation between latitudes (rows) for $D_y(\boldsymbol{r}, \boldsymbol{m})$ and between longitudes (columns) for $D_x(\boldsymbol{r}, \boldsymbol{m})$ increased. This is the direct consequence of assigning the adjacent row and column grid cells larger weights in the computation process for the new $D_y(\boldsymbol{r}, \boldsymbol{m})$ and $D_x(\boldsymbol{r}, \boldsymbol{m})$, respectively. For the case in which perpendicular grid cells were given a higher weight, the opposite trend was visible with higher longitude correlations for $D_y(\boldsymbol{r}, \boldsymbol{m})$ and higher latitude correlations for $D_x(\boldsymbol{r}, \boldsymbol{m})$. Remarkable was that the absolute value for the longitude correlation was much lower than latitude correlation independent of the the weights assigned in the calculation process. Longitude correlation dropped faster over distance while latitude correlation remained high over a long distance (see figure 4.14).

Sensitivity to the direction of the methodology

The directional bias in the methodology resulted in a high latitude (row) correlation. Independent of the weights assigned, latitude correlation was higher than longitude correlation for all weights tested. Yet, no physical reasons are known to assume that precipitation movement correlates more over latitudes compared to longitudes. Instead, it was shown that atmospheric circulation patterns and local orography in most cases steer the movement and occurrence of precipitation [32], [36], [37]. The difference between latitudinal and longitudinal correlation is therefore unwanted. Perpendicular weights for $D_y(\boldsymbol{r}, \boldsymbol{m})$ and parallel weights for $D_x(\boldsymbol{r}, \boldsymbol{m})$ partly counteracted the high latitude correlation as can be seen in figure 4.14 A and B, which can be considered favorable for the credibility of the model.

Nevertheless, a better result was obtained when the directional bias in the current time step was eliminated. As a consequence, latitude correlation for the $D_y(\boldsymbol{r}, \boldsymbol{m})$ dropped and became almost similar to the longitude correlation. The correlation for the $D_x(\boldsymbol{r}, \boldsymbol{m})$ remained high without a clear reason. However, when also replacing the initial field with a field consisting of zeros, latitude and longitude correlation became similar for both $D_y(\boldsymbol{r}, \boldsymbol{m})$ and $D_x(\boldsymbol{r}, \boldsymbol{m})$ as can be seen in figure 4.14 E and F. Hence, removing the directional component of the methodology is most efficient in eliminating the difference between longitudinal and latitudinal correlation. Future modelling approaches should therefore start from an non-directional methodology by using non-differentiated weights and a new computation method in which spatial correlation in the current time step is not defined in a fixed direction. Deviations from this starting point should be made only on arguments substantiated with observed physical limits, such as the observed historical spatial and/or temporal correlation values. In that way, it will be prevented that variation is added to the observed extremes which is caused by the underlying methodology instead of credible modelling of the natural spatial variability of precipitation.

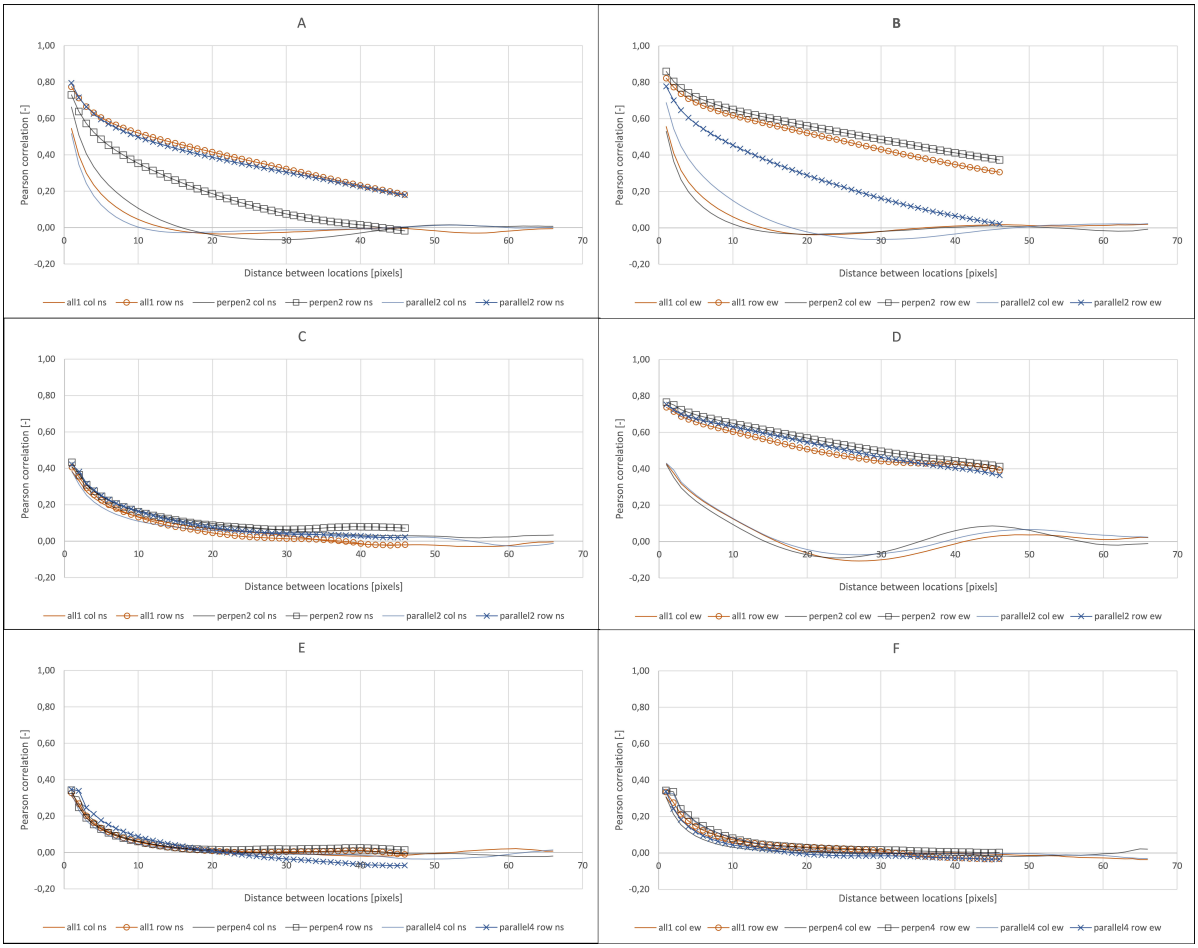

Figure 4.14: Pearson correlation values of vector permutations between latitude (row) and longitude (column) under different conditions. Left column shows the north-south ($D_y(\boldsymbol{r}, \boldsymbol{m})$) permutation, right column shows the east-west ($D_x(\boldsymbol{r}, \boldsymbol{m})$) permutation. Base weights for all figures is 1. Changes in weights are indicated in the legend. Figures A, B) Initial field filled from left to right, new permutation based on past en present values. C, D) Initial field filled from left to right, new permutation only based on past values. E, F) Initial field consist of zeros, new permutation only based on past values.

4.3.6. Extent of variation

The most extreme event for each basin was shown to vary depending on the methodology used to create the underlying vector fields. The events analysed took place on July 15th, 2021 for the Moselle and Rhine basin, and on June 22nd, 2021 for the Ijssel basin. Highest variation, as defined by the standard deviation, was obtained for the methodology based on random initial fields. This was in agreement with the earlier finding that the modelling results are sensitive to the type of initial field used for different iterations, with largest cv for varying initial permutation fields.

Reducing the difference between the weights did not result in lower variability. On the contrary, when weights were brought closer together compared to the weights used in the methodology, i.e. 1.125 for the parallel components and 0.825 for the perpendicular component, variability was shown to be highest. Obtained standard deviations were 4.83, 10,81 and 7,4 [mm/day] for the Rhine, Moselle and Ijssel basin, respectively. A likely explanation for this phenomenon can be the strong directional component in the model methodology itself. Weights closer to each other will counteract this directional component less, especially due to the fact that the past values were weighted relatively less compared to the present, highly directional, values. This explanation was confirmed by the observation that lowest variation was obtained for the methodology with an initial field based on zeros and weights all equal to one. Standard deviations for the Rhine, Moselle and Ijssel basin were 0,81, 2,98 and 2,57 [mm/day], respectively.

In addition, it was found that the distribution of the extremes varied depending on the methodology and basin under consideration. For the Rhine basin, distributions were almost normal around the extreme observed except for the random method with the smaller weights. This method resulted in two distinct peaks on both sides of the extreme event. This meant that the model generated both a distinct group of events with lower mean precipitation values compared to the historical observed value, while at the same time also generated a group with precipitation patterns resulting in higher mean values. A cause can be found in the direction of the initial field. When smaller weights are used, this direction is hardly changed and thereby likely to be maintained leading to either a shift of a larger part of the event over the basin or a shift of the event away from the center of the catchment. In this way, two distinct peaks are created which depend on the prevailing shifting direction of each iteration.

For the Moselle basin, methodologies starting with an initial field of zeros resulted in an even distributions around the extreme value, while the methodologies starting with a random initial field resulted in left-skewed distributions indicating the generation of mainly lower mean precipitation values. The variation for the Ijssel basin was left-skewed, independent of the methodology used. This indicated that shifting of the 2021 extreme of the Ijssel basin led in most cases to a shift away from the catchment and lower modelled mean precipitation values. For an overview of all histograms, see appendix IV.

Summary research model 2

- The Generalized Extreme Value (GEV) fit to the shifted data became worse when more variation in annual extremes was introduced. Less variation let to smaller uncertainty intervals. However, the quality of the GEV fit could not be used to draw conclusions about the usefulness of the shifted time series for risk analysis.

- The difference between the historical and shifted cumulative distribution functions (cdfs) was largest for high values of limit m, small basins and short aggregation times. The range parameter r did not have a considerable influence on the cdf curves.

- Correlation values were highest for larger basins, long aggregation times and vector type 2, with a high value for limit m and a low value for range r. Reduced variability between rainfall extremes was the main reason for the higher correlation values.

- The methodology of research model 2 was sensitive to the initial and boundary conditions. Features such as the initial field, the weights used to relate past, present and neighbouring cells, and the calculation direction should therefore be chosen as neutral as possible in subsequent modelling processes.

- In future development of the methodology of research model 2, parameter m can be used to represent wind speeds while parameter r can represent spatial and temporal correlation. Adding the modelling opportunity to vary these parameters depending on location and season is advised to better represent natural precipitation movement.

4.4. Results and discussion: wind based permutation

Research models 1 and 2 showed that the effect of spatial permutation on the extremes in different basins was dependent on the methodology used to shift precipitation. They indicated that basin size, direction and aggregation time influenced the extent to which extremes were changed by spatial permutation. In addition, it was proved that a fixed approach, in which precipitation patterns were perturbed over fixed directions and distances, could be replaced by a vector based approach, in which precipitation patterns were perturbed by means of semi-random vector fields, mimicking a more natural movement of precipitation. Nevertheless, the spatial shifts introduced by both research models were artificial and not based on historical observed parameters which are known to influence the movement of precipitation.

As described in subsection 4.1.2, circulation patterns do have a large influence on the movement and occurrence of precipitation. Therefore, the goal of model 3 was to research whether it is possible to shift precipitation based on displacement vectors conditioned with the characteristics retrieved from historical wind speeds and -angles.

In the first subsection of this section, the results of the GEV distribution are shown and discussed. Differences were quantified with the AD-test and the width of the uncertainty intervals. Subsequently, the correlation between the historical and shifted cdf is discussed, together with the obtained AD-test statistics. The third subsection shows the spatial and temporal correlation patterns of the shifted precipitation and compares the values with the historical correlation patterns in order to understand if historical behaviour was preserved. Next, differences between means, maxima and standard deviations of precipitation between historical and shifted data are presented. In the fifth subsection, the results of the comparison between displacement vector angles with the historical observed values is shown. Subsequently, the amount of variation the model produces for an extreme event is showed for the three basins, to see if the method produced novel extremes compared to history. The final subsection focuses on the influence of the model on the July 2021 floods for different upper and lower limits for the wind angles and -speeds as defined by a fraction f of the standard deviation.

4.4.1. Generalized extreme value distribution

The AD-test statistics for the GEV distribution were below -0.1 for all combinations of aggregation time, basin and fraction f (see figure 4.15). This confirmed that the 42 years of modelled extremes were still well fitted by a GEV distribution. Lowest average values for each aggregation time and fraction f were obtained for the Rhine basin. Highest average values were seen for the Ijssel basin, except for f = 0.25 and f = 0.5. The range of AD-test statistics was smallest for the Rhine basin and highest for the Ijssel basin and varied between -0.7 and -1.2, and -0.1 and -1.0, respectively. All these results are in line with the earlier observation that larger basins and longer aggregation times lead to smaller standard deviations of precipitation events. Extremes are less spread and as a result the GEV distribution fit is better reflected in lower AD-test statistics.

The individual basins showed different patterns with regard to the AD-test statistics. For the Rhine basin, lowest AD-test statistics were observed which can be directly attributed to the lower influence of spatial permutation on large basins. AD-test statistics did slowly increase when fraction f became higher for all aggregation times. This showed that only high values of f caused the variation between extremes to increase, reducing the quality of the GEV fit to the modelled extremes. Between different aggregation times, no clear trend in AD-test statistics of the Rhine basin was visible.

The AD-test statistics for the Moselle basin showed a more irregular pattern. This was most likely caused by the introduction of random noise and a monotonic reaction to both the values of f and the aggregation time. For the Ijssel basin, a decreasing trend was observed with lowest AD-test statistics for larger values of f. A clear decrease was seen between f = 0.25 and f = 0.5 for the one, two and four days aggregation times. Weekly AD-test statistics were lowest, except for f = 0.5.

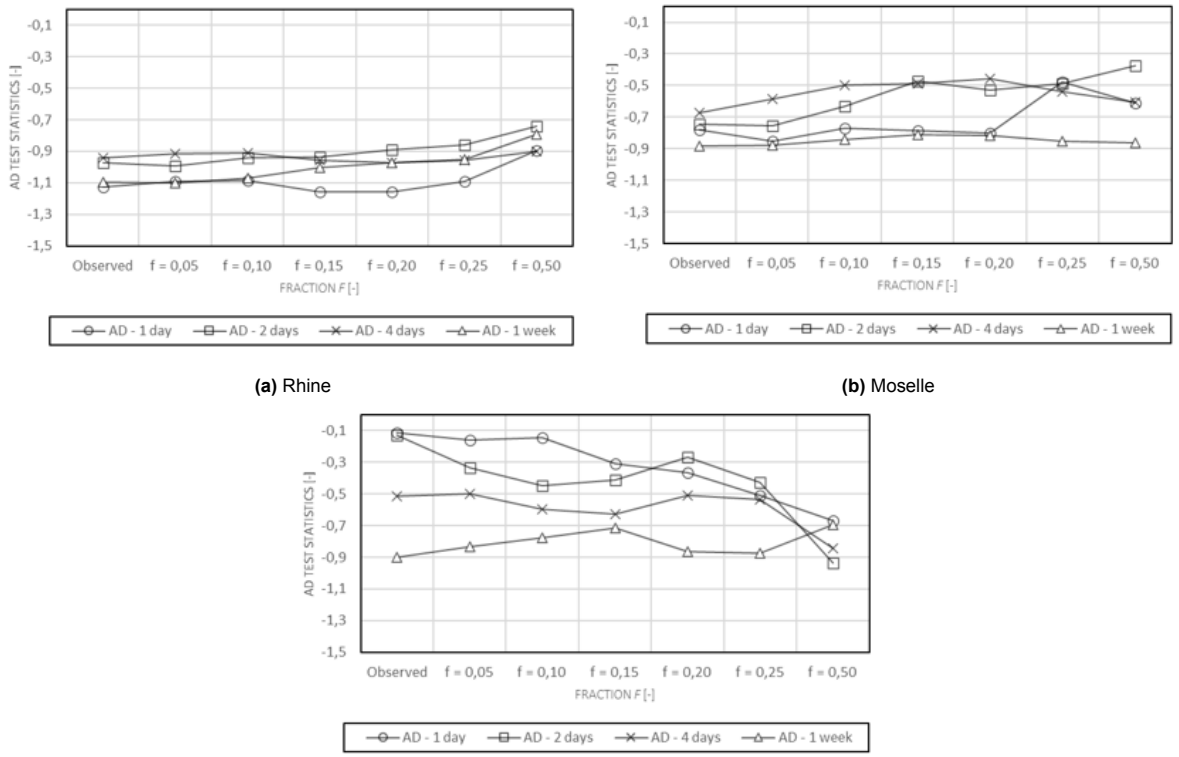

(a) Rhine

(b) Moselle

(c) Ijssel

Figure 4.15: Anderson-Darling test statistics obtained for the Generalized Extreme Value (GEV) distribution of annual precipitation maxima for different combinations of basins, aggregation times and fractions f.

This showed that for smaller basins, a higher value for the fraction f led to a more even distribution of extremes by disrupting the coherence of the historical precipitation pattern. This hypothesis was confirmed by the presence of three very extreme events in the historical data series with values above 44 [mm/day]. Permutation led in all cases to a reduction of one or multiple of these events to values up to 13 [mm/day] lower. As a result, GEV fits became better and AD-test statistics decreased.

Nevertheless, it needs to be noticed that a better GEV fit is not the goal of the development of a spatial permutation model. As indicated in subsection 4.1.2, climate change causes current day precipitation events to change and to become more local. More extreme events are expected at locations where they are not observed yet. A better fit of the GEV distribution caused by a smaller range of extremes can therefore oppose the goal of generating more local extremes. As such, the extent to which the spatial permutation leads to changes in precipitation maxima is a better indicator for the suitability of the model to generate new extremes. These changes do indicate how well the model can create more local variation at different locations which could not be deduced from the GEV fit itself. Hence the changes in maxima can be used to quantify the capability of the model to generate new local extremes on top of the historical observed values in order to mimic present-day climate better.

Switching to the observed uncertainty intervals around the GEV fit, more clear patterns were observed (see figure 4.16). The uncertainty intervals were shown to be sensitive to the aggregation time, with decreasing AD-values for longer aggregation times. This indicated that the variation in extremes was reduced when the aggregation time of the extremes increased. No sensitivity to the value of f was observed. In addition, the magnitude of the uncertainty intervals was related to the magnitude of the extreme precipitation events. The relative lower values in the Rhine basin resulted in smaller uncertainty intervals (±3 [mm/day]), while the Moselle and Ijssel basin had larger values up to 14 [mm/day]. This corresponded with the larger variation and magnitude of the precipitation extremes of these basins to which the GEV was fitted.

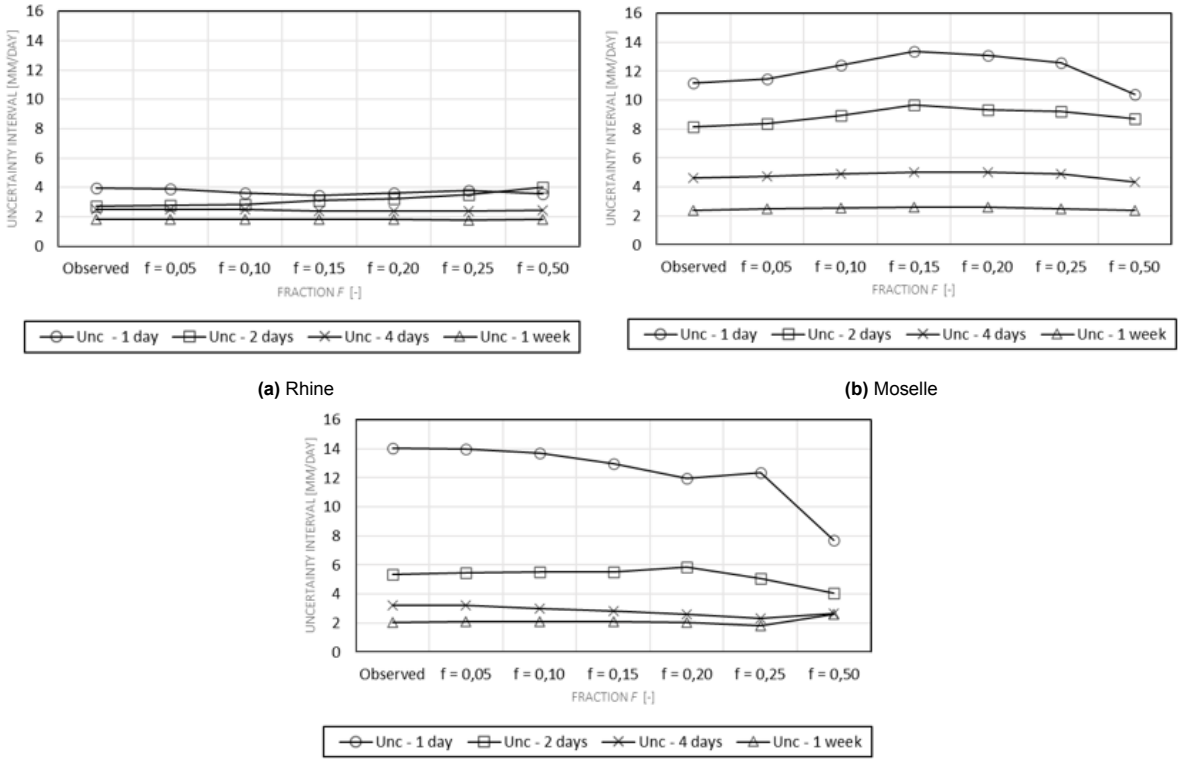

(a) Rhine

(b) Moselle

(c) Ijssel

Figure 4.16: The 5- to 95-percentile uncertainty interval obtained for the Generalized Extreme Value (GEV) distribution of annual precipitation maxima for different combinations of basins, aggregation times and fractions f.

4.4.2. Cumulative distribution function

The AD-test showed that up to a value of f = 0.25 the cdf-curves of the shifted data were not significantly different compared to the historical data. For all basins and aggregation times, values were below 0.16 with the lowest value found to be -1.24. For f = 0.5, AD-test statistics became much larger for all aggregation times for both the Rhine and Moselle basin (see appendix V). The Ijssel basin did not show a strong response and values remain below zero (see figure 4.17).

On top, two different patterns in the AD-test statistics to compare the similarity between the historical and wind-based vector shifted cdfs could be observed. These patterns were related to basin size. The larger basins of the Moselle and the Rhine catchments showed an increase in AD-test statistics when the value of fraction f increased. This increase is explained by the amount of disruption of the precipitation pattern related to the fraction f. As can be seen in figure 4.26, low values of f hardly influence the amount of precipitation modelled over the basin. Low pressure areas are disrupted but since pixels are shifted over the basin, the mean value does not change much resulting in almost similar cdfs and low AD-test statistics. Only at the highest value of f, i.e. f = 0.5, disruption takes place including values from outside the basin boundaries. The spatial correlation of the historical low pressure area was lost. This resulted in much lower mean values which is reflected in a strong increase of AD-test statistics and a shifted cdf curve with values below the historical cdf over the whole range (see appendix V).

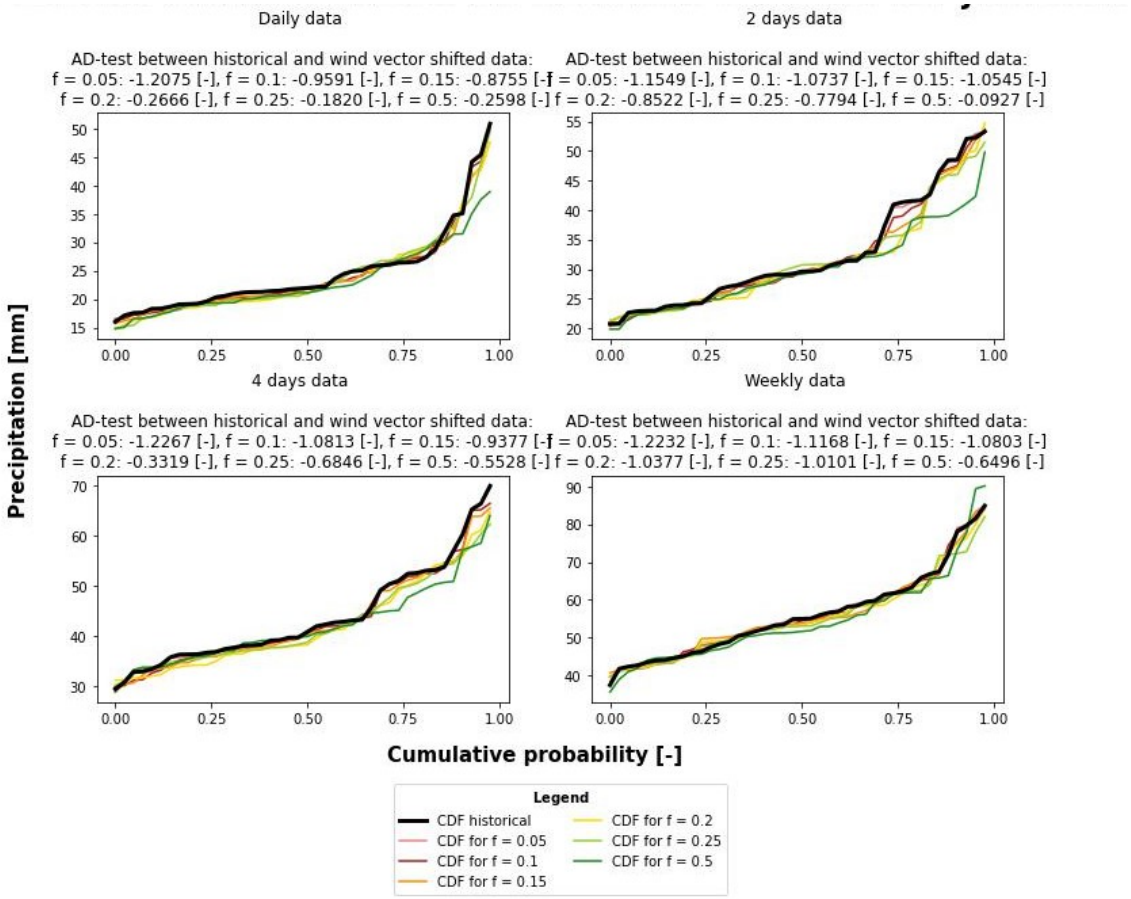

Figure 4.17: Cumulative distribution functions (cdf) of the Ijssel basin for different values of f and aggregation times. Anderson-Darling (AD) test statistics are printed above each figure.

This hypothesis was confirmed by considering the percentage of time a grid cell in a basin sampled a value from outside the basin. As can be clearly seen in figure 4.18, low values of f resulted in almost no sampling from outside the basin except for the boundary cells. As a result, the mean value modelled over the larger Moselle and Rhine basin will not change a lot. Increasing f to 0.5 resulted in a steep increase of the percentage of time a precipitation value from outside the basin was sampled. Thereby, a larger difference between the historical and modelled mean precipitation value emerged.

For the smaller Ijssel basin, a different pattern was observed (see figure 4.17). AD-test statistics were all below zero with an on average increasing trend of AD-test statistics for higher values of f. Though, the effect of the value of f on the similarity between the historical and shifted cdf was small. An explanation can be found when considering the configuration of the majority of the individual annual extremes. These extremes often consisted of low pressure areas which were much larger than the Ijssel basin itself and relatively uniform, i.e. stratiform precipitation events (see figure 4.19). Even when the disruption was high and an increasing percentage of the precipitation was sampled from outside the basin (see figure 4.18), new values were still from the same low pressure area. As a result, the mean value over the basin did not change much. In addition, it was observed that most extreme events were often of the convective type with centers straight above the Ijssel basin (see figure 4.20). For these types of events, higher f values did result in the introduction of pixels with distinct and lower precipitation values over the Ijssel basin. Consequently, the final cdf curve of the shifted data showed a clear deviation of the historical cdf curve for the most extreme events, especially for shorter aggregation times .

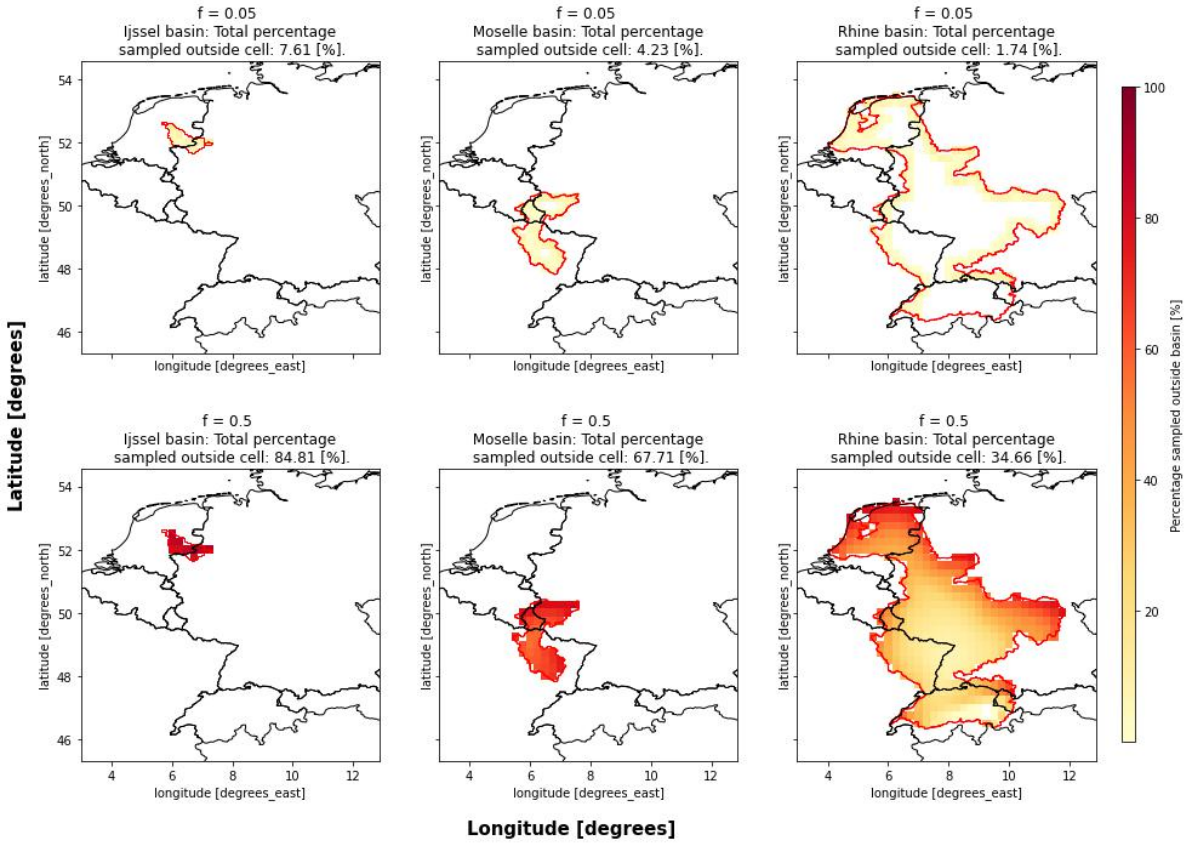

Figure 4.18: Spatial representation of the percentage of time each grid cell sampled a value from outside the basin. Top row shows the values for $f = 0.05$. Bottom row shows the values for $f = 0.5$. Overall percentages are plotted above the sub-figures. From left to right: Ijssel, Moselle and Rhine.

Comparing the AD-test statistics between different aggregation times showed that an aggregation time of one week resulted in the lowest AD-test statistics. Shorter aggregation times caused an increase in AD-test statistics though this relation did not hold for every value of f since absolute differences between AD-test statistics were small. For the Rhine and Moselle basin, all aggregation times showed an increase in AD-test statistics for higher f, while the Ijssel basin showed an irregular pattern with increasing and decreasing AD-test statistics over the different values of fraction f. This is most likely be attributed to random noise introduced by the iterations over the small area of the Ijssel basin.

The Pearson correlation coefficient between the observed and shifted cdf distributions showed a clear relation with fraction f. Higher fractions resulted in a decreased correlation for all basins and all aggregation times. The difference in correlation became larger between aggregation times when fraction f increases. For the Ijssel basin, the smallest correlation value was observed, i.e. 0.961, while the highest value of 0.999 was observed for all basins. Correlation values between aggregation times did not show a clear pattern for individual values of f.

4.4.3. Spatial and temporal correlation of precipitation

Differences in seasonal spatial correlation between the historical and wind vector shifted precipitation data showed a positive correlation with the value of fraction f. Largest differences were seen for f=0.5 and ranged from -0.09 to 0.3 [-]. For f=0.05, differences were as small as -0.02 up to 0.01 [-]. Small values of f led to higher spatial correlation of the shifted data especially in summer. Large values for f showed the opposite trend with lower spatial correlation compared to historical data for all seasons, with maxima during winter. The differences in spatial correlation were lowest in the Alps for all values of f, though this pattern became only visible when the value of f increased.

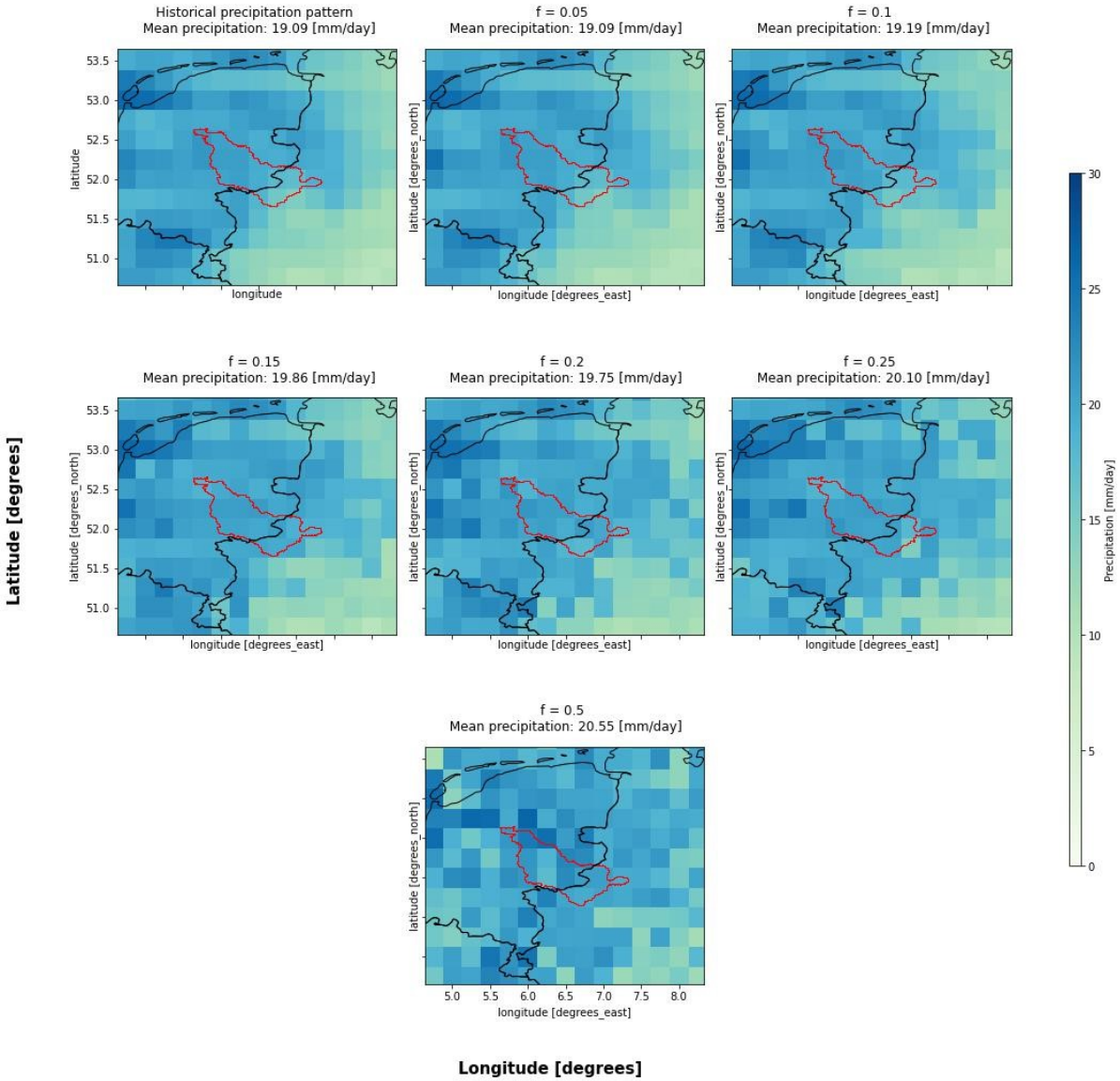

Figure 4.19: Stratiform storm above the Ijssel basin at July 2nd, 1980. Influence of the value of fraction f is shown. Mean values are plotted above each graph.

The above described relation between f and the spatial correlation is a direct result of the modelling approach. By sampling new values of the wind angles randomly from the historical data, the spatial coherence between neighboring cells got partly lost. Even with almost the same historical wind angle, the new proxy angle was chosen from a range of values around the historical value. In the model, no dependence was imposed between the sampled wind angle of the grid cell to the newly sampled angles of its surrounding cells. As such each wind angle was as likely to be chosen creating a more random pattern of displacement vector angles which is directly related to a more random precipitation pattern.

This effect became stronger when the value of f, and thereby the range of possible wind angles to sample from, increased. Only in the Alpine region, almost no difference between spatial correlation values was seen. Both historical and modelled spatial correlation values were low since the orography of this region created local areas separated by mountain ridges having their distinct precipitation and wind angle distributions. As a result, grid cell precipitation values and wind characteristics were not influenced by their neighboring cells and the introduction of additional noise by the model did not change the almost absent spatial correlation in this region.

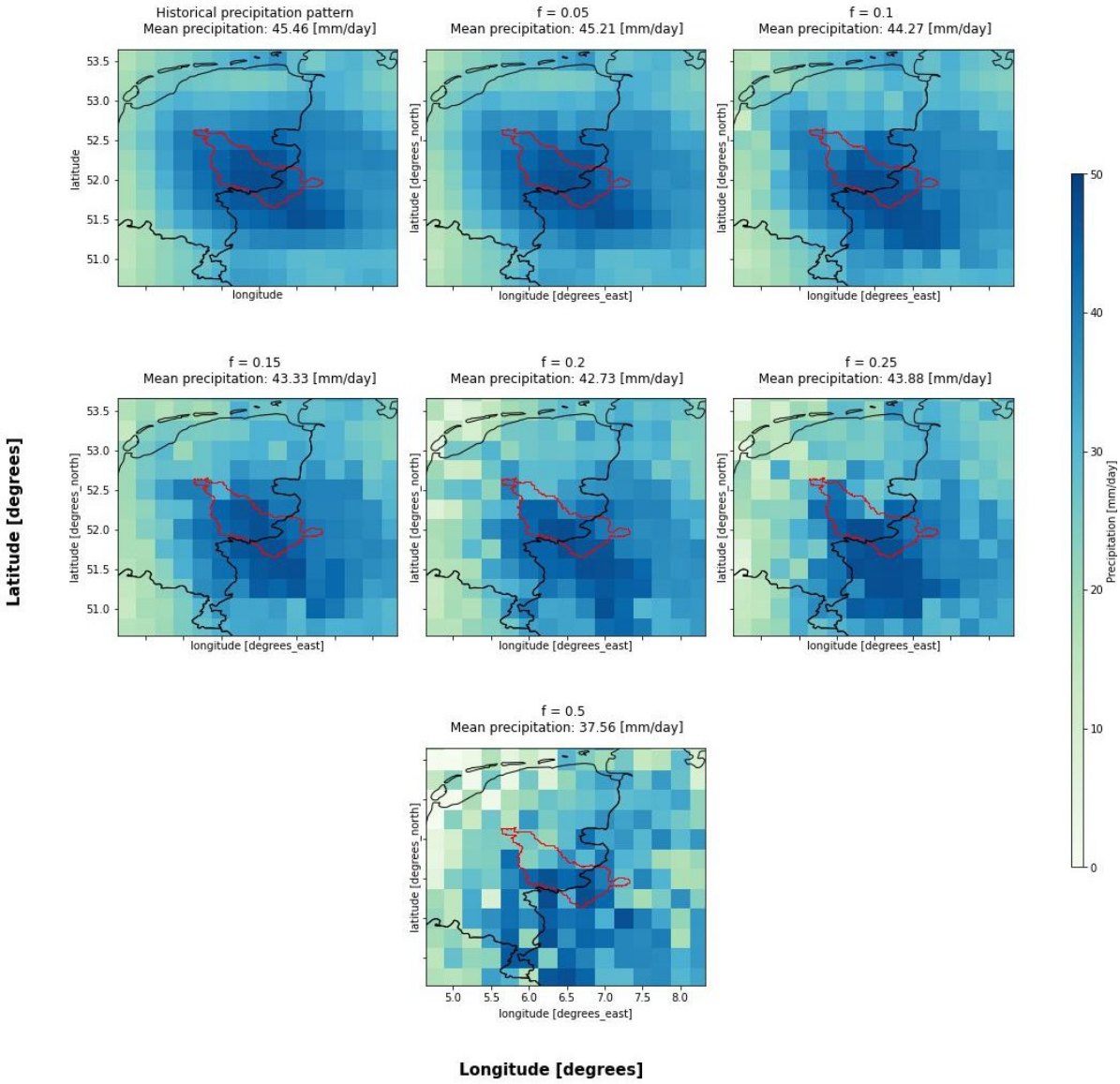

Figure 4.20: Convective storm above the Ijssel basin at September 26th, 1993. Influence of the value of fraction f is shown. Mean values are plotted above each graph.

The mean temporal auto-correlation over the Rhine basin was show to be strongly correlated with the time lag. Largest values were seen for a time lag of one day, after which auto-correlation values dropped quickly (see figure 4.21). For these longer time lags, the lack of temporal correlation in the historical data also resulted in the absence of differences between the historical and modelled correlation. Additional noise created by the model did not reduce the temporal correlation which was already close to zero for the historical data. This is in agreement with the observation made for the almost absent spatial correlation in the Alpine region.

In contrast, for the time lag of one day, differences were observed at higher values of f. The differences were caused by the randomness of sampling, both for the length as well as the direction of the displacement vector. Grid cells in which subsequent sampled displacement vectors were in general similar resulted in higher values of the temporal correlation. Very different displacement vectors resulted in sampling of more diverse precipitation values leading to lower temporal correlations.

Since no relation was imposed to create temporal dependency between days, the pattern of over- or underestimation of the historical correlation by the model was random. Higher values of f did generate more randomness and thereby less consistency in both time and space. This was confirmed by the larger differences between the historical and shifted mean auto-correlation values for higher values of f (compare left and right graph of figure 4.21).

In addition, figure 4.21 shows a clear seasonality. Highest auto-correlation values were seen in winter independent of the time lag and value of fraction f. This can be explained by the stratiform nature of winter storms. These stratiform fronts often cover large areas and have, in general, a relatively continuous and uniform intensity which persists for a long duration. As such, temporal correlation for stratiform storms will be higher, especially compared to convective storms. Convective storms are often local and have a short duration. They are the typical rain showers often observed during the summer season, Their low temporal correlation is also reflected in the lowest correlation values for the summer season, as can be seen in figure 4.21.

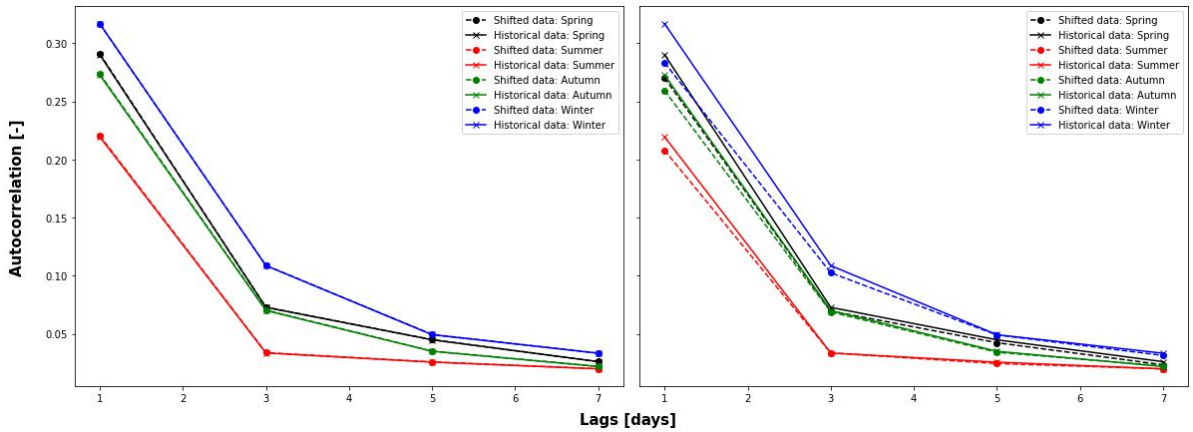

Figure 4.21: Mean auto-correlation over the Rhine basin for the historical and wind based vector shifted precipitation data for f=0.05 (left) and f=0.5 (right). Mean values are shown for time lags of one, three, five and seven days for the four different seasons.

4.4.4. Difference in the mean, maximum and standard deviation of precipitation

The differences in monthly mean precipitation, measured as the historical mean value minus the shifted mean value, increased when the fraction f became larger. Lowest values ranged from -0.5 to 0.5 [mm/day] for f = 0.05, which is 89% and 143% of the historical mean, respectively, while highest values were seen for f = 0.5, ranging from -2.2 to 4.6 [mm/day], which is 41% and 381% of the historical mean (see figure 4.22). Patterns of areas with higher and lower mean precipitation values were consistent over the different values of f. Most extreme differences were seen in the south-east of the basin while differences in the north-west were smaller. Large areas with negative and positive differences were often paired.

This pattern of paired areas can be explained by the general precipitation conditions over the different countries. Comparing the seasonal mean precipitation patterns for Germany [55], France [56] and Italy [57], the areas of underestimation can be related to the areas with high mean precipitation values in the historical data. Permutation resulted in the introduction of lower mean values from the surroundings leading to lower modelled mean precipitation values, i.e. positive differences. The areas in which an overestimation of the mean precipitation was seen were strongly connected to this underestimated areas. Applying the reverse reasoning, these areas were prone to the introduction of higher precipitation values resulting in higher mean values, i.e. negative differences.

With regard to time, it was shown that patterns of mean differences varied over the months. Regarding the whole study area, most widespread differences were seen during October and the winter months. These differences are most likely caused by the prevailing stratiform fronts which are typical for the winter months and span large areas. On grid cell resolution, the most extreme absolute differences were seen during summer when precipitation is often convective and very local. Smallest absolute difference were seen in spring. This observation was made for all values of f.

The difference in maximum precipitation showed the same trend as the mean precipitation. Most extreme differences were again seen below the Alps while in the north the differences were minimal. Between months, patterns differed with varying locations of maximum differences. During the summer months, larger differences were seen more north of the Alps while during winter most extreme difference were observed around the Mediterranean see and in the north of Italy. In addition, differences became larger when the value of f increased. The smallest differences were observed for f = 0.05 and ranged from -45 to 35 [mm/day], i.e. 63% and 179% of the historical values, respectively. For f = 0.5 values from -147 to 126 [mm/day], i.e. 33% and 564% of the historical maximum, respectively, were seen for the most extreme locations (see figure 4.23).

In contrast to the mean values, the patterns observed for the differences in maximum values were very local and more scattered. Differences between neighbouring grid cells were large. A reason for this observation can be found in the methodology underlying the calculation of the differences. These differences are based on the highest values of the historical and observed values in one month. If the shifting approach resulted in the introduction of many low precipitation values into the grid cell at the expense of the historical higher values, the difference will be positive. On the other hand, the introduction of only one very large value will already result in a high negative value since this value will be selected as the monthly maximum. As such, the differences in maxima are more random and depend on the spatial shifting approach. A new round of iterations of model 3 will therefore likely result in a new pattern of observed differences in maxima while the mean patterns will remain approximately the same.

Also the differences in standard deviation showed a positive correlation with the value of fraction f. Larger values of f resulted in larger differences with maxima ranging from -4.42 (55%) to 6.74 [mm/day] (218%) for f = 0.5 and a minimum range of -1.1 (91%) and 1.12 [mm/day] (115%) for f = 0.05. Differences were also larger in the south of the study area, below the Alps, while difference in the north were small. Most extreme differences were seen in October, November, December and January.

The patterns of the differences in standard deviation showed a large similarity with the patterns observed for the mean differences. Areas with negative differences in standard deviation, i.e. larger variation in the vector shifted data compared to the historical data, had larger negative difference in mean precipitation as well. Since the standard deviation is based on the spread of values, the similarity in patterns is caused by the reduction of the magnitude of extremes caused by spatial permutation. As can be seen in appendix V, spatial shifting led to the reduction of the most extreme events over larger areas. This created lower mean values and precipitation values closer to each other. The spread of values and thereby the standard deviation will reduce. This similar response of the mean and the standard deviation to the reduction of the magnitude of extremes resulted in the alike patterns observed for both characteristics.

When considering the standard deviation of mean precipitation values over the different basins for each month, it was observed that shifted standard deviations are in general smaller than the historical standard deviations. The higher the value of fraction f, the smaller the standard deviation over the basin and the larger the positive difference between the historical and shifted standard deviation. This observation can be justified with the same reasoning as the reduced standard deviation on grid cell resolution as described in the paragraph above. Larger values of f led to more disruption and thereby a more extreme reduction of the magnitude of precipitation extremes and the spread of the modelled means, i.e. the standard deviations.

On top, the difference between the modelled and historical standard deviation became smaller when aggregation time increased. On the one hand, this is due to the fact that the standard deviations of longer aggregation times were in general smaller compared to shorter aggregation times. On the other hand, and the direct cause of the smaller standard deviations, is the fact that extremes for longer aggregation times are less extreme compared to shorter aggregation times. As consequence of the summations of multiple days of precipitation, very rainy days are averaged by dryer days in the same time series. This is the case for both the historical data series as well as the shifted data series. Disruption still resulted in some reduction of the most rainy days, but the effect was less visible compared to the shorter duration events.

Last, a strong relation between standard deviation and basin size was observed. Smaller basins did react more strongly on spatial permutation reflected by the varying and even negative values of the difference in standard deviation. Especially in summer months, in which convective storms were more common, spatial permutation led to introduction of larger extremes by shifting convective storms over or out of the small basin. Larger basins did not show this response since the model did not move precipitation over distances large enough to introduce or exclude complete new precipitation fields. The difference in standard deviation for the Rhine basin remained almost constant over the seasons with a slight increase during winter. As such, this indicates that spatial permutation can be especially useful when the area of interest is small. Even small and likely precipitation shifts resulted in more variation in the observed precipitation values, which is not the case for larger basins.

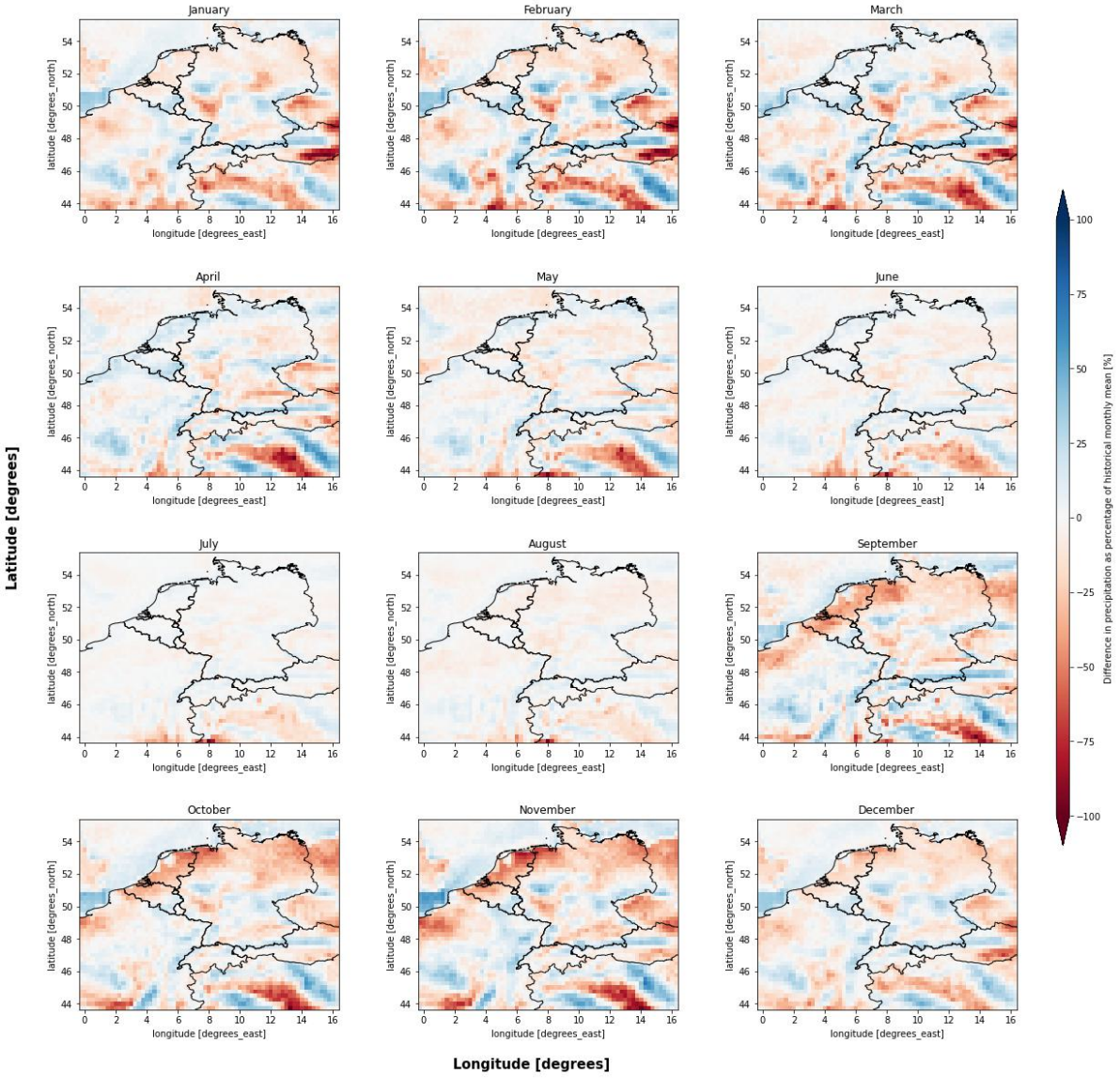

Figure 4.22: Monthly difference between historical and wind based vector shifted mean precipitation for f = 0.5. Differences are calculated as historical minus vector shifted mean precipitation and shown as percentage of the historical monthly mean.

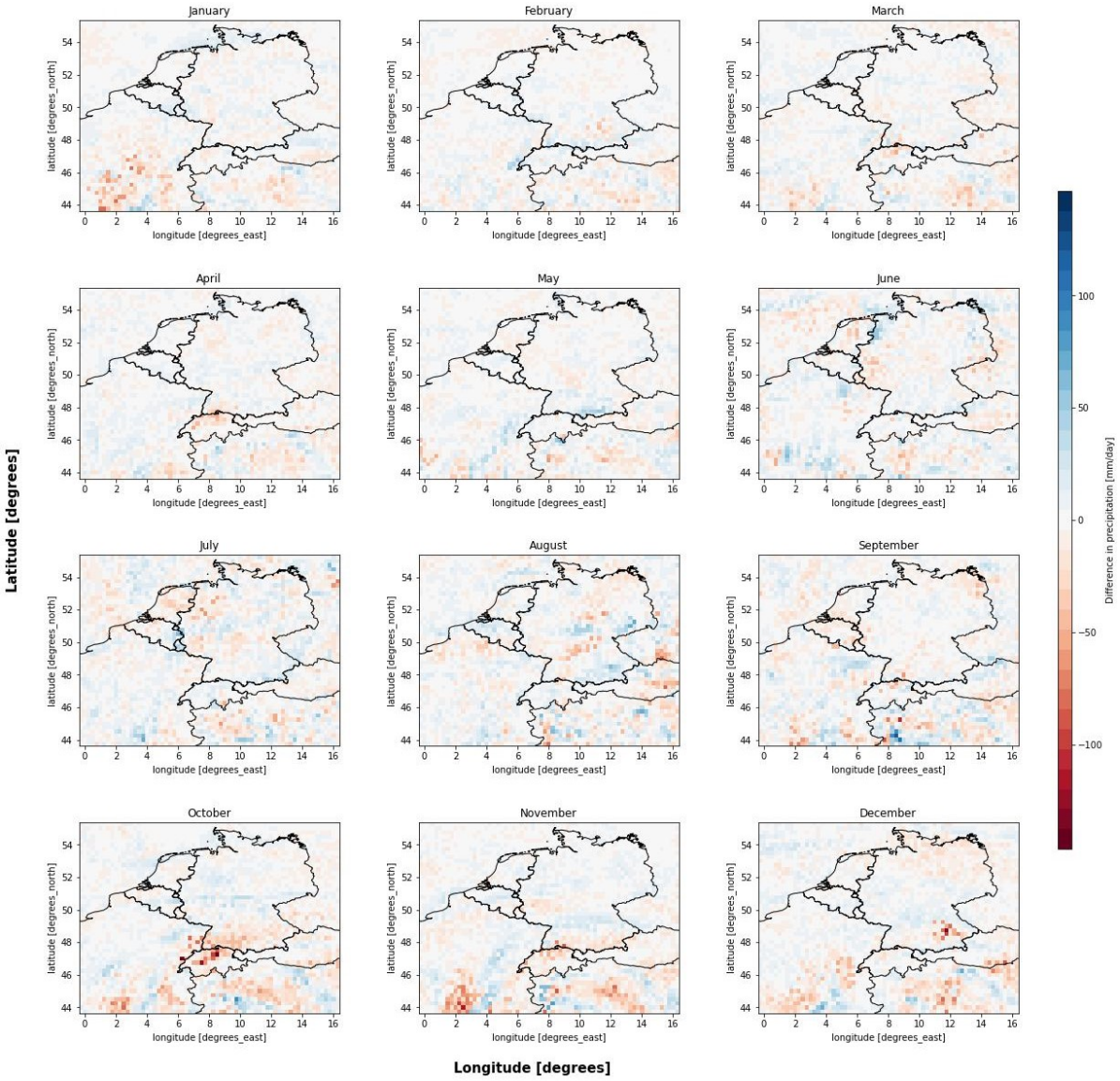

Figure 4.23: Maximum monthly difference between historical and wind based vector shifted maximum precipitation for f = 0.5. Differences are calculated as historical minus vector shifted maximum precipitation.

4.4.5. Comparison of historical and model wind angles

The historical and model wind angles showed a similar pattern for the locations tested. The model was able to mimic the distribution of angles for both mountainous areas, e.g. Bern (Swiss), and lowlands, e.g. Munster (Germany) (see appendix VI). For Bern it was observed that most common angles were either under- or oversampled. This could be caused by the distinct groups of wind speeds and -angles in mountainous areas (see figure VII.1) which made the probability to sample an angle outside the group of the initial historical angle low . Even with larger bounds as set by the fraction f, not much sampling outside the groups could take place. As a result, most deviation was seen in the most preferred angles while the fit is better for areas with relatively rare angle and wind speed combinations.

For Munster, located in a low land area, a slight oversampling of the historical wind speeds and angles was observed for the less common angles. This opposed effect to the observations made for Bern can be explained by the fact that in low land areas wind speeds and angles are more evenly distributed (see figure VII.2). This allowed for sampling over a wider range of wind speeds and angles which created more variation in the sampled wind angles, especially around the sides of the most prevailing groups of angles in the histogram. Though, difference between f = 0.1 and f = 0.5 were not large. This can be an indication that even with small values of f, the sampling range for angles and wind speeds is already large enough to sample further outside the most distinct groups of angles.

4.4.6. Extent of variation

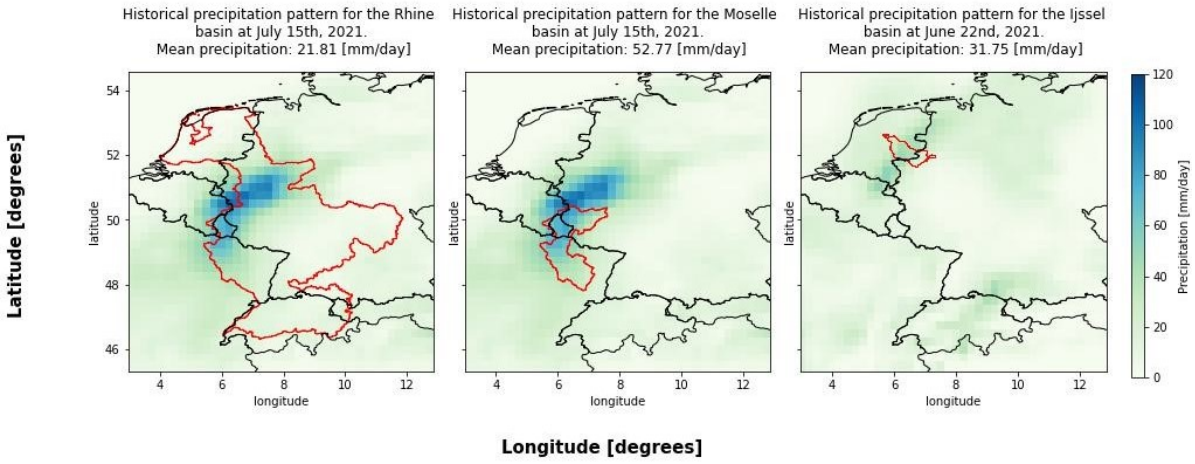

Figure 4.24: The historical precipitation patterns for the single most extreme events in 2021 for each individual basin. From left to right: Rhine, Moselle and Ijssel.

For the most extreme event of each basin, it was examined how much variation the model was able to add with different values of f. Figure 4.24 shows the historical precipitation patterns of the most extreme event of each basin in 2021. The histograms obtained for each basin showed a clear pattern (see figure 4.25). Larger values of f resulted in a larger spread of extreme values indicated by a higher standard deviation of the extreme. Lowest standard deviations for each value of f were observed for the Rhine basin and increased when basin size became smaller (see figure 4.25 A and D).

The histograms of the Rhine basin were extremely right-skewed, indicating that most modelled extremes were larger than the historical observed extreme. An explanation for the skewness can be seen in the historical precipitation pattern (see figure 4.24). The center of the low pressure area was located on the west of the basin. Since the prevailing wind direction during the summer months is south-west, the model will likely sample angles from this direction and thereby shifting the low pressure area more to the east, e.g. over the Rhine basin. As a result, mean precipitation values increased. Larger increases were seen when the value of f became higher since the length of the displacement vectors was allowed to be longer moving the event further over the basin.

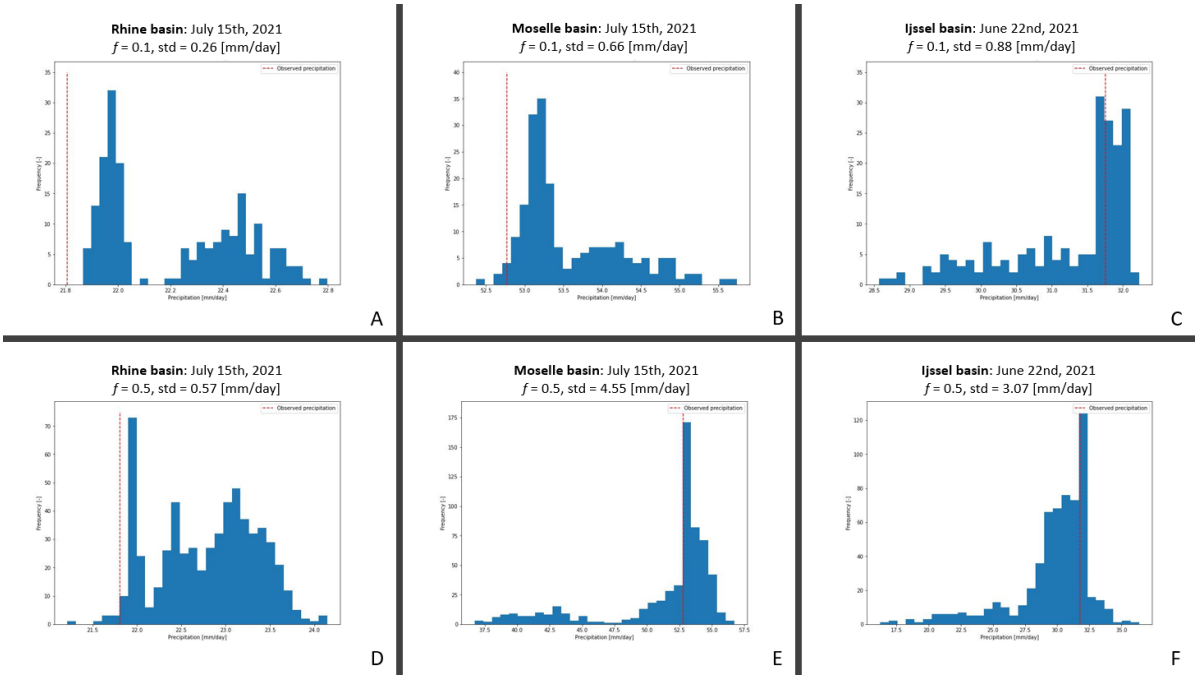

Figure 4.25: Histograms of the variation of 100 runs for the most extreme event in each basin in 2021. Top row shows the results for f = 0.1. Bottom row shows the results for f = 0.5. From left to right: Rhine (July 15th), Moselle (July, 15hth) and Ijssel (June, 22nd)

For the Moselle a transition form a right-skewed histogram, with mostly higher values for the modelled extremes, to a left-skewed histogram, with mostly lower values for the modelled extremes, was observed when the value of f increased (see figure 4.25 B and E). The relation between the shape of the histogram and the value of f can be explained by the limits to the direction and distance of the permutation as opposed by the value of f. Based on a similar reasoning as for the Rhine basin, it can be seen in figure 4.24 that small values of f can shift the center of the precipitation event more over the north side of the basin. This resulted in higher mean values up to 55.75 [mm/day] compared to the historical 52.75 [mm/day] (see figure 4.25). However, when the value of f became large two distinct options were observed. For some iterations, the precipitation event was scattered with the introduction of many low values over the basin resulting in lower mean values and a more left-skewed histogram. The opposite was also seen in other iterations in which the scattered patterns introduced more high precipitation values over the basin. However, mean reductions were more severe compared to mean increases which is likely caused by the prevailing south-west wind angles which promote the shift of the event away from the Moselle basin.

The Ijssel basin showed a left-skewed histogram for all values of f (see figure 4.25 C and F). This indicated that the model produced mostly less extreme precipitation values compared to the historical observed value. The reason for the reduction of the extreme can be found in the location of the historical event which was straight above the basin (see figure 4.24). Even small shifts resulted mainly in the reduction of the mean value observed by introducing lower values of the surrounding grid cells. It therefore needs to be noticed that a larger standard deviations does not mean that there are also more extremes introduced. The standard deviation is a metric which does indicate the spread and thereby the influence of spatial permutation on the observed data. However, it does not give information about the magnitude of the observed values. The magnitude will mainly depend on the position of the historical extremes relative to the basin and the prevailing wind angles. For that reason, the ability of the model to generate more extreme events will depend on the diversity and length of the historical data set. Only when the historical patterns provide sufficient variety in extremes and wind angles, the model will be able to generate new extremes.

4.4.7. Influence on the July 2021 flood

Figure 4.26 displays the influence of the model on the July 15th, 2021 event in the Moselle basin. The results showed that the mean precipitation became higher for the lower values of f. The mean value was increased due to the shifting of cells with larger amounts of precipitation over the basin. Lower mean precipitation values were seen when the value of f increased since lower precipitation values were shifted over the basin originating from location outside of the low pressure area. The amount of disruption showed a positive correlation with the value of f, leading to a loss of spatial correlation for the highest values of f. This indicates that for the modelling approach of model 3 only small values of f can be used to add more variation. Too large values cause to much disruption of the spatial pattern leading to unrealistic precipitation patterns as was seen for the July, 2021 event.

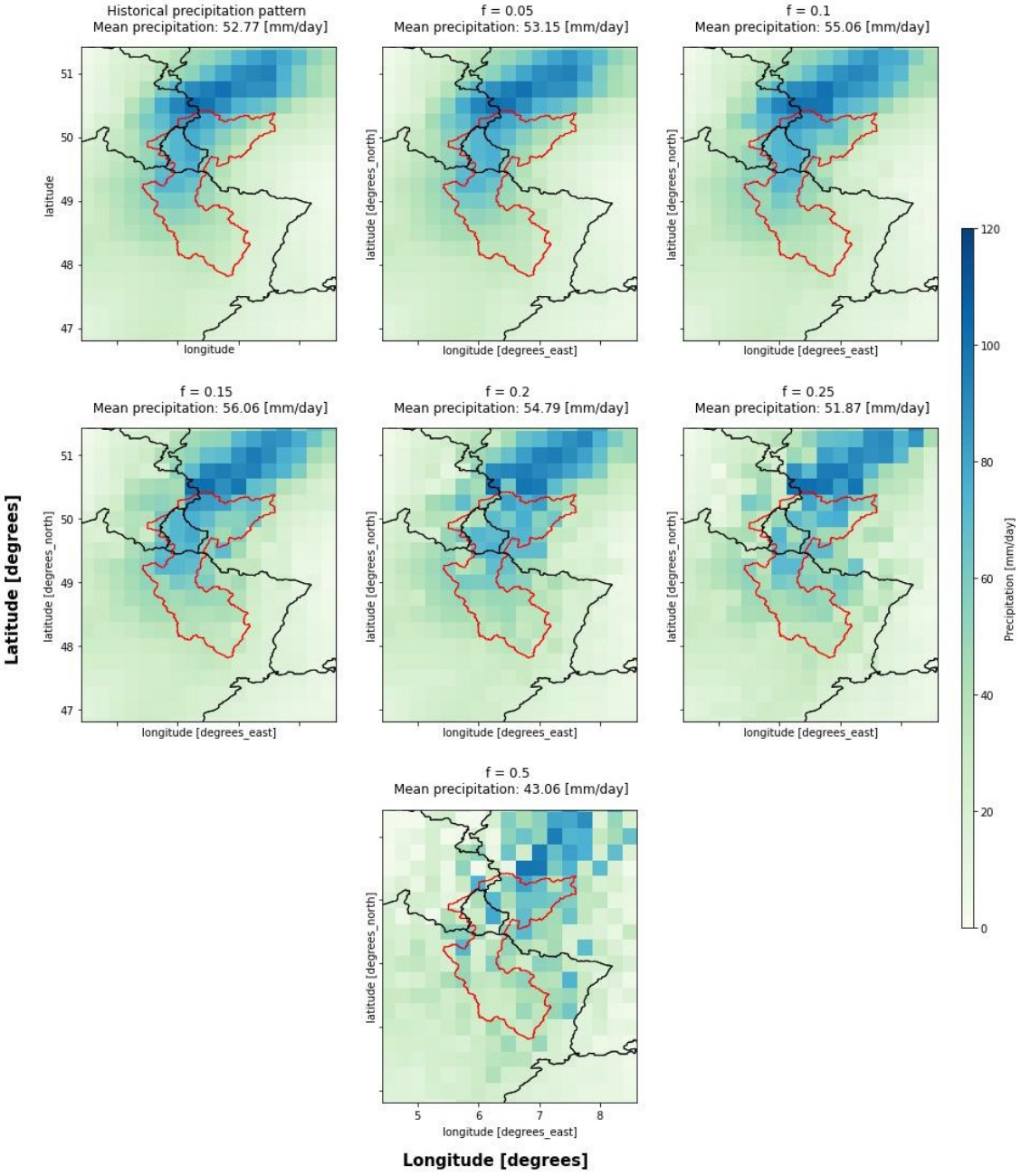

Figure 4.26: Visual representation of the effect of model 3 on the modelled precipitation in the Moselle catchment on July 15th, 2021. Shifts are shown for all values of fraction f.

Summary model 3

- The Generalized Extreme Value (GEV) fit to the shifted data showed the same response to aggregation time, basin size and introduced variation as research model 2. The GEV fits were not sensitive to the value of fraction f.
- The difference between the historical and shifted cumulative distribution functions (cdfs) became larger when fraction f increased for the Moselle and Rhine basin. For the Ijssel basin, no response in the shifted cdf curve to the value of fraction f was observed.
- The correlation between observed and modelled mean precipitation values increased when fraction f increased for all combinations of basin and aggregation time tested.
- Spatial and temporal correlation were reduced when the value of f increased as result of the loss of coherence of the observed precipitation patterns.
- Larger values for fraction f resulted in larger differences between the historical and shifted precipitation mean, maximum and standard deviation. Explanations could be found in the underlying methodology for the maximum values, while disturbed rainfall characteristics where the reason for larger differences between the historical and shifted mean and standard deviation of precipitation.
- The methodology of model 3 was able to produce displacement vectors with the same distribution of angles as the historical wind angle distribution.
- The amount of variation added to the historical observed extremes became higher when fraction f increased. However, the magnitude of the shifted extremes depended on basin size and shifting direction.
- Temporal and spatial correlation was not explicitly incorporated in the methodology of model 3. This resulted in a trade-off between the amount of variation introduced and the similarity between the historical and shifted precipitation characteristics. Future attempts should focus on incorporating correlation more explicitly to reduce this trade-off.

5

Project discussion

The central objective of this research was to examine the effects and benefits of spatial permutation on the generation of new extreme precipitation events in the Rhine basin. In the past, much research has been done the the generation of new extreme events with temporal resampling. By means of creating similar groups of weather patterns, historical data was resampled into new precipitation series. The largest drawback of this method is that it will not introduce new extremes with durations shorter than the temporal resolution of the historical data. As such, especially small basins with times of concentration shorter than the temporal resolution of the precipitation data will not be exposed to new and more extreme values.

Spatial permutation was therefore proposed as a new methodology to introduce extreme events from surrounding areas into the area of interest. Recent extreme precipitation events have shown that especially very local and not yet observed rainfall configurations can have a severe impact on local communities. This led to a growing demand for more local, varying and extreme precipitation series which can be used for risk analysis. Yet, substantiated permutation is a difficult topic. The occurrences and characteristics of precipitation have been shown to be highly dependent on the prevailing circumstances and location [32], [36], [43]. In addition, most research into the opportunities of spatial permutation is limited to local scale initiatives [8] and knowledge about the potential of larger scale spatial permutation is scarce. Consequently, this research was set up with a clear gradient of complexity in the models generated to analyse step by step the potential of spatial permutation.

The first step in this process was the development of research model 1 which showed that spatial permutation does affect precipitation statistics but that basin size, aggregation time and direction influence the results. Especially the confirmation that direction is of importance for spatial permutation was an important finding which has not been seen back that clearly in research model 2 and model 3. The main reason is the fact that only in research model 1 the direction of shifts was known precisely. As such, observed changes in statistics and extremes could be related to direction or other causing factors without the noise created by a more random approach as was used in the subsequent models.

In addition, research model 1 has been the only model in this research for which time series longer than 42 years were generated, i.e 378 years. In retrospective, it would be advised to generate longer time series for the two other models as well, especially for the analysis of the cdf distributions. The parameters fitted for this process do depend on the sample size, since their sensitivity to outliers increase when sample size is relatively small [58]. This sensitivity was especially observed for the Ijssel basin which had some very extreme events in the historical data series. As such, comparison of the cdfs and conclusions drawn from their corresponding AD-test statistics should be considered with care. For the GEV distributions, results can be considered more robust even for the small sample size. Hossain *et.al.* [59] showed that using L-moments as parameter estimation technique was less sensitive to small sample sizes, outliers and variability compared to other techniques like the maximum likelihood estimate and the Bayesian method.

Besides the findings done based on research model 1 and the generation of longer data series compared to the other models, it must be noticed that the shifts applied are far from realistic. Low pressure areas associated with extreme rainfall do often follow preferred tracks which are non-linear and depend on the location of origin [60]. In addition, they are impacted by the presence of orographic elements like the Alps, which was not considered in the shifting methodology of research model 1. Therefore, research model 2 was developed in which a deepening step was made to study how precipitation can be moved in a more physical and realistic way.

The added level of complexity in research model 2 compared to research model 1 was created by shifting from a fixed permutation based approach to a vector based approach. The choice to use vectors to shift precipitation was based on the notion that wind data are leading for precipitation movement [8] [61]. Their direction and speed can be quantified and visualized by means of vectors, and with the methodology of research model 2 these patterns could be mimicked. Yet, the resulting vector fields did highly depend on the choices made for the model parameters. Whereas the effect of the parameter for the upper and lower limit m on the vector length could be clearly seen in the resulting vector field, the response to the weights used and the range parameter r was more complex.

Nevertheless, understanding the complexity of the range, limit and the weights was important since these parameters reflect two important characteristics of precipitation movement: spatial and temporal correlation. Spatial correlation of precipitation depends on the location of interest. In low land areas coherence is generally high and the vector in a grid cell is influenced by and does influence the values of vectors in its neighboring cells to a large extent. This leads to the often observed large stretch vector fields such as the westerlies over Northern Europe. In mountainous areas, spatial correlation can be much lower as result of orographic separation of different areas and the local effects of topography. Subsequently, the influence of one grid cell on its surrounding grid cells will be less [62]. These correlation patterns observed in the wind vector fields influence the precipitation patterns in these regions directly and are therefore important to capture in the model. Though, research model 2 allowed for imposing a degree of spatial correlation by increasing or decreasing the value of r, no variations of this value for different grid cells could be set. This led to the loss of variability characteristics especially when comparing distinct orographic regions.

A way forward would be to condition the parameters m and r on historical observed characteristics of precipitation, like the wind data used in model 3. In such, the strength of research model 2 to include spatial and temporal correlation will be maintained while at the same time introducing seasonality and spatial variable characteristics into the model. Nevertheless, the methodology of research model 2 also need to be redefined to limit the effect of the modelling direction on the final results. Starting with an initial field of zeros and equalizing the weights used will be the first steps. Further options need to be researched.

In model 3, the use of historical wind data as starting point did account to a certain extent for the variability of spatial correlation of vectors over the study area. The historical wind data clearly showed a reduced spatial correlation over the Alps while high values were seen over the low lands of northern Europe. However, the diversity of sampling options for new angles could be high when the value of fraction f, determining the sampling limits of the proxy vectors, increased or when natural variability was already large in the grid cell. This, together with the lack of any spatial correlation relation imposed in the model, led to a reduction of spatial correlation in the modelled displacement vector fields. For the largest values of f, this was confirmed by the loss of spatial coherence of the precipitation events. An improvement of the model could therefore be made by imposing a spatial correlation relation on the chosen displacement vectors. This relation can have many formats but options include:

1. To keep the historical wind angle and only varying the length of the displacement vector.
2. To impose a second round of iterations over the displacement vectors and calculate the average $D_x\left(\vec{V_p}\right)$ and $D_y\left(\vec{V_p}\right)$ based on N of the surrounding grid cells. N will be set larger if spatial correlation is high in the historical data and smaller when spatial correlation can be considered low (see appendix VIII.1).

The loss of temporal correlation is related to the loss of spatial correlation and will likely improve when a spatial correlation is represented better on a cell-by-cell basis, However, for the current method the same discussion point holds. In research model 2, temporal correlation was maintained to a certain extent by imposing weights on the past and present vector values. The research model was highly sensitive to the choice of the weights and a well argued reasoning for the choice of weights is needed to use this methodology in a more physical based approach. Using the historical temporal correlation coefficients can be one option to relate past and present. Especially since the auto-correlation between precipitation values was shown to be highest over a time step of one day, this would fit into the current methodology applied in model 3 which also has a time step of one day. A weighted selection method should than be developed for the permutations $D_x\left(\vec{V_p}\right)$ and $D_y\left(\vec{V_p}\right)$ at time *t = t*. Vectors with the same direction and with a similar value of wind speed as the proxy vector sampled at time step *t = t-1* will be given a higher probability to be sampled as a new proxy vector at time *t = t* (see appendix VIII.2).

Considering the outcomes of model 3 a clear trade-off between the noise generated by the value of f and the similarity of the historical and modelled precipitation and vector fields was seen. The same was also observed for the values of m and r in research model 2. More noise resulted in less similarity and vice versa. The optimal ratio between these two standards is disputable. On the one hand, more noise means a higher probability that new extremes are generated which is the final purpose of the spatial shifting approach and can be useful for a better representation of the current weather pattern in risk modelling. On the other hand, the modelled precipitation and vector patterns need to maintain a certain similarity with the historical patterns to maintain their credibility. To much deviation points towards violation of physical boundaries which are present in reality. This is unwanted and will make the model more controversial for further applications.

Finding the optimal balance between noise and similarity is important but will to a certain point always be a subjective choice of the modeller. Providing scenarios with different combination of parameters can be a good way to leave the choice of the optimal value to the final user. Clear communication about the influential parameters, which sensitivity can be derived by additional sensitivity studies, and the trade-offs between different standards is in that case indispensable. For further studies a closer look into the acceptable range of noise and similarity is therefore advised. Together with the generation of longer time series and more explicit incorporation of temporal and spatial correlation, this information is expected to improve the spatial shifting approach as proposed in model 3.

Yet, despite the improvements proposed, it is believed that the application of the spatial permutation methodology of model 3 can already be an useful contribution to the toolbox of weather generators. In contrast to research models 1 and 2 it has been shown that model 3 could permute precipitation in a substantiated and credible way. No fixed shifting direction or distances was needed and the methodology did not heavily rely on underlying assumptions except for the choice of fraction f. Besides, it maintained the characteristics of the historical precipitation patterns while at the same time generated new extremes in different regions of the study area. The methodology also gives way to a broader use on pan-European scale as long as sufficient wind data is available. However, careful examination of the results, especially in orographically complex areas, is advised to ensure that the model does not introduce physical unrealistic new precipitation events.

Finally, the results have shown that especially smaller basins, with times of concentration higher than the temporal resolution of the data, can benefit from the introduction of new extremes from neighbouring locations. For larger basins the direct effect was less but potential can be seen in the combination of a spatial and a temporal sampling approach. New time series can be generated by temporal resampling and an additional iteration with spatial resampling can generate supplementary variation. This will make the rainfall series useful for both small and large catchments. The final effect of a combined approach will need to be proven by subsequent research into the opportunities which spatial resampling can offer.

Summary project discussion

- Research model 1 showed that permutation direction, distance, aggregation time and basin size determine the outcome of the model. The longer time series generated by research model 1 made the statistical analysis more robust, though care should be taken about the dependency between the observed extremes.

- Research model 2 showed that precipitation can be shifted based on semi-random vectors. It provided a framework for including spatial and temporal correlation explicitly in the generated vector fields.

- Research model 2 was sensitive to the initial and boundary conditions. Therefore, it is recommended to base the value of the independent variables limit m and range r on historical observed physical parameters like wind direction and -speed.

- Model 3 proofed that wind direction and -speed can be used to condition displacement vectors. However, a large trade-off was observed between the number of newly generated extremes and the similarity between the historical and modelled rainfall characteristics.

- To reduce this trade-off it is recommended to include spatial and temporal correlation more explicitly in the methodology of model 3. Options suggested include:

  - Maintain the historical wind angle for each displacement vector. Only vary the length.
  - Use a convolution matrix to equalize the displacement vectors after their creation (see appendix VIII.1).
  - Use a weighted selection method for the displacement vectors of the current day based on the displacement vectors of the day before (see appendix VIII.2).

  It is expected that the quality of the temporal correlation will benefit from the improvement of the spatial correlation and visa versa.

- To apply spatial permutation on Pan-European scale, research model 2 and model 3 are considered suitable. However, sufficient (wind)data and improvement of the methodologies to reduce the drawbacks as described above is recommended to increase the quality of the results.

- For future research it is advised to look into the possibilities to combine the current temporal resampling algorithms with the developed spatial permutation approaches. As such, it is foreseen that generated data series will be more divers and suitable for risk assessment in both small and large areas.

6

Conclusion

Weather generators (WGs) are powerful models which are used to generate long term precipitation series for flood risk analysis. They are based on different types of temporal resampling algorithms which combine similar days into new weather sequences. Their use has been proven useful for large basins with a time of concentration longer than the temporal resolution of the precipitation data. For smaller areas, temporal resampling is not able to generate new extreme events since the time of concentration is shorter than the temporal resolution. As such, no more extreme values can be observed than the maxima in the historical data. Yet, during last years local and severe storms have shown their devastating effect on local communities. These storms had never been observed before but their frequency is expected to increase due to climate change. This raised the question whether spatial permutation could contribute to a better representation of these local extremes in long term weather series.

To answer this question for the Rhine basin, four different consecutive research questions were formulated. Each question provided information for the next question. In the first part, a literature review described the main characteristics of precipitation regimes. Regimes can be distinguished by their temporal and spatial variability and the precipitation amounts observed. The main factors influencing precipitation regimes are atmospheric circulation patterns, topography and climate change and their influence depends on location and season. Combining the characteristics and influencing factors resulted in the subdivision of Europe in seven different areas. The Rhine basin was located in two of them. The biggest part concerned Western Europe characterized by prevailing westerlies, low wind speeds, relative flat orography and mean precipitation values around 5 [mm/day]. The Alps formed the second area distinguished by varying mean precipitation values over the months, large orographic elements, low wind speeds and very divers wind directions.

In the second part, fixed spatial permutation proved that shifting does affect extreme precipitation patterns and statistics. A strong dependence of direction was confirmed when the area of interested covered distinct precipitation regimes, e.g. the Rhine basin. Small basins reacted more strongly on spatial permutation with a larger variation in modelled extremes. This demonstrated that spatial permutation can be particularly useful to introduce more variability in precipitation for small basins. An increase in shifting distance resulted in larger difference between historical and modelled precipitation, while aggregation time showed the opposite relation. Nevertheless, the fixed approach conflicted with the highly dynamic character of precipitation as described in the literature review. This contradiction was addressed in the third part.

The third part showed that a more random vector based approach can be used to move precipitation more naturally over the Rhine basin. Strongest effects on extreme precipitation were again seen for small basins and short aggregation times. In addition, spatial and temporal correlation was incorporated in the methodology and was shown to be important for coherent precipitation shifting. A lack of correlation resulted in highly scattered precipitation patterns.

However, the sensitivity of the model to the weights assigned, the direction of calculations, the initial and boundary conditions caused the outcomes of research model 2 to be highly dependent on the assumptions made. To reduce the influence of these assumptions a more physically based methodology was developed.

Historical wind vectors formed the physical base of the last model developed in this research approach. Observed angles and speeds were used to conditions the displacement vectors. The variation between historical and displacement vectors was set by the fraction f and was proved to influence the results strongly. Too high values created non-coherent precipitation patterns while too low values constrained the capability of the model to generate new extremes. Spatial and temporal correlation was lost by the lack of the methodology to take this explicitly into account. Nevertheless, the main characteristics and influencing factors of precipitation regimes could be mimicked by the generated displacement vector fields. Thereby, model 3 was considered to have a high potential for substantiated permutation of precipitation.

To harvest the potential of spatial permutation and to contribute to a better representation of very local, destructive precipitation events in stochastic weather series several steps were suggested. First, spatial correlation of displacement vectors should be accounted for preferably with the possibility to alter correlation values depending on the grid cell location and season. Values can be extracted from historical precipitation sorted by season and related to distance by variogram analysis. Auto-correlation should be taken into consideration especially over short durations, i.e. one day, though a better representation of spatial correlation is expected to already contribute to this objective. Furthermore, the justifiable ratio between noise and variation remains a point of interest and research into optimization of these standards will contribute to a better transparency of the model results. Last, a promising contribution of spatial resampling was seen in combination with temporal resampling. The effects of this combination of both temporal and spatial variation are not known. However, many applications are anticipated for areas of interest concerning both small and large catchments spread over different precipitation regimes.

References

[1] EPA, *Climate change indicators: Heavy precipitation*, 2021. [Online]. Available: https://www.epa.gov/climate-indicators/climate-change-indicators-heavy-precipitation#tab-5 (visited on 06/01/2022).

[2] J. De Ceulaer, *Overstromingen in belgië en buurlanden zijn op één na duurste natuurramp van 2021*, 2021. [Online]. Available: https://www.demorgen.be/nieuws/overstromingen-in-belgie-en-buurlanden-zijn-op-een-na-duurste-natuurramp-van-2021~bec71362/?referrer=https%3A%2F%2Fwww.google.com%2F (visited on 06/01/2022).

[3] B. Jongman, S. Hochrainer-Stigler, L. Feyen, *et al.*, "Increasing stress on disaster-risk finance due to large floods," *Nature Climate Change*, vol. 4, no. 1, pp. 264–268, 2014, 10.1038/NCLIMATE2124.

[4] D. Maraun and M. Widmann, "Weather generators," in *Statistical Downscaling and Bias Correction for Climate Research*. Cambridge University Press, 2018, pp. 201–219. DOI: 10.1017/9781107588783.014.

[5] B. Wright, J. Smith, G. Villarini, and M. Baeck, "Estimating the frequency of extreme rainfall using weather radar and stochastic storm transposition," *Journal of Hydrology*, vol. 488, no. -, pp. 150–165, 2013, http://dx.doi.org/10.1016/j.jhydrol.2013.03.003.

[6] K. Breinl, T. Turkington, and M. Stowasser, "Stochastic generation of multi-site daily precipitation for applications in risk management," *Journal of Hydrology*, vol. 498, no. -, pp. 23–35, 2013, https://doi.org/10.1016/j.jhydrol.2013.06.015.

[7] V. Nguyen, B. Merz, Y. Hundecha, U. Haberlandt, and S. Vorogushyn, "Comprehensive evaluation of an improved large-scale multi-site weather generator for germany," *International Journal of Climatology*, vol. 12, no. -, pp. 4933–4956, 2021, 10.1002/joc.7107.

[8] U. Haberlandt, A.-D. Ebner von Eschenbach, and I. Buchwald, "A space-time hybrid hourly rainfall model for derived flood frequency analysis," *Hydrology and Earth System Sciences*, vol. 12, no. 6, pp. 1353–1367, 2008. DOI: 10.5194/hess-12-1353-2008. [Online]. Available: https://hess.copernicus.org/articles/12/1353/2008/.

[9] K. Slager. "High water in limburg in the summer of 2021 had more impact than river floods in 1993 and 1995." (2021), [Online]. Available: https://www.deltares.nl/en/news/high-water-in-limburg-in-the-summer-of-2021-had-more-impact-than-river-floods-in-1993-and-1995/.

[10] G. Arduino, P. Reggiana, and E. Todini, "Recent advances in flood forecasting and flood risk assessment," *Hydrology and Earth System Sciences*, vol. 9, no. 4, pp. 280–284, 2005, https://doi.org/10.5194/hess-9-280-2005.

[11] P. Eagleson, "Dynamics of flood frequency," *Water Resources Research*, vol. 8, no. 4, pp. 878–898, 1972, https://doi.org/10.1029/WR008i004p00878.

[12] S. Ullrich, M. Hegnauer, D. Nguyen, B. Merz, J. Kwadijk, and S. Vorogyshyn, "Comparative evaluation of two types of stochastic weather generators for synthetic precipitation in the rhine basin," *Journal of Hydrology*, vol. 601, no. -, pp. 69–85, 2021.

[13] J. Skamarock W.C.and Klemp, J. Dudhia, D. Gill, *et al.*, "A description of the advanced research wrf," *NCAR Technical Note NCAR/TN-475+STR*, vol. 3, no. -, 2008, https://doi.org/10.5065/D68S4MVH.

[14] V. Nourani and N. Farboudfam, "Rainfall time series disaggregation in mountainous regions using hybrid wavelet-artificial intelligence methods," *Water Resources Research*, vol. 168, no. -, pp. 306–318, 2019, https://doi.org/10.1016/j.envres.2018.10.012.

[15] F. Serinaldi and C. Kilsby, “Simulating daily rainfall fields over large areas for collective risk estimation,” *Journal of Hydrology*, vol. 512, no. -, pp. 285–302, 2014, http://dx.doi.org/10.1016/j.jhydrol.2014.02.043.

[16] M. Booij, “Extreme daily precipitation in western europe with climate change at appropriate spatial scales,” *International Journal of Climatology*, vol. 22, no. -, pp. 69–85, 2002, 10.1002/joc.715.

[17] M. Dubrovsky, “Creating daily weather series with use of the weather generator,” *Environmetrics*, vol. 8, no. 5, pp. 409–425, 2013, https://doi-org.tudelft.idm.oclc.org/10.1002/(SICI)1099-095X(199709/10)8:5<409::AID-ENV261>3.0.CO;2-0.

[18] H. Yeo, S.-J. Park, B. M. Kim, *et al.*, “The observed relationship of cloud to surface longwave radiation and air temperature at ny-ålesund, svalbard,” *Tellus B: Chemical and Physical Meteorology*, vol. 70, p. 1 450 589, Jan. 2018. DOI: 10.1080/16000889.2018.1450589.

[19] H. Henderson-Sellers and K. McGuffie, “North atlantic oscillation,” in *The future of the world’s climate*. Elsevier Science, 2012, ISBN: 978-0-12-386917-3. DOI: https://doi.org/10.1016/C2010-0-67318-4.

[20] H. Hersbach, B. Bell, P. Berrisford, *et al.*, “Era5 hourly data on pressure levels from 1979 to present,” *Copernicus Climate Change Service (C3S) Climate Data Store (CDS)*, Jun. 14, 2018, https://doi.org/10.1038/s41558-018-0260-4. [Online]. Available: https://cds.climate.copernicus.eu/cdsapp#!/dataset/reanalysis-era5-pressure-levels?tab=overview (visited on 05/25/2022).

[21] N. Earth, *Admin 0 – countries*, 2018. [Online]. Available: https://www.naturalearthdata.com/downloads/10m-cultural-vectors/10m-admin-0-countries/ (visited on 05/25/2022).

[22] J. Hoogeveen, *Hydrological basins in europe*, 2009. [Online]. Available: https://data.apps.fao.org/map/catalog/srv/eng/catalog.search#/metadata/1849e279-67bd-4e6f-a789-9918925a11a1 (visited on 05/27/2022).

[23] The SciPy community, *Scipy.stats.anderson_ksamp*, 2022. [Online]. Available: https://docs.scipy.org/doc/scipy/reference/generated/scipy.stats.anderson_ksamp.html (visited on 06/08/2022).

[24] The SciPy community, *Scipy.stats.pearsonr*, 2022. [Online]. Available: https://docs.scipy.org/doc/scipy/reference/generated/scipy.stats.pearsonr.html (visited on 06/08/2022).

[25] ECMWF, *Era5: How to calculate wind speed and wind direction from u and v components of the wind?* 2022. [Online]. Available: https://confluence.ecmwf.int/pages/viewpage.action?pageId=133262398 (visited on 08/14/2022).

[26] A. M. Society, *Precipitation regime*, 2012. [Online]. Available: https://glossary.ametsoc.org/wiki/Precipitation_regime#:~:text=Characteristics%20of%20the%20seasonal%20distribution%20of%20precipitation%20at%20a%20particular%20place. (visited on 08/15/2022).

[27] M. C. Peel, B. L. Finlayson, and T. A. McMahon, “Updated world map of the köppen-geiger climate classification,” *Hydrology and Earth System Sciences*, vol. 11, no. 5, pp. 1633–1644, 2007. DOI: 10.5194/hess-11-1633-2007. [Online]. Available: https://hess.copernicus.org/articles/11/1633/2007/.

[28] X. Lana, M. Martinez, C. Serra, and A. Burgueno, “Spatial and temporal variability of the daily rainfall regime in catalonia (north-eastern spain), 1950-2000,” *International journal of Climatology*, vol. 24, pp. 613–641, 2004. DOI: 10.1002/joc.1020. [Online]. Available: https://rmets-onlinelibrary-wiley-com.tudelft.idm.oclc.org/doi/pdf/10.1002/joc.1020.

[29] I. Emmanuel, H. Andrieu, E. Leblois, and B. Flahaut, “Temporal and spatial variability of rainfall at the urban hydrological scale,” *Journal of Hydrology*, vol. 430-431, pp. 162–172, 2012, ISSN: 0022-1694. DOI: https://doi.org/10.1016/j.jhydrol.2012.02.013. [Online]. Available: https://www.sciencedirect.com/science/article/pii/S0022169412001126.

[30] A. Karagiannidis, A. Bloutsos, P. Maheras, and C. Sachsamanoglou, “Some characteristics of precipitation in europe,” *Theoretical and Applied Climatology*, vol. 91, pp. 193–204, Feb. 2008. DOI: 10.1007/s00704-007-0303-7.

[31] C. Xiao, W. Yuan, and R. Yu, “Diurnal cycle of rainfall in amount, frequency, intensity, duration, and the seasonality over the uk,” *International Journal of Climatology*, vol. 38, no. 13, pp. 4967–4978, 2018. DOI: https://doi.org/10.1002/joc.5790. [Online]. Available: https://rmets.onlinelibrary.wiley.com/doi/abs/10.1002/joc.5790.

[32] R. Lindsey and L. Dahlman, “Climate variability: North atlantic oscillation,” Aug. 2009. [Online]. Available: https://www.climate.gov/news-features/understanding-climate/climate-variability-north-atlantic-oscillation.

[33] L. Zubiate, F. McDermott, C. Sweeney, and M. O’Malley, “Spatial variability in winter nao–wind speed relationships in western europe linked to concomitant states of the east atlantic and scandinavian patterns,” *Quarterly Journal of the Royal Meteorological Society*, vol. 143, no. 702, pp. 552–562, 2017. DOI: https://doi.org/10.1002/qj.2943.

[34] J. Wibig, “Precipitation in europe in relation to circulation patterns at the 500 hpa level,” *International Journal of Climatology*, vol. 19, no. 3, pp. 253–269, 1999. DOI: https://doi.org/10.1002/(SICI)1097-0088(19990315)19:3<253::AID-JOC366>3.0.CO;2-0.

[35] J. Álvarez-Rodríguez and T. Estrela, “Regionalization and drought characterisation in europe,” *ARIDE Technical Report*, vol. 9, Dec. 2000.

[36] R. Houze Jr., “Orographic effects on precipitating clouds,” *Reviews of Geophysics*, vol. 50, no. 1, Jan. 2012. DOI: https://doi.org/10.1029/2011RG000365.

[37] A. Anders, “Precipitation patterns and topography,” *Vignette Collection*, Nov. 2016. [Online]. Available: https://serc.carleton.edu/vignettes/collection/25201.html.

[38] A. Stockham, S. D.M., F. J.G., and A. P. Draude, “Quantifying the rain-shadow effect: Results from the peak district, british isles,” *Bulletin of the American Meteorological Society*, vol. 99, no. 4, pp. 777–790, 2018. DOI: 10.1175/BAMS-D-17-0256.1.

[39] D. Touma, A. Michalak, D. Swain, and N. Diffenbaugh, “Characterizing the spatial scales of extreme daily precipitation in the united states,” *Journal of Climate*, vol. 31, no. 19, pp. 8023–8037, 2018. DOI: 10.1175/JCLI-D-18-0019.1.

[40] G. D. Jenerette, R. L. Scott, and A. R. Huete, “Functional differences between summer and winter season rain assessed with modis-derived phenology in a semi-arid region,” *Journal of Vegetation Science*, vol. 21, no. 1, pp. 16–30, 2010. DOI: https://doi.org/10.1111/j.1654-1103.2009.01118.x.

[41] S. Curtis, “Means and long-term trends of global coastal zone precipitation,” *Nature News*, Apr. 2019. DOI: https://doi.org/10.1038/s41598-019-41878-8.

[42] K. Trusilova, M. Jung, G. Churkina, U. Karstens, M. Heimann, and M. Claussen, “Urbanization impacts on the climate in europe: Numerical experiments by the psu–ncar mesoscale model (mm5),” *Journal of Applied Meteorology and Climatology*, vol. 47, no. 5, pp. 1442–1455, 2008, ISSN: 15588424, 15588432. [Online]. Available: http://www.jstor.org/stable/26172226 (visited on 04/11/2022).

[43] H. Xiangping, B. Huang, and F. Cherubini, “Impacts of idealized land cover changes on climate extremes in europe,” *Ecological Indicators*, vol. 104, pp. 626–635, 2019, ISSN: 1470-160X. DOI: https://doi.org/10.1016/j.ecolind.2019.05.037. [Online]. Available: https://www.sciencedirect.com/science/article/pii/S1470160X19303838.

[44] European Environmental Agency, *Heavy precipitation in europe*, 2021. [Online]. Available: https://www.eea.europa.eu/data-and-maps/indicators/precipitation-extremes-in-europe-3/assessment-1 (visited on 06/14/2022).

[45] E. Aalbers, G. Lenderink, and E. van Meijgaard, “Local-scale changes in mean and heavy precipitation in western europe, climate change or internal variability?” *Climate Dynamics*, vol. 50, pp. 4745–4766, 2018. DOI: https://doi.org/10.1007/s00382-017-3901-9.

[46] J. López-Moreno, S. Goyette, and M. Beniston, “Climate change prediction over complex areas: Spatial variability of uncertainties and predictions over the pyrenees from a set of regional climate models,” *International Journal of Climatology*, vol. 28, no. 11, pp. 1535–1550, 2008. DOI: https://doi.org/10.1002/joc.1645.

[47] C. Frei, R. Schöll, S. Fukutome, J. Schmidli, and P. Vidale, "Future change of precipitation extremes in europe: Intercomparison of scenarios from regional climate models," *Journal of Geophysical Research: Atmospheres*, vol. 111, no. D6, 2006. DOI: https://doi.org/10.1029/2005JD005965.

[48] EEA, *Elevation map of europe*, [Online; accessed April 14, 2022], 2009. [Online]. Available: https://www.eea.europa.eu/ds_resolveuid/558D91E1-3DB0-4639-9F70-2012CC4453A5.

[49] J. Min and S. Halim, "Rainfall modelling using generalized extreme value distribution with cyclic covariate," *Mathematics and Statistics*, vol. 8, no. 6, pp. 762–772, 2020, 10.13189/ms.2020.080617.

[50] D. Hawkins, *Identification of Outliers* (Monographs on Statistics and Applied Probability). Springer Netherlands, 2013, ISBN: 9789401539944. [Online]. Available: https://books.google.nl/books?id=ONjyCAAAQBAJ.

[51] J. Higgins and S. Green, *Cochrane handbook for systematic reviews of interventions version 5.1.0*, 2011. [Online]. Available: www.handbook.cochrane.org (visited on 06/14/2022).

[52] W. Zhang, K. Furtado, P. Wu, *et al.*, "Increasing precipitation variability on daily-to-multiyear time scales in a warmer world," *Science Advances*, vol. 7, no. 31, eabf8021, 2021. DOI: 10.1126/sciadv.abf8021. [Online]. Available: https://www.science.org/doi/abs/10.1126/sciadv.abf8021.

[53] A. Basist, G. Bell, and V. Meentemeyer, "Statistical relationships between topography and precipitation patterns," *Journal of Climate*, vol. 7, no. 9, pp. 1305–1315, 1994. DOI: 0.1175/1520-0442(1994)007<1305:SRBTAP>2.0.CO;2. [Online]. Available: https://journals.ametsoc.org/view/journals/clim/7/9/1520-0442_1994_007_1305_srbtap_2_0_co_2.xml.

[54] H. Carlson, "Check your confidence: Size really does matter," *Journal of Chemical Information and Modeling*, vol. 53, 8 Aug. 2013. DOI: 10.1021/ci4004249.

[55] C. Jung and D. Schindler, "Precipitation atlas for germany (gepra)," *Atmosphere*, vol. 10, no. 12, 2019, ISSN: 2073-4433. DOI: 10.3390/atmos10120737. [Online]. Available: https://www.mdpi.com/2073-4433/10/12/737.

[56] J. Meersmans, M. Martin, E. Lacarce, *et al.*, "A high resolution map of french soil organic carbon. agronomy of sustainable development," *Agronomy for Sustainable Development*, vol. 32, pp. 841–851, Oct. 2012. DOI: 10.1007/s13593-012-0086-9.

[57] A. Crespi, M. Brunetti, G. Lentini, and M. Maugeri, "1961–1990 high-resolution monthly precipitation climatologies for italy," *International Journal of Climatology*, vol. 38, no. 2, pp. 878–895, 2018. DOI: https://doi.org/10.1002/joc.5217. [Online]. Available: https://rmets.onlinelibrary.wiley.com/doi/abs/10.1002/joc.5217.

[58] J. Zamboni, *The advantages of a large sample size*, 2018. [Online]. Available: https://scienc ing.com/calculate-tscore-5135749.html.

[59] I. Hossain, A. Khastagir, and M. Aktar, "Comparison of estimation techniques for generalised extreme value (gev) distribution parameters: A case study with tasmanian rainfall," *Int. J. Environ. Sci. Technol.*, vol. 19, pp. 7737–7750, 2022. DOI: https://doi-org.tudelft.idm.oclc.org/10.1007/s13762-021-03693-5.

[60] M. Hofstätter, B. Chimani, A. Lexer, and G. Blöschl, "A new classification scheme of european cyclone tracks with relevance to precipitation," *Water Resources Research*, vol. 52, no. 9, pp. 7086–7104, 2016. DOI: https://doi.org/10.1002/2016WR019146. [Online]. Available: https://agupubs.onlinelibrary.wiley.com/doi/abs/10.1002/2016WR019146.

[61] L. Back and C. Bretherton, "The relationship between wind speed and precipitation in the pacific itcz," *Journal of Climate*, vol. 18, no. 20, pp. 4317–4328, 2005. DOI: 10.1175/JCLI3519.1. [Online]. Available: https://journals.ametsoc.org/view/journals/clim/18/20/jcli3519.1.xml.

[62] Q. Zhu, J. Chen, L. Zhu, X. Duan, and Y. Lio, "Wind speed prediction with spatio–temporal correlation: A deep learning approach," *Energies*, vol. 11, no. 705, 2018. DOI: 10.3390/en11040705.

Summary of notebooks used for research model 2

All notebooks can be found at the Fathom-global Github page in the folder: *axa-internal/wflow_axa/src/1-prepare/SWG_Nynke* in the branch SWG. The first part can be found in the folder *model2_code*. The second part can be found in the folder *model2_sensitivity*. Requesting access may be needed to view to code.

I.1. Code of model 2

model2_CDF_AD: code used to perform the Anderson-Darling test to quantify the difference between the cumulative distribution functions (cdf) of the observed and shifted annual precipitation maxima. Code returns both the AD-test statistics and a graph of the two cdfs.

model2_CDF_AD_oneclick: code used to perform the Anderson-Darling test to quantify the difference between the cumulative distribution functions (cdf) of the observed and shifted annual precipitation maxima. Code returns both the AD-test statistics and a graph of all the cdfs of one vector type. Code is written such that it can be run with 'one click' without the need for further input.

model2_CDF_pearson: code used to calculate the Pearson correlation coefficient to quantify the correlation between the cumulative distribution functions (cdf) of the observed and shifted annual precipitation maxima. Code returns the Pearson correlation coefficient, the 5- and 95-percentile intervals and a graph of the two cdfs.

model2_CDF_pearson_oneclick: code used to calculate the Pearson correlation coefficient to quantify the correlation between the cumulative distribution functions (cdf) of the observed and shifted annual precipitation maxima. Code returns the Pearson correlation coefficient, the 5- and 95-percentile intervals and a graph of all the cdfs of one vector type including the confidence intervals. Code is written such that it can be run with 'one click' without the need for further input.

model2_coord_to_precip: code used to convert numpy.arrays with shifted longitude and latitude coordinates into precipitation values based on the historical observed precipitation data. Code returns a xr.Dataset with the new precipitation values.

model2_GEV_AD: code used to perform the Anderson-Darling test to quantify the goodness of fit of the Generalized Extreme Value (GEV) distribution to the observed and shifted annual precipitation maxima. Code returns both the AD-test statistics and a graph of all the GEV distributions of one vector type.

model2_GEV_AD_oneclick: code used to perform the Anderson-Darling test to quantify the goodness of fit of the Generalized Extreme Value (GEV) distribution to the observed and shifted annual precipitation maxima. Code returns both the AD-test statistics and a graph of all the GEV distributions of one vector type. Code is written such that it can be run with 'one click' without the need for further input.

model2_GEV_AD_unc_analysis: code used to examine the underlying causes of the differences in AD values for the GEV fit of varying combinations of basins and aggregation times. Code returns a figure with the observed and shifted annual maxima for different aggregation times and vector types.

model2_histogram_extremes: code used to generate a N number of repetitions of one year to determine the extent of variation the model can generate under different starting conditions. Code returns a histogram of all repetitions with the historical value and standard deviation indicated.

model2_pearson_cor_analysis: code used to generate the correlation figures between the observed and shifted precipitation value for different basins for an aggregation time of one day. Code returns for each basin a figure in which the shifted precipitation is plotted against the observed precipitation including the corresponding Pearson correlation coefficient.

model2_precipitation_fields_figure: code used to generate a figure in which the historical and observed spatial precipitation pattern is shown including the differences in [mm/day] between the two patterns.

model2_save_base42: code used to generate the base xr.Dataset with 42 years of historical observed precipitation values.

model2_test_coords: code used to check visually if the longitude and latitude coordinates between the observed and shifted data have the similar direction.

model2_short_ani: code used to generate a short vector animation of one month to show the differences in vector fields between different vector types characterized by their values of limit m (or a and b (old notation)) and range r.

model2_visualize_extremes: code used to generate a figure in which one extreme event and the influence of the different shifts and vector types are shown for the Moselle basin. In addition, the codes include an option to generate a short animation of the period before and after the extreme event under consideration.

model2_workflow: code used to generate new coordinate sets to shift the historical precipitation patterns, convert them to precipitation values, generate an animation and finally store them as a new xr.Dataset.

I.2. Code to analysis the model sensitivity

Sensitivity_initial_field: code used to generate an N number of random displacement vector fields with a length of one year with varying initial fields. Mean rainfall values are calculated at different points in time for the Ijssel, Moselle and Rhine basin.

Sensitivity_initial_field_zeros: code used to generate an N number of random displacement vector fields with a length of one year with initial fields filled with zeros. Mean rainfall values are calculated at different points in time for the Ijssel, Moselle and Rhine basin.

Sensitivity_past_all1: code used to generate an N number of random displacement vector fields with a length of one year with a fixed initial field for each iterations. All weights of the past weight's matrix are set to one. Current displacement vector values are not used in the calculation. Maximum rainfall values are calculated at different points in time for the Ijssel, Moselle and Rhine basin. Spatial correlation is calculated for latitude and longitude.

Sensitivity_past_all1_zeros: code used to generate an N number of random displacement vector fields with a length of one year with an initial field consisting of zeros for each iterations. All weights of the weight's matrix are set to one. Current displacement vector values are not used in the calculation. Maximum rainfall values are calculated at different points in time for the Ijssel, Moselle and Rhine basin. Spatial correlation is calculated for latitude and longitude.

Sensitivity_past_parallel4_zeros: code used to generate an N number of random displacement vector fields with a length of one year with an initial field consisting of zeros for each iterations. Parallel weights of the past weight's matrix are set to four. All other weights are set to one. Current displacement vector values are not used in the calculation. Maximum rainfall values are calculated at different points in time for the Ijssel, Moselle and Rhine basin. Spatial correlation is calculated for latitude and longitude.

Sensitivity_past_perpen4_zeros: code used to generate an N number of random displacement vector fields with a length of one year with an initial field consisting of zeros for each iterations. Perpendicular weights of the past weight's matrix are set to four. All other weights are set to one. Current displacement vector values are not used in the calculation. Maximum rainfall values are calculated at different points in time for the Ijssel, Moselle and Rhine basin. Spatial correlation is calculated for latitude and longitude.

Sensitivity_weights_all1: code used to generate an N number of random displacement vector fields with a length of one year with a fixed initial field for each iterations. All weights of the past and current weight's matrix are set to one. Maximum rainfall values are calculated at different points in time for the Ijssel, Moselle and Rhine basin. Spatial correlation is calculated for latitude and longitude.

Sensitivity_weights_parallel2: code used to generate an N number of random displacement vector fields with a length of one year with a fixed initial field for each iterations. All parallel weights of the past and current weight's matrix are set to two. Other weights are set to one. Maximum rainfall values are calculated at different points in time for the Ijssel, Moselle and Rhine basin. Spatial correlation is calculated for latitude and longitude.

Sensitivity_weights_perpen2: code used to generate an N number of random displacement vector fields with a length of one year with a fixed initial field for each iterations. All perpendicular weights of the past and current weight's matrix are set to two. Other weights are set to one. Maximum rainfall values are calculated at different points in time for the Ijssel, Moselle and Rhine basin. Spatial correlation is calculated for latitude and longitude.

Sensitivity_weights_past_parallel2: code used to generate an N number of random displacement vector fields with a length of one year with a fixed initial field for each iterations. All parallel weights of the past weight's matrix are set to two. Other weights are set to one. Current displacement vector values are not used in the calculation. Maximum rainfall values are calculated at different points in time for the Ijssel, Moselle and Rhine basin. Spatial correlation is calculated for latitude and longitude.

Sensitivity_weights_past_perpen2: code used to generate an N number of random displacement vector fields with a length of one year with a fixed initial field for each iterations. All perpendicular weights of the past weight's matrix are set to two. Other weights are set to one. Current displacement vector values are not used in the calculation. Maximum rainfall values are calculated at different points in time for the Ijssel, Moselle and Rhine basin. Spatial correlation is calculated for latitude and longitude.

Summary of notebooks used for model 3

All notebooks can be found at the Fathom-global Github page in the folder: *axa-internal/wflow_axa/src/1-prepare/SWG_Nynke/model3_code* in the branch SWG. Requesting access may be needed to view to code.

colormaps: text file with code to import colormaps used for figures for the final report.

model_data: text file with explanation of the data used in the notebooks of model 3.

model3_autocorrelation_angles: Calculates the autocorrelation of the wind angles and wind speeds of the historical and shifted data series for time lags of one, three, five and seven days. Returns figure with the spatial patterns of the autocorrelation values for each season.

model3_autocorrelation_time: Calculates the autocorrelation of the precipitation patterns of the historical and shifted data series for time lags of one, three, five and seven days. Returns figure with the spatial patterns of the autocorrelation values for each season.

model3_built_anomalies: code used in the initial phase to visualize different wind characteristics such as mean and maximum windspeed and the change of windspeed over one day.

model3_CDF_AD_cell_basin_oneclick: code used to generate the probability density (pdf) curves of the precipitation values observed in one grid cell. Histograms are returned to compare the observed and shifted precipitation values per grid cell. Testing of different statistics to quantify the difference between the historical and shifted pdfs is done. QQ-plots can be plotted to compare grid cell data.
model3_CDF_AD_oneclick: code used to generate the Anderson-Darling test statistics for the cumulative distribution functions.

model3_CDF_pearson_oneclick: code used to calculate the Pearson correlation coefficient between the sorted annual maxima of the observed and shifted data sets. 5- and 95-percentile uncertainty intervals around the cumulative distribution functions are calculated and plotted.

model3_CDF_pearson_oneclick_non_sorted: code used to calculate the Pearson correlation coefficient between the unsorted annual maxima of the observed and shifted data sets. 5- and 95-percentile uncertainty intervals around the cumulative distribution functions are calculated and plotted.

model3_compare_cor: code used to generate the figures to compare the historical and shifted precipitation patterns both in time and in space for different seasons.

model3_compare_precip_fields: code used to generate the figures to compare the historical and shifted precipitation patterns on their monthly mean, maximum and standard deviation.

model3_correlation_space: Calculates the spatial correlation of the longitude and latitude component of the historical and shifted vectors and the historical and shifted precipitation patterns. Correlation values are calculated compared to the 5x5 square surrounding the grid cell of interest. Code returns figure of mean correlation value for each grid cell per season.

model3_cov_analysis: code used to calculate the coefficient of variation between windspeeds and -angles (not used in the report). Last part of the code was used to visualize the historical windspeed and -angle distribution at different locations and compare these with the shifted data by means of histograms.

model3_cov_vectors: code used to calculate the coefficient of variation (cov) (standard deviation / mean) of the historical and observed longitude and latitude components of the vectors, the wind angles and the vector lengths. Returned figures include the cov values of the observed and historical data series per season and the absolute difference between the two data series.

model3_datasets_delta_degrees: code to convert historical u- and v-components from [m/s] to [degrees] and save them as a new XArray.Dataset.

model3_datasets_displacement_vectors: code to generate the final datasets with the displacement vectors and the new precipitation values.

model3_displacement_vectors: code in which the methodology of model 3 is applied step by step and converted into a final definition used to generate the displacement vectors for different fractions *f*.

model3_extremes_basins: code to visualize the spatial pattern of an extreme event over the basin of interest.

model3_final_datasets: code to generate final datasets with displacement vectors and components in degrees.

model3_final_datasets_wa_wsp: code to generate final datasets with displacement vectors and components in degrees including wind angle and -speed.

model3_GEV_AD_oneclick: code to generate generalized extreme values (GEV) distribution and the corresponding AD-values and uncertainty intervals.

model3_july2021: code to visualize the observed and shifted precipitation patterns for the July 2021 event for all three models.

model3_per_sampling: code used to count the number of times a grid cell inside a basin samples a precipitation value outside a basin. Returns figure of the Ijssel, Moselle and Rhine basin showing the spatial pattern of percentage of time a grid cell in the basin samples from outside the basin. Overall percentages are plotted above the figure. A second attempt to generate figures which plot the percentage of time and outside grid cell was included in the figure is added, but the code did not work yet. Potential for further research.

model3_practise_pdf:: code used the practise the generation of a probability density function (pdf) for the historical and shifted precipitation values. Different options are tested and visualized.

model3_sensitivity_fraction: code to visualize the sensitivity of different model parameters to the value of fraction f (results are not used in the report).

model3_std_basins_different_durations: code to calculate the differences in standard deviation of precipitation for different durations between the observed and shifted data.

model3_std_hist_vs_noise: code used to compare the noise generate by the shifting of the historical precipitation with the standard deviation of the historical precipitation per month. Returns figure for each month in which the noise is shown as percentage of the historical standard deviation.

model3_test_bias_windangle: code to test whether a bias in wind angle sampling can be explained by a skewed sampling distribution. Note: bias appeared to be an error in the used data, so the output of this code was not relevant at the end for the report.

model3_variation: code to generate the histograms for one extreme event to determine the extent of variation model 3 can generate for different values of fraction f.

model3_wind_direction_angle: code to test the definitions used in other notebooks to convert angles to directions and calculate windspeed from components.

III

Precipitation and wind characteristics of the Rhine basin

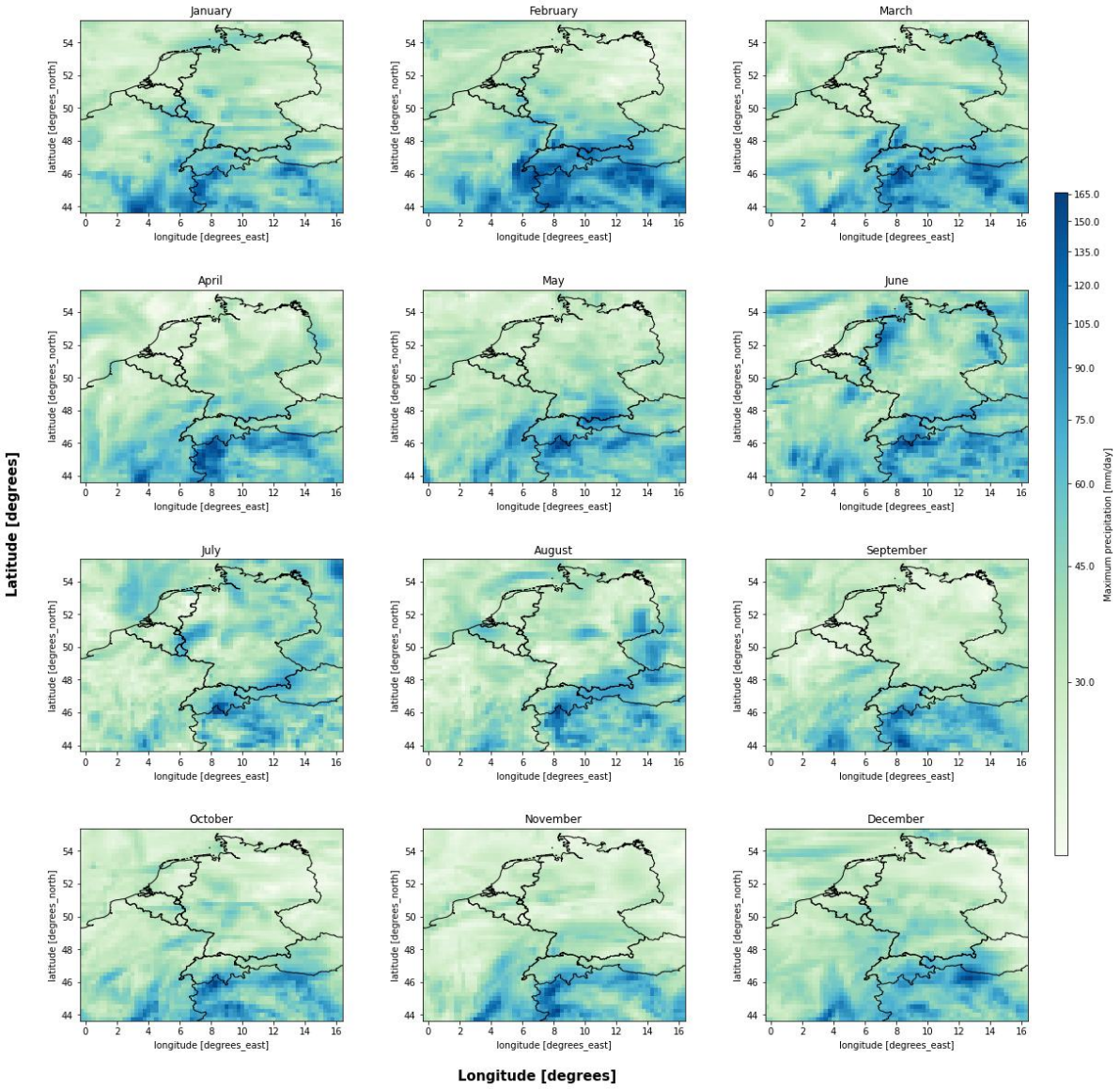

Figure III.1: Maximum historical daily precipitation values [mm/day] observed over the Rhine basin. Data was retrieved from the ERA5 reanalysis data set from 1980-2021. Values shown are average values over each month.

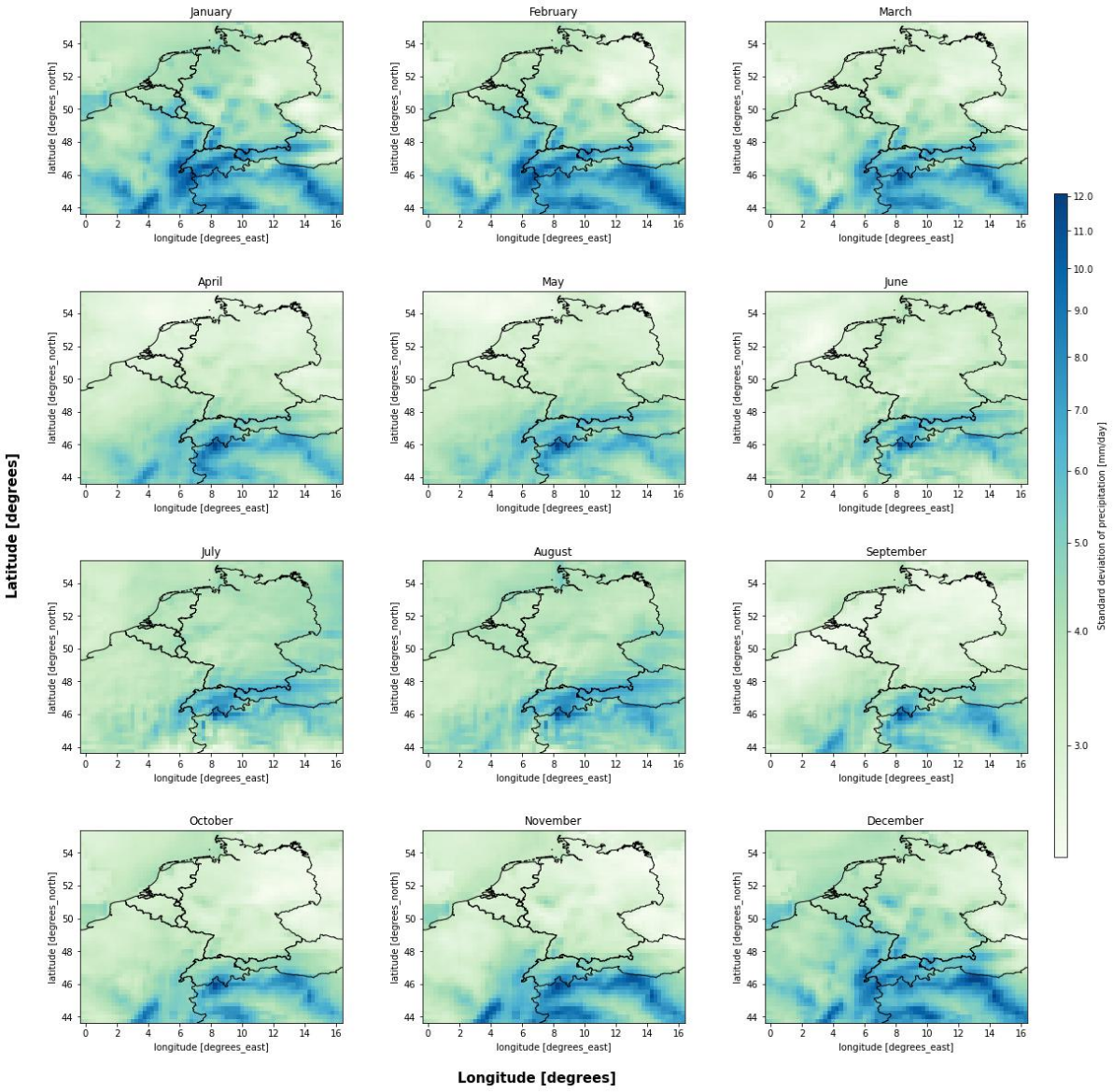

Figure III.2: Standard deviation of historical daily precipitation values [mm/day] observed over the Rhine basin. Data was retrieved from the ERA5 reanalysis data set from 1980-2021. Values shown are average values over each month.

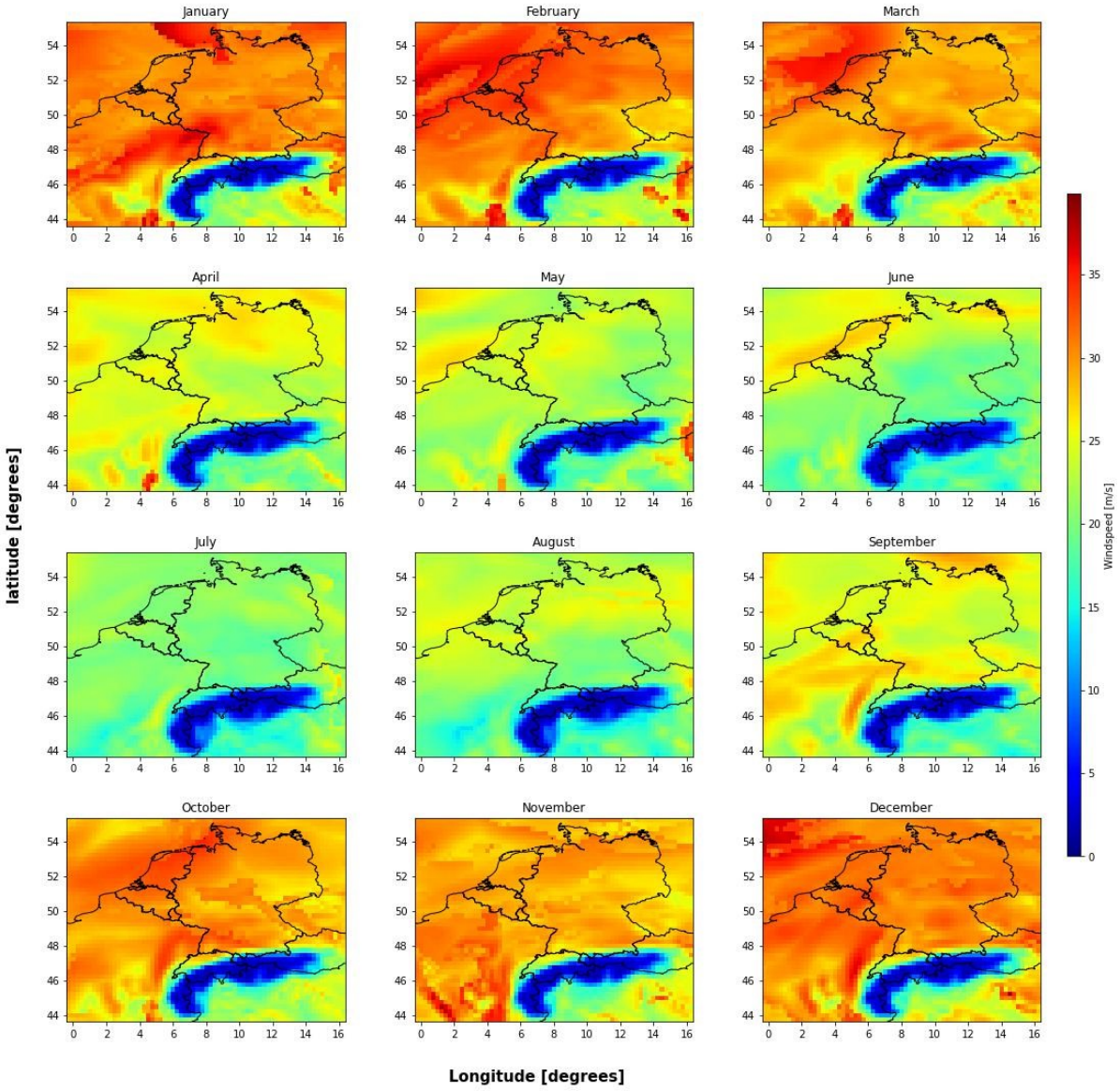

Figure III.3: Maximum historical daily wind speed values [m/s] observed over the Rhine basin. Data was retrieved from the ERA5 reanalysis data set from 1980-2021. Values shown are average values over each month.

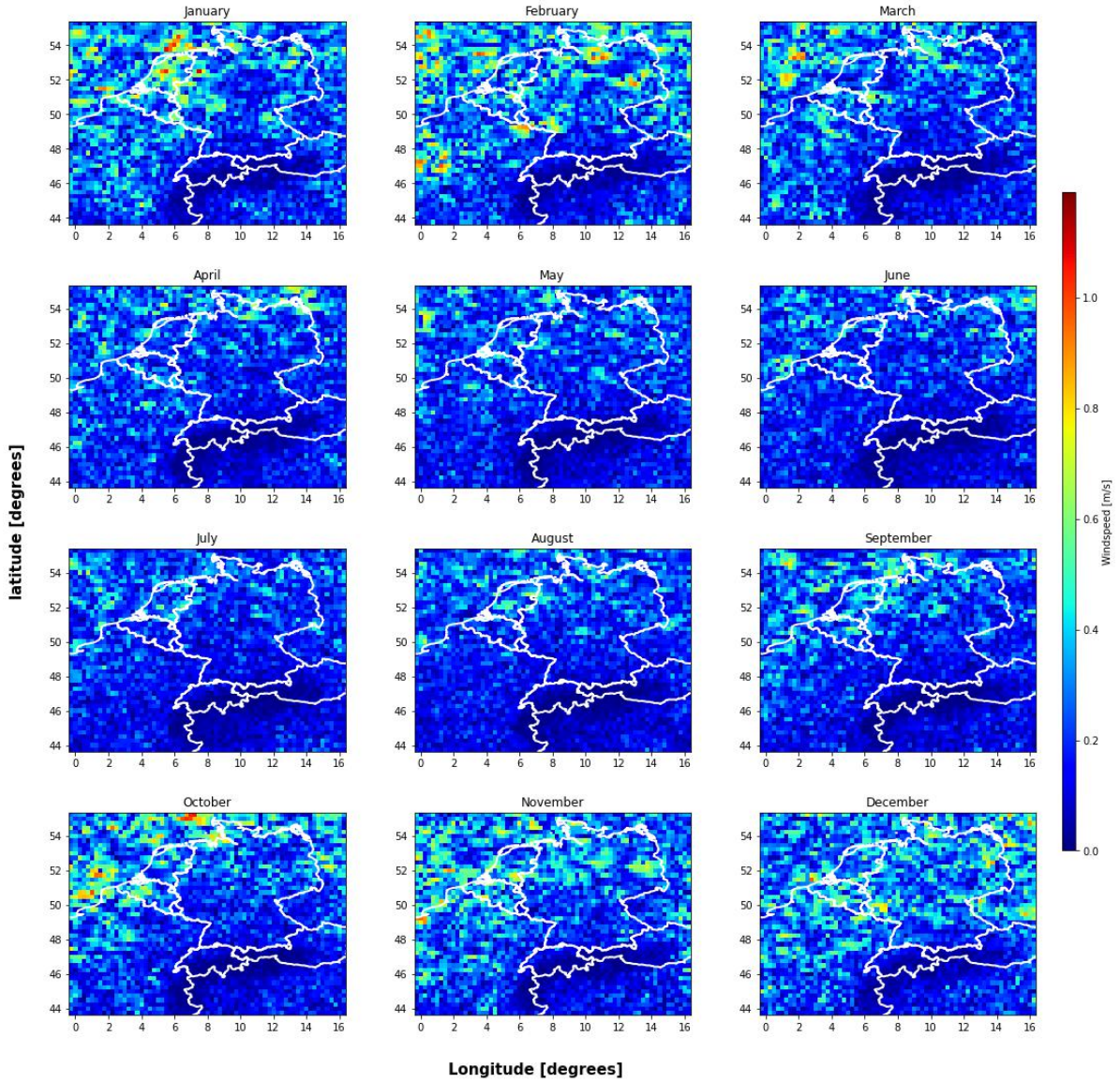

Figure III.4: Minimum historical daily wind speed values [m/s] observed over the Rhine basin. Data was retrieved from the ERA5 reanalysis data set from 1980-2021. Values shown are average values over each month.

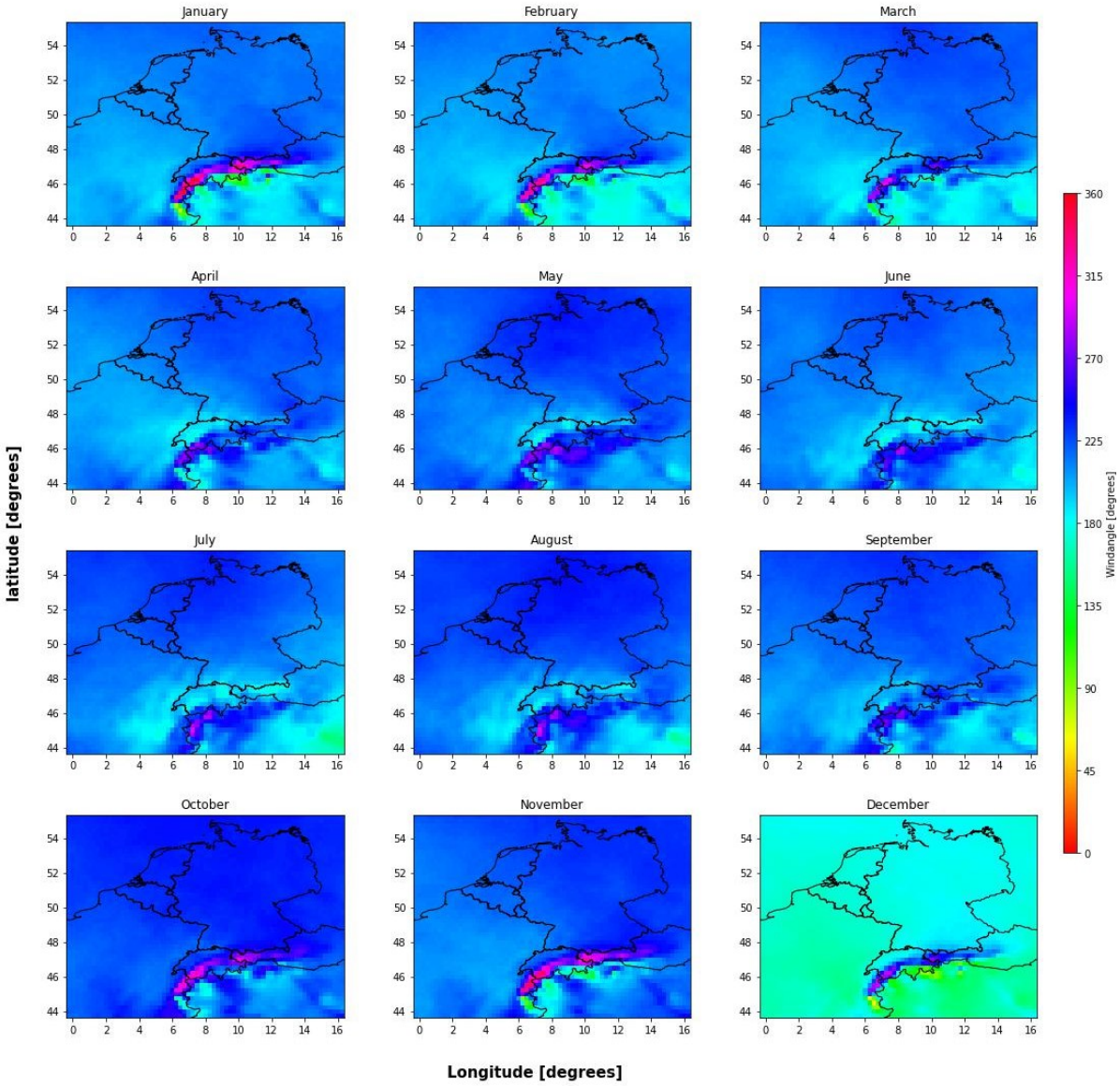

Figure III.5: Average wind angle [degrees] observed over the Rhine basin. Data was retrieved from the ERA5 reanalysis data set from 1980-2021. Values shown are average values over each month.

IV

Histograms of variation for different methodologies for each basin

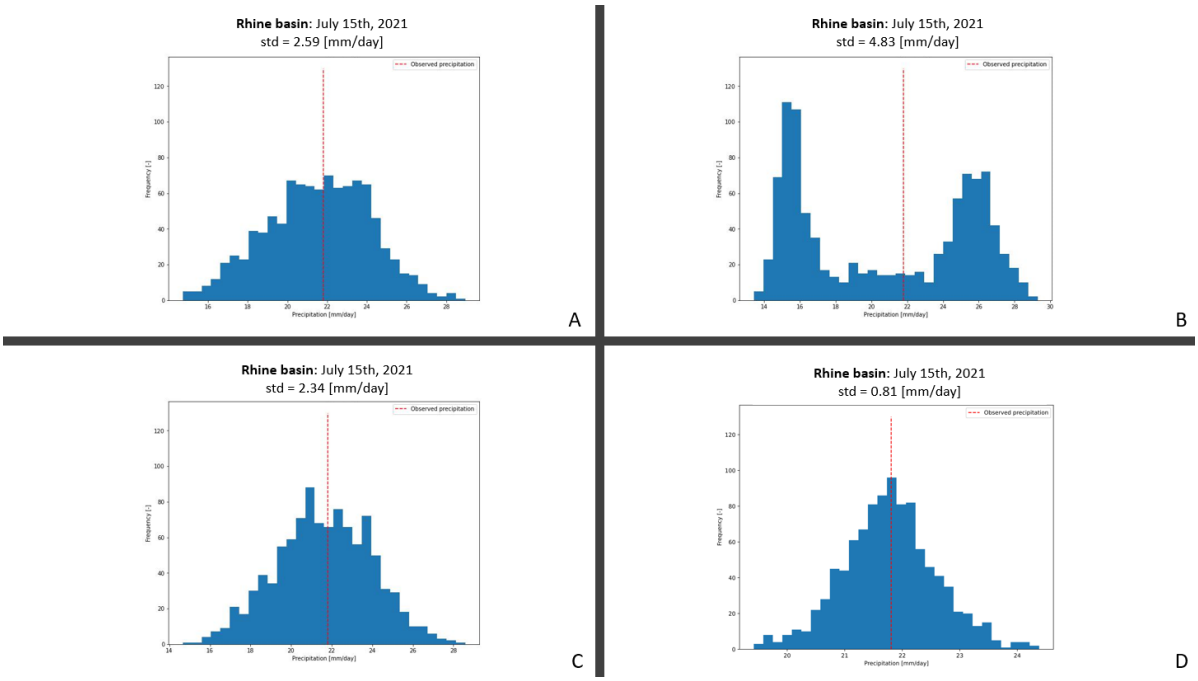

Figure IV.1: The extent of variation generated by different methodologies for the most extreme event in the Rhine basin in 2021 at July 15th, 2021. Methodologies are indicated by the letters: A) Random initial fields and weights 1.5 for parallel cells and 0.75 for perpendicular cells (standard methodology of toy model 2), B) Random initial fields and weights 1.125 for parallel cells and 0.825 for perpendicular cells, C) Initial field with zeros and weights 1.5 for parallel cells and 0.75 for perpendicular cells, D) Initial field with zeros and weights all one. Standard deviations are printed above each figure.

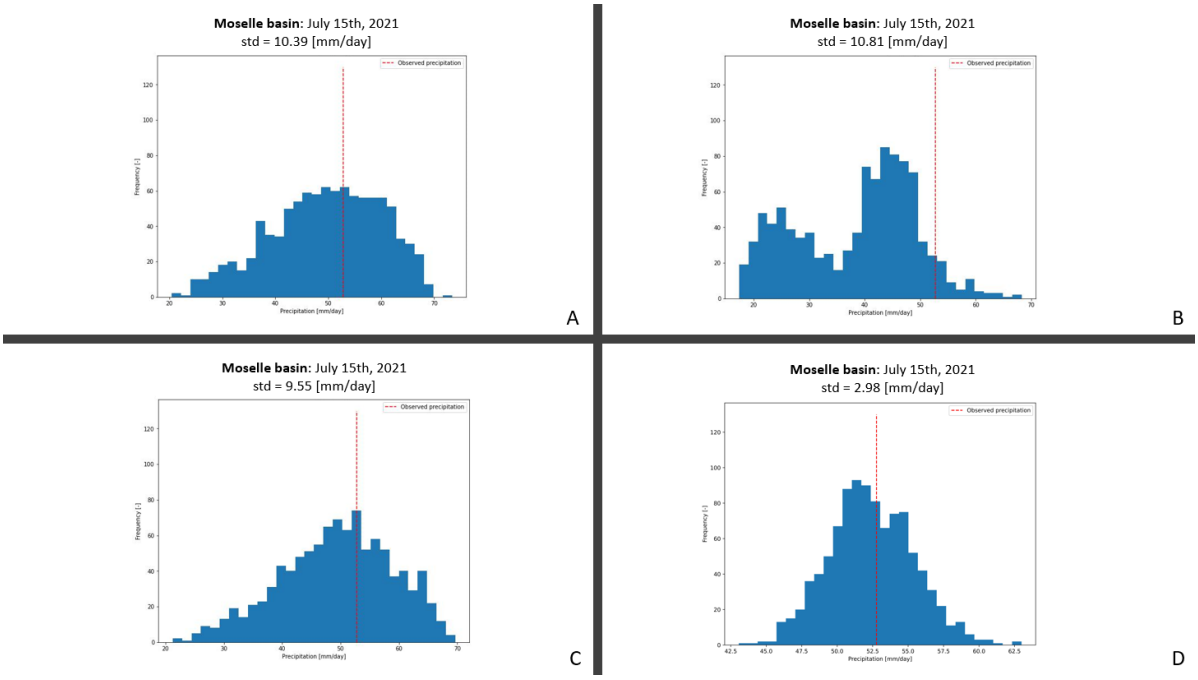

Figure IV.2: The extent of variation generated by different methodologies for the most extreme event in the Moselle basin in 2021 at July 15th, 2021. Methodologies are indicated by the letters: A) Random initial fields and weights 1.5 for parallel cells and 0.75 for perpendicular cells (standard methodology of toy model 2), B) Random initial fields and weights 1.125 for parallel cells and 0.825 for perpendicular cells, C) Initial field with zeros and weights 1.5 for parallel cells and 0.75 for perpendicular cells, D) Initial field with zeros and weights all one. Standard deviations are printed above each figure.

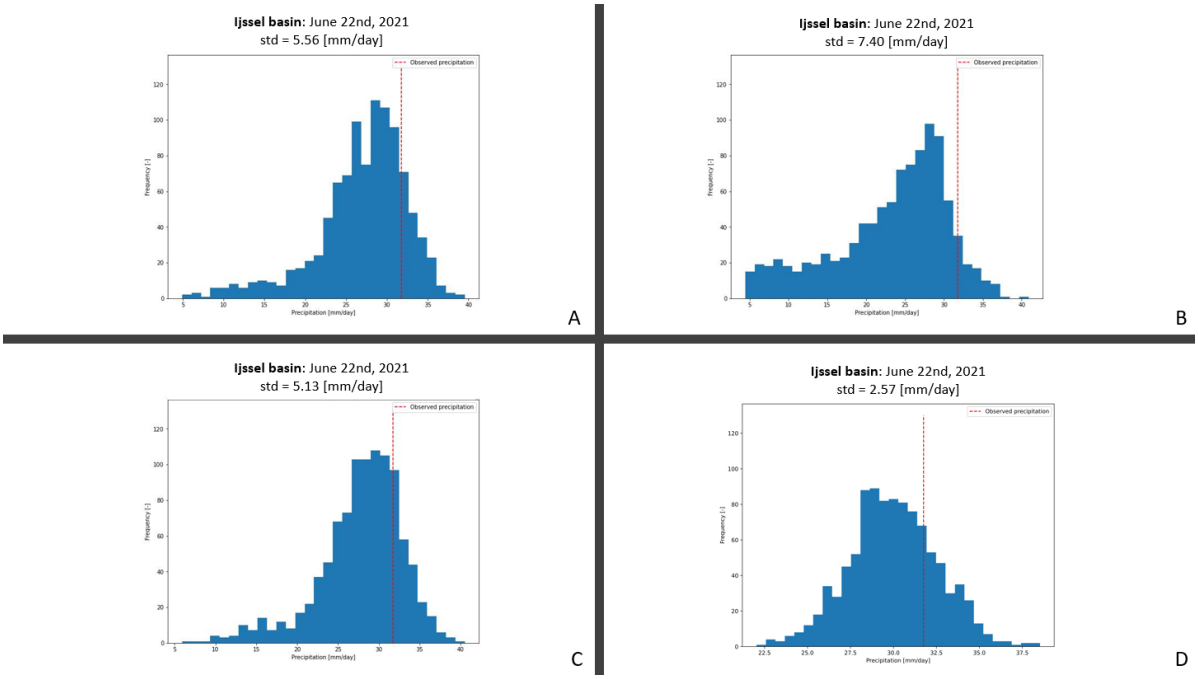

Figure IV.3: The extent of variation generated by different methodologies for the most extreme event in the Ijssel basin in 2021 at June 22nd, 2021. Methodologies are indicated by the letters: A) Random initial fields and weights 1.5 for parallel cells and 0.75 for perpendicular cells (standard methodology of toy model 2), B) Random initial fields and weights 1.125 for parallel cells and 0.825 for perpendicular cells, C) Initial field with zeros and weights 1.5 for parallel cells and 0.75 for perpendicular cells, D) Initial field with zeros and weights all one. Standard deviations are printed above each figure.

V

Cdf curve of the Rhine and Moselle basin with AD-values

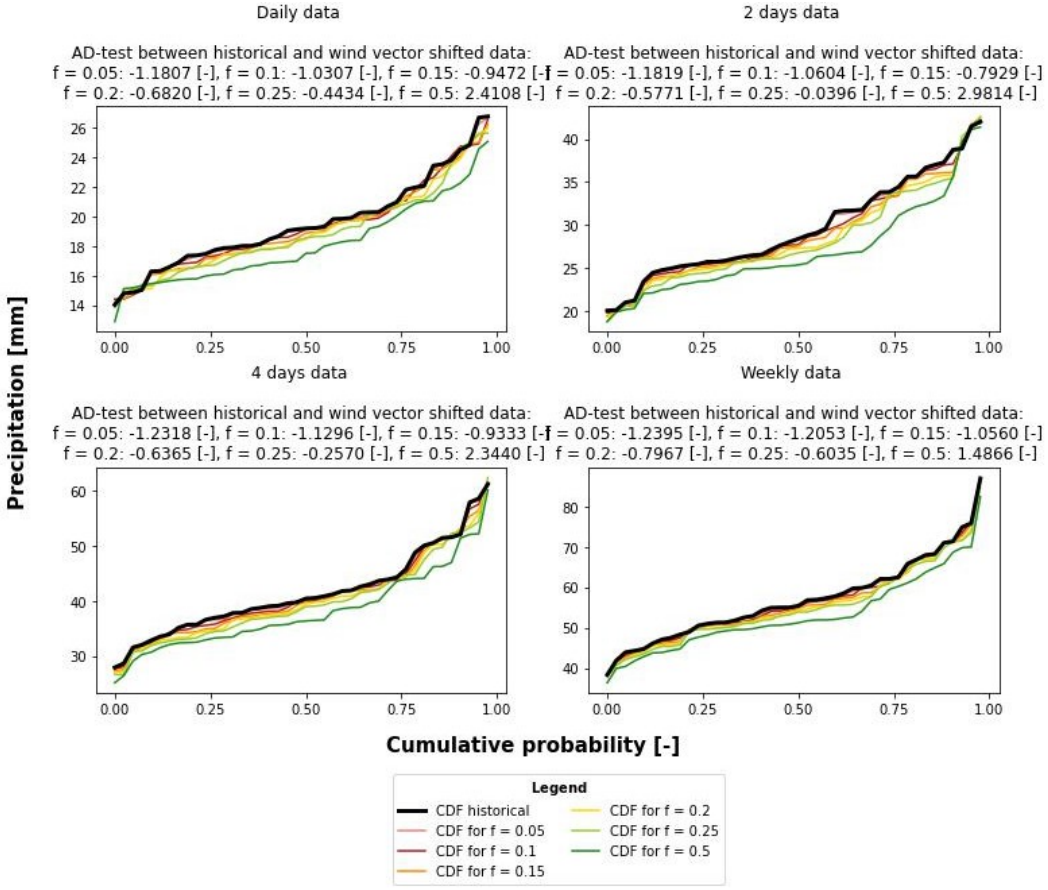

Figure V.1: Cumulative distribution function (cdf) of the Rhine basin for different durations and values of fraction f. AD-test statistics are shown above each graph. Note the strong decrease in extremes when the value of fraction f increases till f = 0.5 (dark green line) for all durations

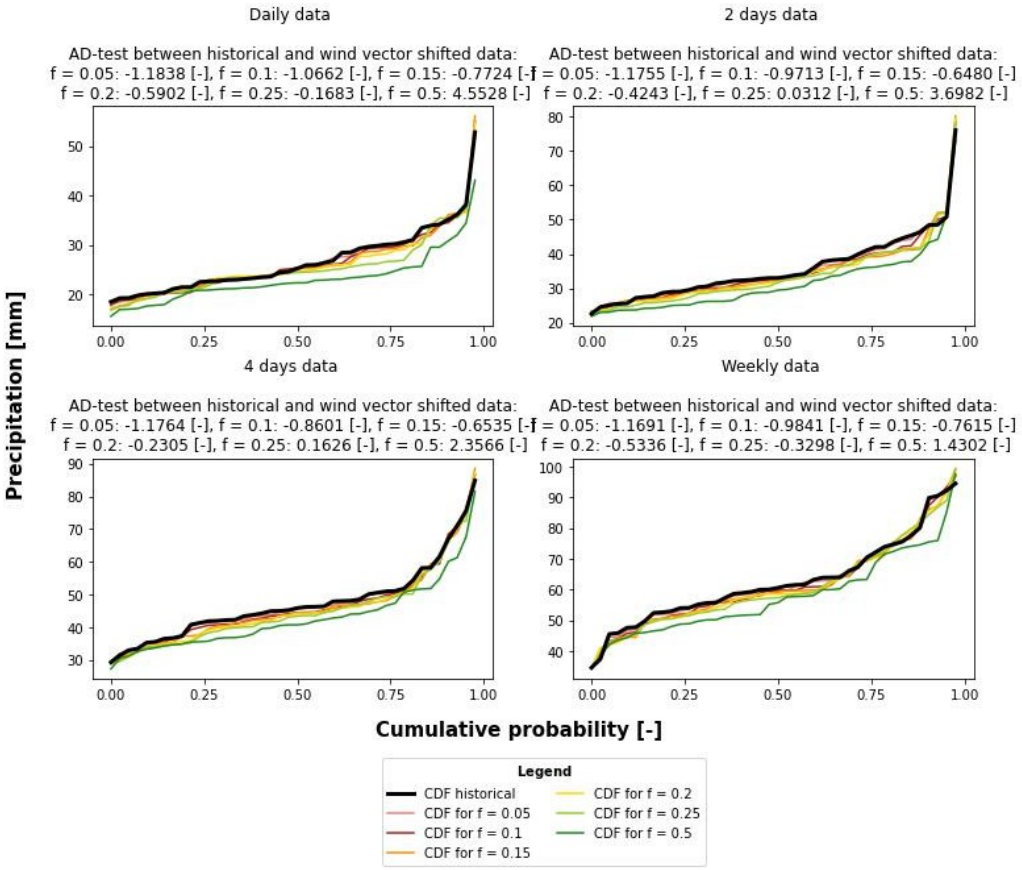

Figure V.2: Cumulative distribution function (cdf) of the Moselle basin for different durations and values of fraction f. AD-test statistics are shown above each graph. Note the strong decrease in extremes when the value of fraction f increases till f = 0.5 (dark green line) for all durations

VI

Histograms of the angle distribution

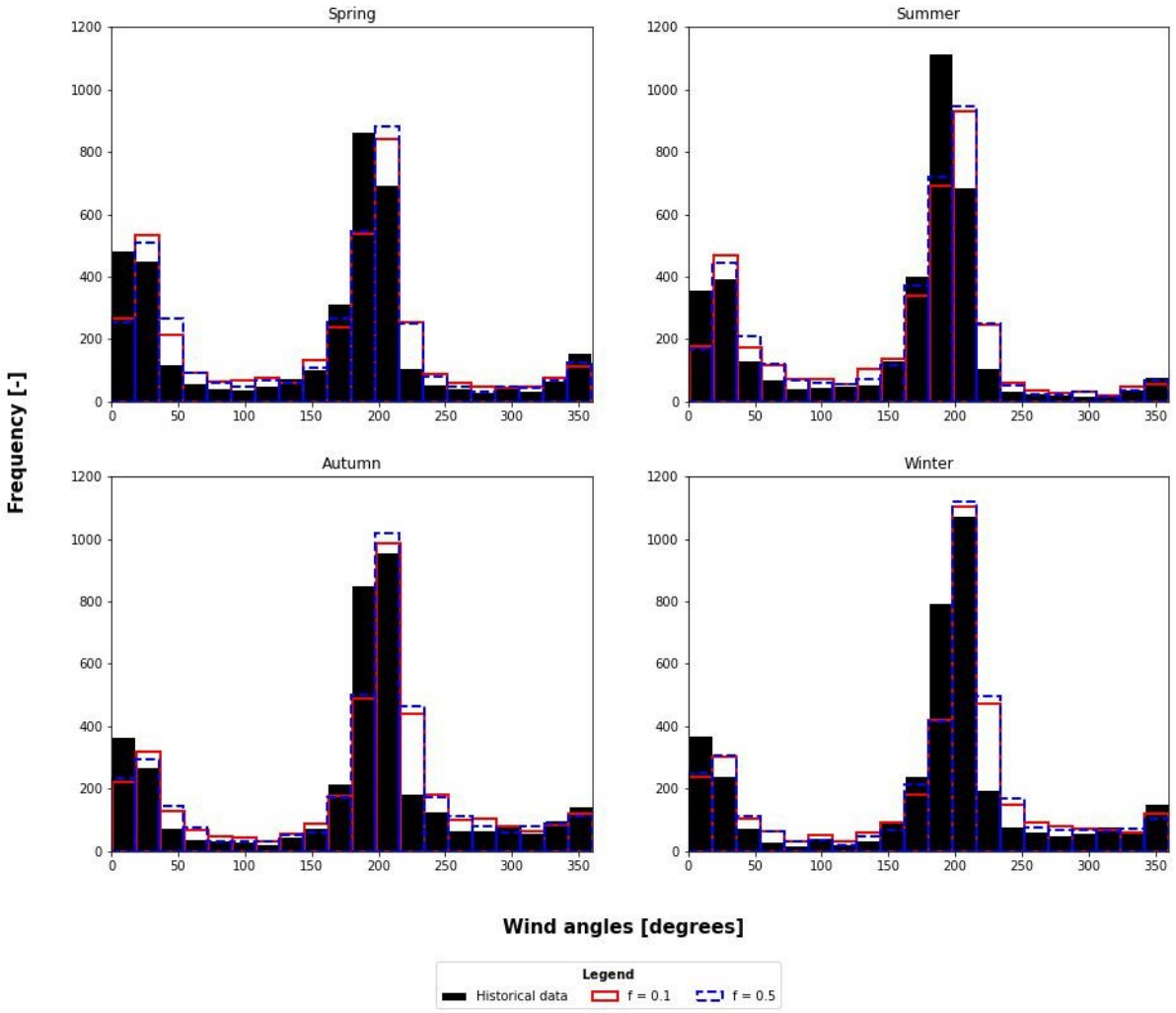

Figure VI.1: Seasonal histograms of the historical (black) and modelled wind angles for two different values of *f*: 0.1 (red) and 0.5 (blue), for the city of Bern (Swiss).

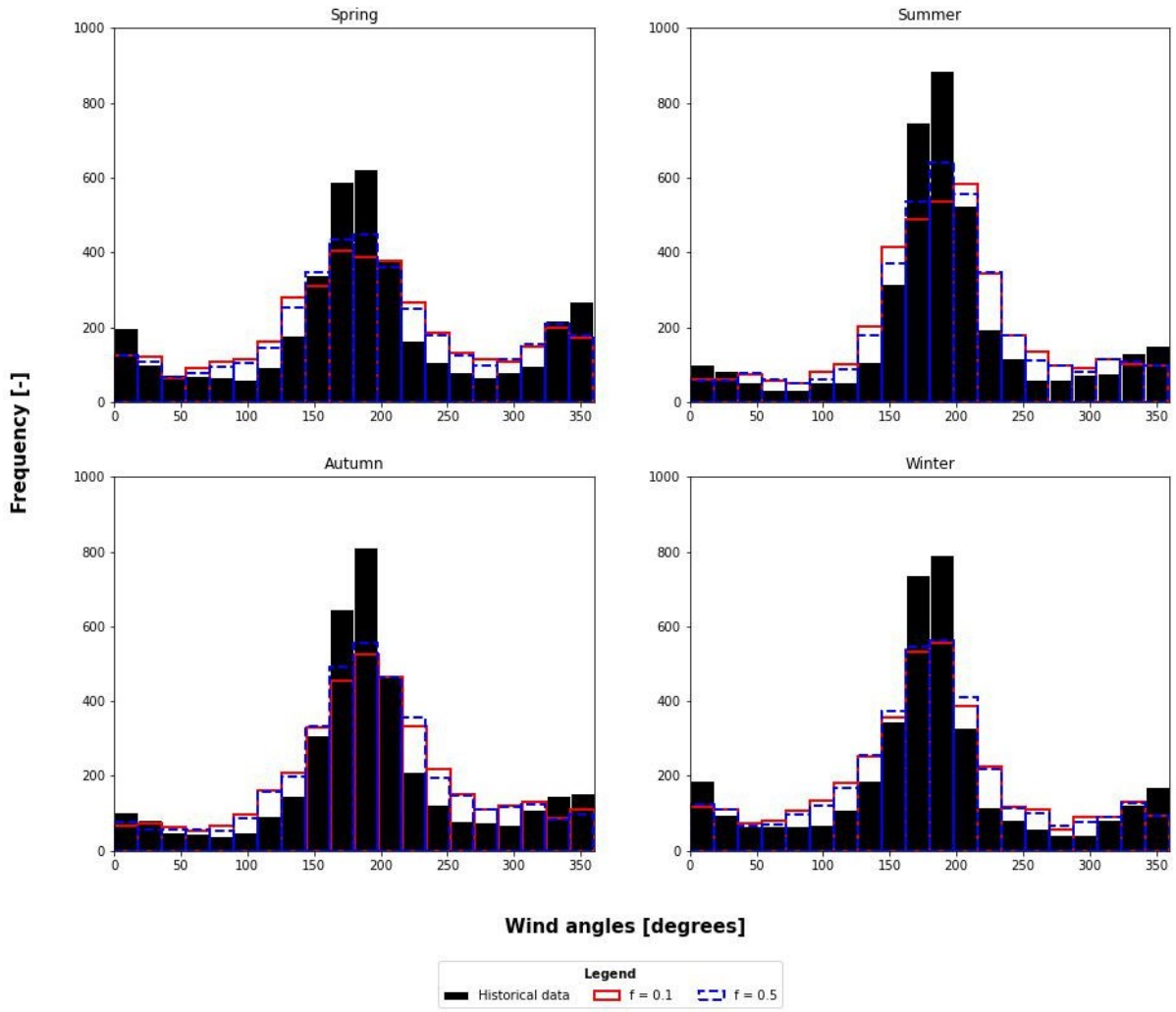

Figure VI.2: Seasonal histograms of the historical (black) and modelled wind angles for two different values of *f*: 0.1 (red) and 0.5 (blue), for the city of Munster (Germany).

VII

Wind speed and wind angle distribution

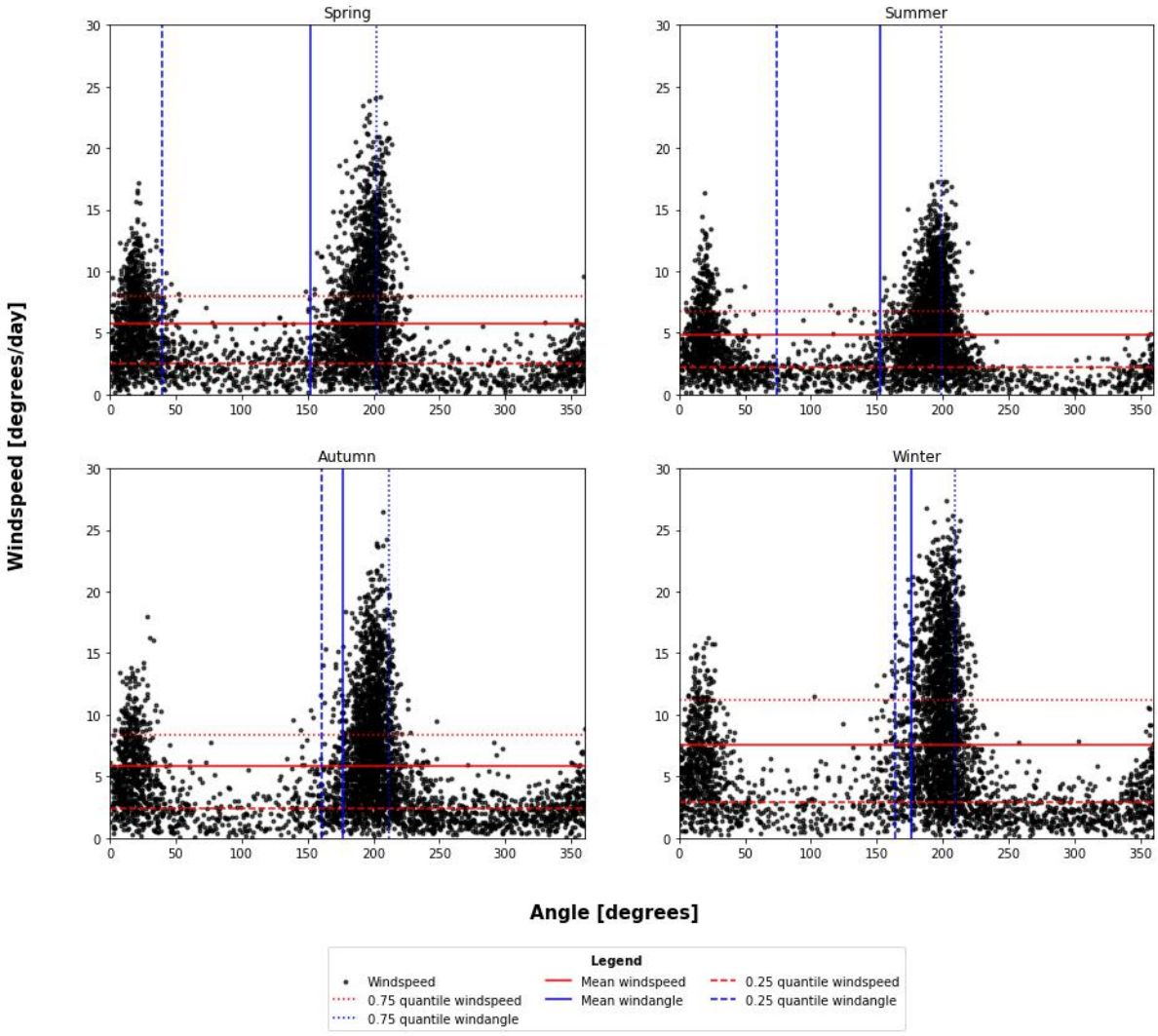

Figure VII.1: Seasonal scatter plot of wind angle vs. wind speed for the city of Bern (Swiss).

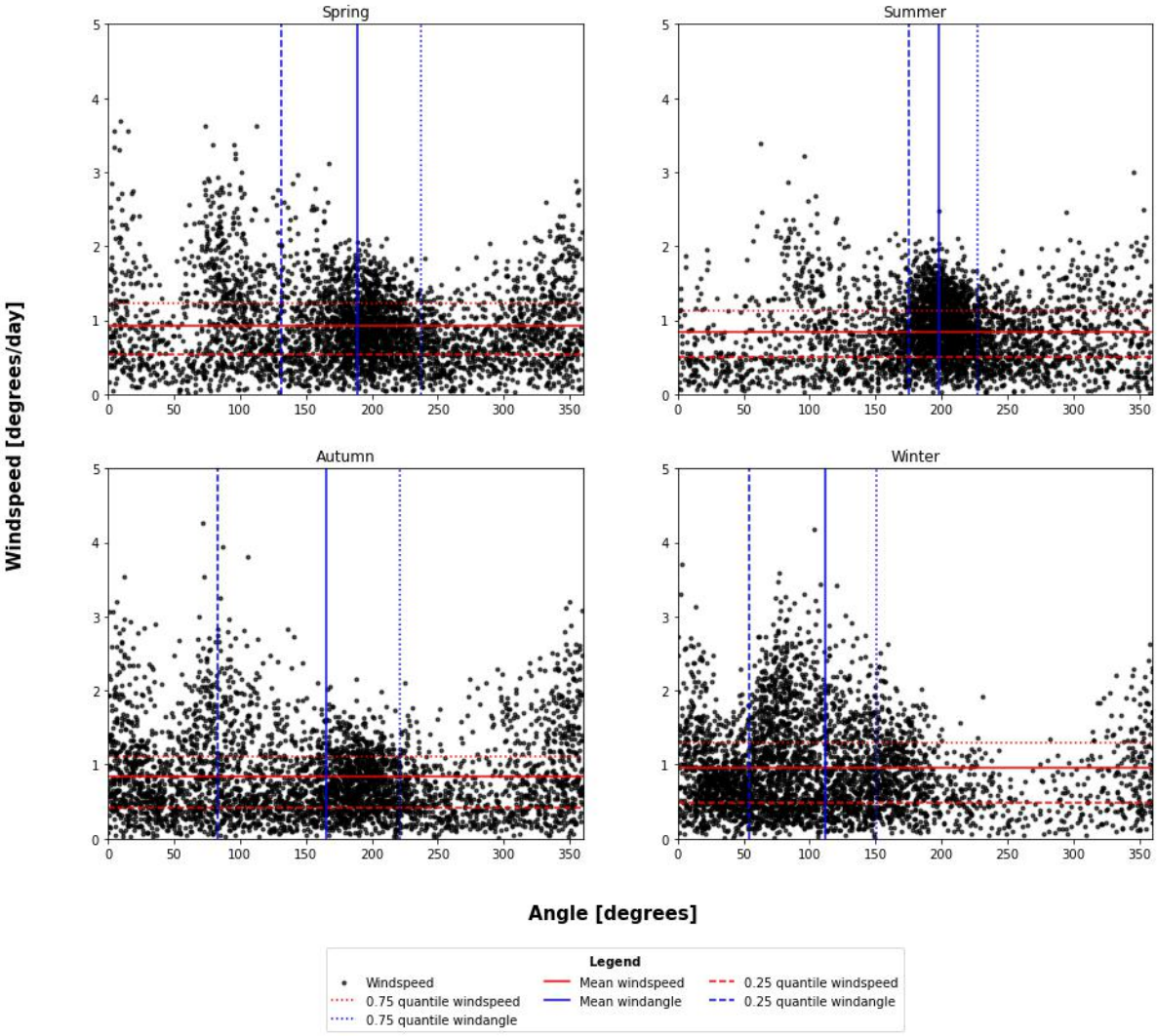

Figure VII.2: Seasonal scatter plot of wind angle vs. wind speed for the city of Munster (Germany).

VIII

Recommendations correlation

VIII.1. Improvement spatial correlation

On the next page, a schematic representation of the use of a convolution matrix to explicitly include spatial correlation in the methodology of model 3 is presented. Foreseen advantages and challenges are described in the enumerations below.

Advantages:

- The spatial correlation between vectors in neighboring grid cells will increase. It is expected that the resulting spatial correlation will show a smaller difference with the historical spatial correlation value.
- By increasing the size of the convolution matrix, the spatial correlation between grid cells can be extended over larger distances. This can be used to reflect large correlation distance in uniform areas, like lowlands. Decreasing the size of the convolution matrix can be used to create the opposite effect for areas with low historical correlation values, like mountainous areas.
- Varying the weights of the convolution matrix can be used to introduce directional correlation. This can be useful in areas which are characterised by different precipitation regimes, e.g. at foothills or at small islands.

Challenges:

- The realisation of an objective method to determine the different weights when a convolution matrix with varying weights is seen as most appropriate.
- The determination of the appropriate size of the convolution matrix. This can potentially be done by defining a cut-off value of the historical spatial correlation between two cells. Cells with values lower than this cut-off value should not be involved in the convolution process.

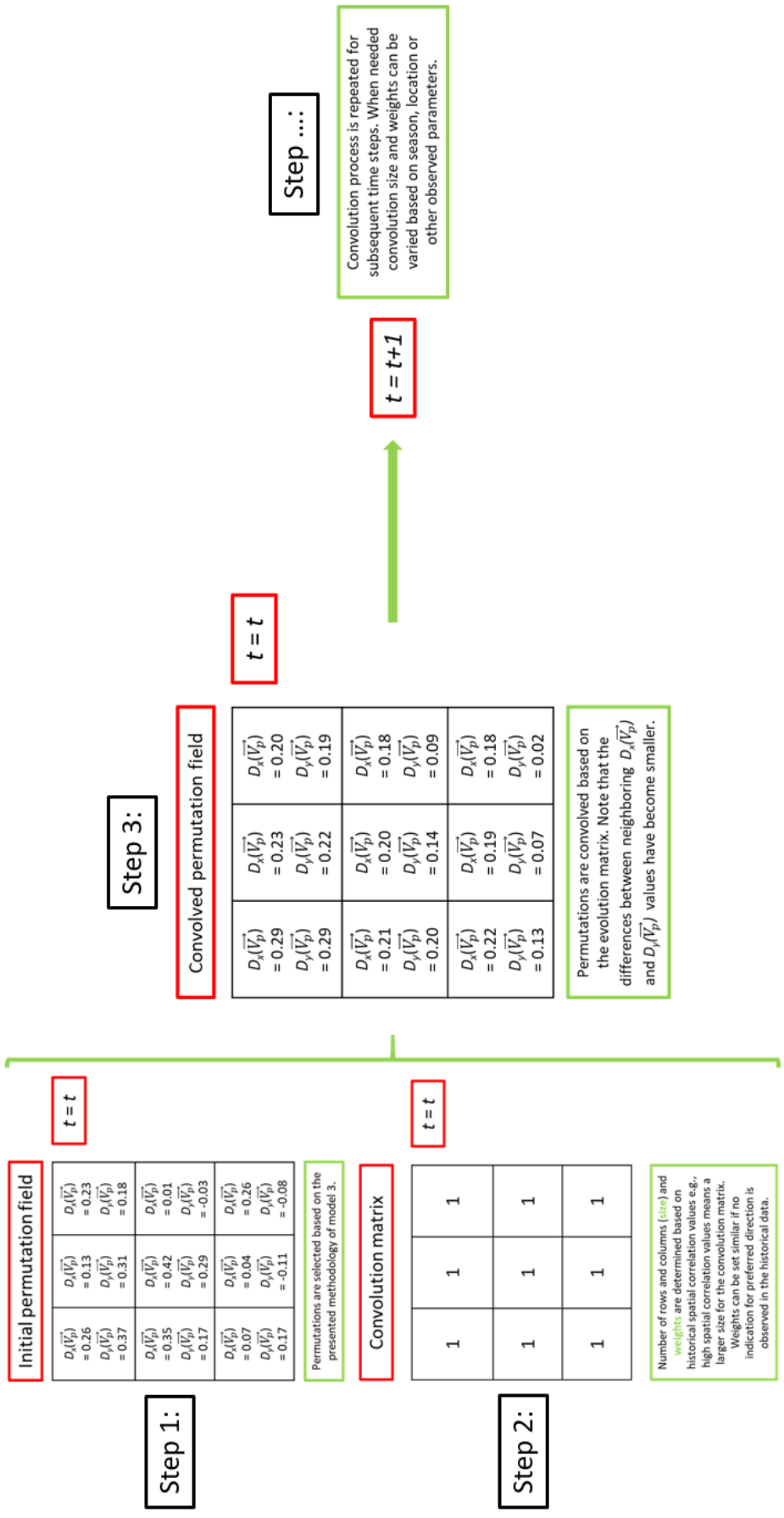

Figure VIII.1: Visual representation of the elaboration of the proxy vector selection to include more spatial correlation in the methodology of model 3.

VIII.2. Improvement temporal correlation

On the next page, a schematic representation of the use of an elaborated approach of choosing a proxy vector to explicitly include temporal correlation in the methodology of model 3 is presented. Foreseen advantages and challenges are described in the enumerations below.

Advantages:

- The temporal correlation between vectors in one grid cell will increase. It is expected that the resulting temporal correlation will show a smaller difference with the historical temporal correlation value.
- Randomness is maintained by allowing the model to 'escape' from the quadrant with the highest weights.
- The method can be implemented as new part in the methodology of model 3. There is no need to change the rest of the methodology.

Challenges:

- The realisation of an objective method to determine the weights which need to be given to each quadrant of proxy vectors.
- The inclusion of spatial correlation in this method should create a dependency between the weights of quadrants of neighbouring cells at one time step to prevent an improvement of the temporal correlation at the expense of the spatial correlation.

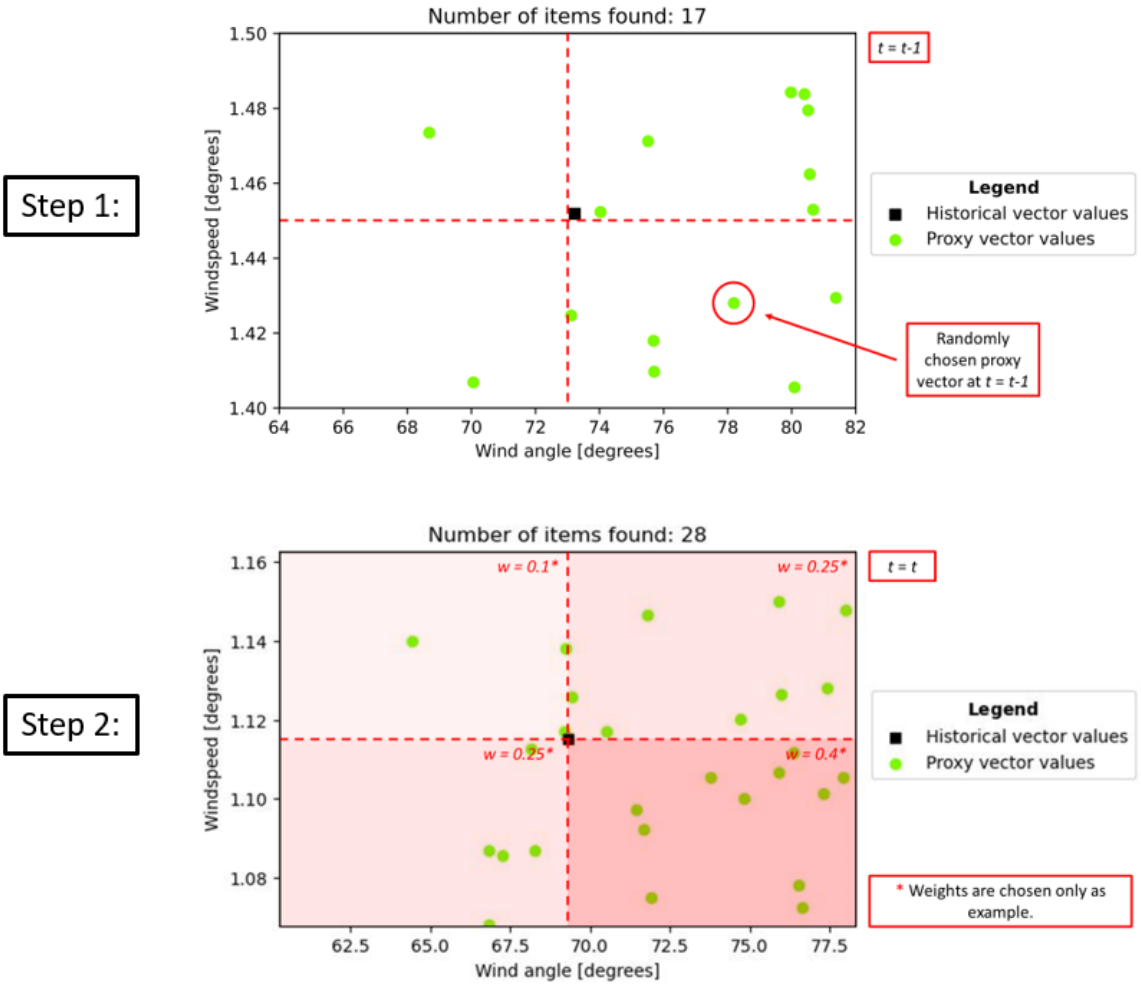

Figure VIII.2: Visual representation of the elaboration of the proxy vector selection to include more temporal correlation in the methodology of model 3.


TUDelft